BOUNDARY VALUE PROBLEMS IN DIELECTRIC SPECTROSCOPY

by

Zdzisław Andrzej, Delecki

A Doctoral Dissertation
Submitted to the School of Graduate Studies and Research
of the University of Ottawa
in partial fulfillment of the requirements
for the Degree of

DOCTOR OF PHILOSOPHY

in

Electrical Engineering

Ottawa-Carleton Institute
for Electrical Engineering
Department of Electrical Engineering
University of Ottawa
Ottawa, Canada

The essential in the being of a man of my type lies precisely in what he thinks and how he thinks, not in what he does or suffers.

ALBERT EINSTEIN in *"Why I Left Canada" by L. Infeld* (1966)

I hereby declare that I am the sole author of this paper. I authorize the University of Ottawa to lend this thesis to other institutions or individuals for the purpose of scholarly research.

Z.A. Delecki

I further authorize the University of Ottawa to reproduce this dissertation by photocopying or by other means, in total or in part, at the request of other institutions or individuals for the purpose of scholarly research.

Z.A. Delecki

ACKNOWLEDGEMENTS

It is a pleasure to express the author's most sincere gratitude to his advisor, Dr. S.S. Stuchly, for his encouragement, guidance, criticism and generous supplemental financial support throughout this work.

The author would also like to thank the advisory committee members Dr. M. Stuchly, Dr. G. Costache and Dr. J. Wight for their many useful suggestions and helpful criticism to improve the focus and scope of this work.

The author is indebted to his colleagues: Dr. J. Kozlowski, Mr. K. Esselle and Mr. M. Radojičić who unselfishly contributed their time and energy to read the manuscript at its various stages and gave fine and constructive comments.

The author would also like to express his appreciation to Ms. Elizabeth Sullivan of the Academic Computing Centre for allowing him unlimited access to the university computing facilities.

The author would like to express sincere thanks to his wife for making a very conceivable effort to keep his spirits high.

The author wishes to acknowledge the doctoral scholarship provided by the Natural Sciences and Engineering Research Council of Canada during the course of this research.

ABSTRACT

A description of the electromagnetic field within material media is critically reviewed. A method of the transverse-longitudinal decomposition of Maxwell's equations permits us to formulate a new form of the quasi-stationary boundary condition for the magnetic field density at the interface of dielectric media possessing finite permittivity. This concept leads to an explicit formula for the surface impedance. Its application to an open-ended coaxial line sensor decouples the internal and external field problems. A method for the solution of the external problem is developed for a semi-infinite dielectric space with mixed boundary conditions on circular annuli. This is evaluated by applying the Finite Hankel Transform (FHT). Extended tables of roots for application of the FHT are presented for the first time. Finally, a new approach to calculating the experimental errors in determination of dielectric properties is presented.

CONTENTS

LIST OF FIGURES

LIST OF TABLES

LIST OF SYMBOLS

a	Radius of the inner conductor of a coaxial line unless otherwise stated
A_E	Normalization constant for electric waves (TM)
A_H	Normalization constant for magnetic waves (TE)
b	Radius of the outer conductor of a coaxial line unless otherwise stated
$\vec{\mathbf{b}}$	Microscopic magnetic flux density vector
$\vec{\mathbf{B}}$	Macroscopic magnetic flux density vector
$\vec{\mathbf{B}}_o = \mu_o \vec{\mathbf{H}}$	Free space magnetic flux density vector
$\vec{\mathbf{B}}_{eff} = \overline{\vec{\mathbf{b}}}$	Effective (spatial average) magnetic flux density vector in matter
C_a	Lumped capacitance of the aperture
c_c	Coupling coefficient of the aperture
C_f	Lumped capacitance of the terminal region
d	Radius of the finite flange
$\vec{\mathbf{d}}$	Microscopic electric flux density (displacement) vector
$\vec{\mathbf{D}}$	Macroscopic electric flux density (displacement) vector
$\vec{\mathbf{D}}_o = \epsilon_o \vec{\mathbf{E}}$	Free space electric flux density (displacement) vector
$\vec{\mathbf{D}}_{eff} = \overline{\vec{\mathbf{d}}}$	Effective (spatial average) flux field density vector
e	Natural logarithm basis: $2.7182818\cdots$
$\vec{\mathbf{e}}$	Microscopic electric field density vector
$\vec{\mathbf{E}}$	Macroscopic electric field density vector
E	Scalar macroscopic electric field density
$\vec{\mathbf{E}}_{eff} = \overline{\vec{\mathbf{e}}}$	Effective (spatial average) electric field density vector
$\mathcal{F}(\kappa)$	Finite Hankel transform
G_a	Lumped Conductance of the aperture
$G^{(-)}(\rho, z\,; \rho', z')$	Green's function corresponding to the region $z < 0$
$G^{(+)}(\rho, z\,; \rho', z')$	Green's function corresponding to the region $z > 0$
$\vec{\mathbf{h}}$	Microscopic magnetic field density vector
$\vec{\mathbf{H}}$	Macroscopic magnetic field density vector
$\vec{\mathbf{H}}_{eff} = \overline{\vec{\mathbf{e}}}$	Effective (spatial average) magnetic field density vector in matter
$\vec{\mathbf{d}}$	Microscopic electric flux density (displacement) vector

$\Im$	Imaginary part of a complex function (number)
$\vec{\mathbf{j}}$	Microscopic volumetric current density vector
$\vec{\mathbf{J}}$	Macroscopic volumetric current density vector
$\vec{\mathbf{J}}_e$	Electric volumetric current density vector
$\vec{\mathbf{J}}_F$	"Free" volumetric current density vector
$\vec{\mathbf{J}}_m$	Magnetic volumetric current density vector
$\vec{\mathbf{J}}_{et}$	Electric current density vector tangential to a discontinuity
$\vec{\mathbf{J}}_{mt}$	Magnetic current density vector tangential to a discontinuity
$\vec{\mathbf{J}}_{e\zeta}$	Electric current density vector normal to a discontinuity
$\vec{\mathbf{J}}_{m\zeta}$	Magnetic current density vector normal to a discontinuity
$J_m(\kappa\rho)$	Bessel function of the first kind of order m and argument $\kappa\rho$
$\vec{\mathbf{K}}$	Surface electric current density
$\mathcal{K}_m(\kappa\rho)$	Kernel of Hankel transform
$\ell = a/b$	Ratio of the inner and outer radii of a coaxial region
$\vec{\mathbf{M}}$	Space-Averaged magnetization moment density
$\vec{\mathbf{n}}$	Unit normal vector to an arbitrary surface
$\mathcal{P}^+$	Finite Hankel transform of Ψ^+
$\vec{\mathbf{P}}$	Space-Averaged dipole moment density
$Q'_{\alpha\beta}(\vec{\mathbf{x}}, t)$	Covariant tensor of rank two of the quadrupole moment density
$\Re$	Real part of a complex function (number)
$\vec{\mathbf{S}}$	The time-averaged Poynting vector
$\vec{\mathbf{S}}^*$	Complex Conjugate Poynting vector
$\overline{S}(\rho)$	Nonvanishing radial component of power density
S_a	the aperture plane
S_v	Surface surrounding volume V
S_t	Reference surface separating terminal region from the coaxial line
S_a	Surface of the aperture of the coaxial sensor
$\vec{\mathbf{x}}$	Arbitrary 3-D field point position vector
$\vec{\mathbf{x}}'$	Arbitrary 3-D source point position vector

$w(\vec{\mathbf{x}}')$	Convolution kernel of a spatial averaging procedure
V	volume or voltage depending on context
$\tilde{y}$	Normalized admittance
$\tilde{Y}_a$	Aperture admittance
$\tilde{Y}_o$	Characteristic admittance of a line or waveguide
$\tilde{Y}_s$	Surface admittance of a dielectric interface
$Y_m(\kappa\rho)$	Neumann function of order m or alternatively Bessel function of the second kind
$\mathcal{Y}_0$	Intrinsic admittance of a medium
$\mathcal{Z}_0$	Intrinsic impedance of a medium
$z_o = \sqrt{\frac{\mu_o}{\epsilon_o}}$	Characteristic impedance of free space
$\tilde{Z}_s$	Complex surface impedance
γ_c	Propagation constant of the TEM wave in coaxial line
γ_n	Complex propagation constant of the TE-wave
$\tilde{\Gamma}$	Complex reflection coefficient (exact value)
$\tilde{\Gamma}_o$	Complex reflection coefficient of the TEM-wave
$\tilde{\Gamma}_m$	Measured complex reflection coefficient
$\tilde{\Gamma}_n$	Complex backward scaterring coefficient of the TM waves
δ	Type of dispersion of biological dielectrics
$\delta(\vec{\mathbf{x}} - \vec{\mathbf{x}}')$	Dirac delta function
$\delta_{m\,0}$	Constant defined on page 43
$\Delta\tilde{\Gamma}$	Complex uncertainty in reflection coefficient
$\Delta\tilde{\epsilon}$	Complex uncertainty in permittivity
$\Delta\phi_{max}$	Maximal deviation of the phase angle
$\tilde{\epsilon}$	Complex permittivity
ϵ'	Real part of the complex permittivity
ϵ''	Imaginary part of the complex permittivity (loss factor)
ϵ_∞	High frequency complex permittivity in Debye's model
ϵ_L	Low frequency complex permittivity in Debye's model
ϵ_o	Free space permittivity: $8.885 \times 10^{-12} \left[\frac{C^2\, s^2}{m^3\, kg}\right]$
ε	Relative permittivity
ζ	Variable along the normal to a surface in local coordinate system
ζ_o^+	Discontinuity point denoting limit from above

ζ_o^-	Discontinuity point denoting limit from below
ζ_{pen}	Conventional penetration depth
ζ_p	New penetration depth
θ	Elevation angle in spherical coordinate system
$\vartheta(\omega) = \sqrt{\frac{\tilde{\varepsilon}\omega}{\varepsilon_c(\omega)}}$	Discontinuity operator
$\tilde{\Theta}_n$	Forward Scattering Coefficient of the aperture
κ	Argument of the finite Hankel transform domain
$\kappa_{Em\,n}$	Eigenvalue of the first boundary value problem in (4.2.4)
$\kappa_{Hm\,n}$	Eigenvalue of the second boundary value problem in (4.2.5)
λ	Wavelength of electromagnetic wave
μ_o	Free space permeability: $4\pi \times 10^{-7}\left[\frac{kg\,m}{C^2}\right]$
π	Constant: $3.1415926\cdots$
ρ	Volumetric charge density or radial variable in cylindrical coordinate system
ρ_F	"Free" volumetric charge density
ρ_m	Magnetic volumetric charge density
σ	Surface charge density or conductivity of a medium (depending on context)
$\Phi^+(\phi)$	Scalar wave function for the region $z > 0$
$\chi_{E\,m\,n} = (\kappa_{E\,m\,n})b$	Scaled eigenvalue of transcendental equation (4.2.8)
$\chi_{H\,m\,n} = (\kappa_{H\,m\,n})b$	Scaled eigenvalue of transcendental equation (4.2.9)
ψ	Resolution angle on Smith Chart
Ψ	Scalar field in coaxial waveguide
$\Psi_{E\,m\,n}$	Solution of the field equation in coaxial waveguide corresponding to electric modes
$\Psi_{H\,m\,n}$	Solution of the field equation in coaxial waveguide corresponding to magnetic modes
$\Psi^+(\rho\,,\,z)$	Scalar wave function for dielectric region $z > 0$
$\Psi_t^+(\rho\,,\,z\,,\,\phi)$	Total scalar wave function for dielectric region $z > 0$
ω	Angular frequency
ω_o	Angular frequency at resonance
∇	del operator
∇_t	transverse del operator
$⨍$	Cauchy's principal value integral
$\tan\delta$	Loss tangent

I. Introduction

1.1 The Motivation

Both scientific and technological advances exhibit a need for general theories. One basic methodological tool used in the development of scientific theories is the method of analogy. This method has the following underlining philosophy: An equivalence relation is established between two systems; one is real and the another conceptual. The equivalence relation indicates the similar aspects of the two systems.

In the electromagnetic theory, there are many examples of equivalence relations. Permittivity is one of quantities of which the conceptual model is of great practical interest. The permittivity is a direct consequence of an essential field concept and describes the interaction between the field and the dielectric. The dielectric body affects the electromagnetic waves by polarization and magnetization within its volume and at its boundaries, while the wave, when it penetrates into the dielectric sample, induces charges and currents. The mechanism of interaction between fields and matter is not completely described by the macroscopic theory which gives only a large scale (average) description of the observed behavior.

Electromagnetic fields are often not measured in a free and infinite space, but are confined within boundaries. Scattering and diffraction of waves at boundaries provide essential means for measuring the interaction between electromagnetic waves and dielectric materials using various equivalence relations. The determination of electromagnetic scattering from dielectric boundaries, both in bounded and unbounded regions, is of increasing interest to researchers investigating the biological effects of electromagnetic fields, frequency characteristics of dielectric materials, sub-surface radar, electromagnetic imaging, tomography, remote sensing techniques and industrial applications of microwaves such as heating, drying, acquametry, etc. The quantitative evaluation of the response of biological materials biased by a static magnetic field to weak, varying electromagnetic fields form the basis for the nuclear magnetic resonance phenomena.

The interaction of wide-band microwave signals with a passive component containing a dielectric cannot be completely understood without knowledge about the dispersive properties of both the passive component and the dielectric material.

Various approaches to the solution of field problems have been applied in the past. The conventional one is the differential approach which is based on the direct solution of the wave equation. This approach had predominated over the integral and series approach for the most of the last century. During the last three decades many new integral and series techniques have been proposed with interesting theoretical and computational features.

The purpose of the dissertation is to obtain better understanding of the influence of matter on electromagnetic fields by investigation of:

- theoretical aspects of boundary value problems from the standpoint of dielectric reflection spectroscopy; and
- applied aspects of dielectric spectroscopy.

The theoretical aspects can be summarized as the following aims:

1. to propose a unified approach encompassing the existing methods;
2. to verify the published analysis of dielectric sensors which have a good theoretical foundation;
3. to develop and verify techniques which are appropriate for field computations and thus suitable for dielectric spectroscopy.

The applied aspects have the following goals:

1. to find compromises between mathematical complexity and accuracy for practical problem solving;
2. to develop computational tools for the uncertainty analysis in measurements of dis-

persive materials;

3. to develop a computational basis for dielectric sensor design;
4. to determine limits for the use of dielectric sensors.

The first goal is restricted to determination of stationary scattered electromagnetic fields from various discontinuities created by a dielectric medium. When the medium has a fixed shape and location with respect to the microwave measurement system it is called the test sample. The shape and size of the test sample is determined by the dimensions of a sample holder.

The application of the appropriately analyzed electromagnetic fields is to use expressions for these fields to determine the dispersive properties of the complex permittivity of the test sample. The link between the practical and theoretical aspects of this question is emphasized in the uncertainty analysis. In the experimental part, numerical data obtained by an application of the theory developed here to particular cases of scattered field, the complex dielectric constant and related uncertainties are compared with the experimental data previously published. The use of a topological method represents a novel approach to uncertainty analysis.

Electromagnetic scattering from a lossy or lossless homogeneous dielectric and coated with dielectric conducting bodies has been determined numerically by using the electric or magnetic field integral equation formulations known as EFIE and MFIE, respectively [1]. Since the advent of the high speed digital computer, solving boundary value problems by numerical methods has become an area for intense research. In the past, ten years it has been the basic engineering tool for the solution of microwave problems [2]. Frequently used numerical techniques are the finite difference method, finite element method and method of moments. A special case of the finite element method is the boundary element method

[1] J A. Stratton, "Electromagnetic Theory", McGraw-Hill, New York, 1941, p 466

[2] G J. Burke and A.J Poggio, "Numerical Electromagnetic Code (NEC) - Method of Moments", Technical Document 116, Naval Ocean Systems Center, San Diego, USA, 1980, pp 1-179

which also has some of the advantages of the method of moments. Although numerical techniques allow us to solve a great number of problems which were not amenable to analytical solutions in the past, they do not supply information about the accuracy of the obtained values despite the fact that they are based on mathematically convergent procedures. One way to overcome this problem is to apply the technique to a problem with a known analytical solution and then to compare values computed by the two methods in order to determine the accuracy of the numerical technique. Therefore, there is a need to enlarge the set of the problems having analytical solutions. Different transformations and semi-analytical techniques are used for this purpose.

1.2 Organization of the Dissertation

This dissertation consists of three parts:

- The first part (Chapters I-II) sets the stage. It contains a limited review of the most important aspects of electromagnetics, namely Maxwell's equations, upon which electromagnetic field theory is constructed.
- The second part (Chapters III and IV) contains the main contributions of the dissertation to the solution of a few applied electromagnetic problems. This part is concerns only the field equations and boundary problems in the presence of dielectric and perfectly conducting boundaries.
- The third part (Chapters V-VI) verifies the theoretical results by comparing them with available experimental data. Results important to dielectric spectroscopy include a new approach to uncertainty analysis.

In Chapter II, the basic results of the field theory are described. Electromagnetic field laws of conservation and balance are explained. These basic principles may be expressed either in a differential or an integral form in regions where the variables change sufficiently smoothly. They are equivalent to differential field equations within a region, while at surfaces of discontinuities to they are equivalent to discontinuity conditions. The field equations and discontinuity conditions form an under-determined system of equations, which cannot yield unique solutions unless further equations are supplied. Ideas leading to the *mixed* formulation of Maxwell's equations are also presented. These allow us to have an insight into the nature of the electromagnetic field in the matter. The properties of materials are considered in the scope of the field theory concept. The set of vector fields provides vectorial description of materials. Relations between these vectors are called constitutive equations. The constitutive equations and field equations together, along with discontinuity and boundary conditions, lead to a definite theory, which is useful in predicting answers to particular problems. For some of the special problems, this has been proven through theorems of existence and uniqueness.

The most familiar constitutive equations relate electromagnetic field vectors:

- The electric displacement is proportional to the electric field $\vec{\mathbf{D}} = \tilde{\epsilon}\vec{\mathbf{E}}$;
- The magnetic induction is proportional to the magnetic intensity $\vec{\mathbf{B}} = \mu\vec{\mathbf{H}}$.

In this aspect, however, the scope of interest exceeds this simplification, thus a tensorial description of interrelation between field quantities is attempted. The dielectric as a certain class of material media is defined later by means of the field theory model and attention is focused only to this class of materials.

Although this dissertation is devoted to interaction between dielectric material and fields, the perspective, from which it is viewed, includes the principles of balance in a material medium in the form of conservative relations. However, the detailed theory of dielectrics is excluded from the thesis.

In Chapter III, a new formulation of the discontinuity condition is presented for the magnetic field. It permits us to find an explicit expression for the surface impedance. The analysis of electromagnetic fields at the interface with a dielectric material is fundamental for interaction between field and matter in dielectric reflection spectroscopy. These interactions depend on:

- the type of the wave incident upon the dielectric body;
- the spatial geometry of the body;
- electrical properties of the material medium of the body.

For dielectric reflection spectroscopy, it is obvious that these elements contribute to the value of the reflection coefficient. The first and third element may be easily included into a solution when the interface is a flat semi-infinite dielectric space. However, when the interface is an arbitrary surface, a transformation of the wave-front of the incident wave into an equivalent plane wave may be used. A conformal transformation of the region is an alternative method to obtain a solution. In practical situations, the interface of a sample is separated by a window from the line or waveguide. Influence of windows is usually eliminated by the calibration procedure.

In Chapter IV, the results of the preceding chapter are used to solve an open-ended coaxial line sensor in order to determine the reflected fields in terms of the permittivity of the dielectric. The Green's function for the coaxial line region is modified compared to that given in published results. The concept of the surface admittance developed in Chapter III is applied to decouple the internal and external field problems. The new method for the solution of mixed boundary problems in the external dielectric region is implemented to determine electromagnetic fields.

In Chapter V, calculated and experimental data are compared for two different coaxial sensors imbedded in three liquid dielectric media. The lumped element model of the input admittance for coaxial probes used in dielectric reflection spectroscopy is derived.

In Chapter VI, the uncertainty analysis is carried out using conformal mapping techniques for the measurement technique based on the infinite sample method.

The general summary, discussion and conclusions follow in Chapter VII.

II. Preliminaries

2.1 Electromagnetic Fields in Matter

The theoretical framework for electromagnetic properties of matter is based on the classical form of Maxwell's equations [3]:

$$\nabla \times \vec{\mathbf{E}} = -\frac{\partial \vec{\mathbf{B}}}{\partial t} , \tag{2.1.1}$$

$$\nabla \times \vec{\mathbf{H}} = \vec{\mathbf{J}} + \frac{\partial \vec{\mathbf{D}}}{\partial t} , \tag{2.1.2}$$

$$\nabla \cdot \vec{\mathbf{J}} = -\frac{\partial \rho}{\partial t} . \tag{2.1.3}$$

The requirement that both circulation and source densities should be defined follows from the completeness of the vector field description [4]. The source density for magnetic flux density $\vec{\mathbf{B}}$ is found by taking the divergence of (2.1.1), integrating it with respect to time and setting the constant of integration equal to zero

$$\nabla \cdot \vec{\mathbf{B}} = 0 . \tag{2.1.4}$$

By repeating the same procedure with (2.1.2), eliminating the electric current density $\vec{\mathbf{J}}$ from the result and using (2.1.3), the source density for the displacement vector (or alternatively electric flux density) is

$$\nabla \cdot \vec{\mathbf{D}} = \rho . \tag{2.1.5}$$

In general the field equations contain a high level of indeterminacy since equations (2.1.1)-(2.1.3) correspond to sixteen unknown scalar functions.

Although Maxwell's equations for the electromagnetic fields in vacuum are linear (and hence, the sum of two solutions is again a solution), in the material media they may not be [5]. An important attribute of linearity is the superposition principle. The conventional

[3] C T Tai, "Dyadic Green's Functions in Electromagnetic Theory", Intext Educational Publishers, San Francisco-Toronto-London, 1971, pp 17-27

[4] A P Wills, "Vector Analysis with an Introduction to Tensor Analysis", Prentice-Hall, Inc , 1950 pp 121-122

[5] W F Brown, "Dielectrics", Encyclopedia of Physics, edited by S Flugge, Vol XVII, Springer-Verlag, Berlin, 1956 pp 1-153

approach to dielectric properties is based on a phenomenological model of the response of a dielectric to weak oscillatory fields. The response of the same dielectric may be altered by placing it in a strong electric or magnetic field characterized by the same time dependence. Therefore the equations relating electromagnetic field quantities in a material medium are essentially non-linear [6]. However, for weak fields, the relationship is linear.

The presented form of the electrodynamic field equations does not contain the complete symmetry between electricity and magnetism due to the fact that a single electric charge can exist on a particle, while a single magnetic pole has not been observed so far. The way to achieve a formal form of symmetry will be shown later in this section.

In vacuum, the microscopic and macroscopic forms of Maxwell's equations are equivalent. In the presence of matter, the electric displacement is a function of the electric field; the magnetic induction is a function of the magnetic intensity. In classical electromagnetics these relations are usually assumed to be linear. The total polarizibility is a vector function of the space charge distribution and a distance with respect to some origin. It is usually separated into three parts: electronic, atomic and dipolar. The electronic contribution arises from the displacement of the electron shell relative to the nucleus. The ionic contribution comes from the displacement of a charge ion with respect to other ions. The dipolar polarizability arises from molecules with a permanent electric dipole moment that can change orientation in an applied electric field.

In order to overcome the complexity of microscopic electromagnetic fields within the matter, the macroscopic fields are derived from microscopic equations of electrodynamics [7] using a suitable spatial averaging procedure. The fundamental assumption of the analysis is that the macroscopic quantities are spatial averages of the corresponding microscopic ones. Denoting the microscopic electric field by $\vec{e}$, multiplying it by a suitably

[6] J Meixner, "Einige Folgerungen aus einer Identitat fur Electromagnetische Felder", Acta Physica Polonica, V XXVII, 1965, pp 113-121

[7] G Russakoff, "A Derivation of the Macroscopic Maxwell Equations", American Journal of Physics, Vol 38, No 10, October 1970, pp 1188-1195

chosen testing function $w(\mathbf{x}')$, being real and positive, and integrating over some volume, large as compared to molecular sizes and surrounding $\mathbf{x}' = 0$, we obtain the convolution integral which defines the macroscopic electric field density within material medium in the form:

$$\vec{\mathbf{E}} = \bar{\vec{\mathbf{e}}} = \int_V w(\mathbf{x}')\vec{\mathbf{e}}(\mathbf{x} - \mathbf{x}')d^3\mathbf{x}' \ , \tag{2.1.6}$$

where $\bar{\vec{\mathbf{e}}}$ denotes the spatial average electric field density and the bar is used to indicate the average quantity.

Two possible choices of testing functions are:

$$w(\mathbf{x}') = \begin{cases} \frac{3}{4\pi R^3}, & \text{if } |\mathbf{x}'| \leq R; \\ 0 & \text{if } |\mathbf{x}'| > R \ , \end{cases} \tag{2.1.7}$$

and

$$w(\mathbf{x}') = (\pi R^2)^{-3/2} \, e^{-r^2/R^2} \ , \tag{2.1.8}$$

where R is radius of a sphere, large when compared to molecular sizes of the substance and $R << \lambda/2\,\pi$ for time harmonic monochromatic fields [8].

The first testing function (2.1.7) is known in classical literature [9] as an averaging function over the volume of a sphere having a radius $|\mathbf{x}| = R$. Although conceptually simple, it has the disadvantage of an abrupt discontinuity at R. The second function does not contain this disadvantage, therefore it is used [7] to derive macroscopic equations in the medium. If we write the microscopic Maxwell's equation of the form (2.1.1)-(2.1.3):

$$\nabla \times \vec{\mathbf{e}} = -\frac{\partial \vec{\mathbf{e}}}{\partial t} \ , \tag{2.1.9}$$

$$\nabla \times \vec{\mathbf{h}} = \vec{\mathbf{j}} + \frac{\partial \vec{\mathbf{d}}}{\partial t} \ , \tag{2.1.10}$$

$$\nabla \cdot \vec{\mathbf{j}} = -\frac{\partial \rho_F}{\partial t} \tag{2.1.11}$$

[8] R W P King, "Quasi-Stationary and Nonstationary Currents in Electric Circuits" Encyclopedia of Physics, ed by S Flugge Vol XVI, Springer-Verlag, Berlin, 1958, pp 165-172

[9] J D Jackson, "Classical Electrodynamics", John Wiley & Sons, New York, 1975, pp 226-235

and apply the convolution integral (2.1.6) to all microscopic fields and sources involved, $\vec{\mathbf{e}}$, $\vec{\mathbf{d}}$, $\vec{\mathbf{b}}$, $\vec{\mathbf{h}}$, $\vec{\mathbf{j}}$, ρ, and use the commutative property of differentiation in time and integration in space, we obtain the macroscopic approximation of electromagnetic fields within the matter formally analogous to (2.1.1)-(2.1.5):

$$\nabla \times \vec{\mathbf{E}}_{eff} = -\frac{\partial \vec{\mathbf{B}}_{eff}}{\partial t} \tag{2.1.12}$$

$$\nabla \times \vec{\mathbf{H}}_{eff} = \bar{\vec{\mathbf{j}}} + \frac{\partial \vec{\mathbf{D}}_{eff}}{\partial t} \tag{2.1.13}$$

$$\nabla \cdot \bar{\vec{\mathbf{j}}} = -\frac{\partial \bar{\rho}}{\partial t} \tag{2.1.14}$$

$$\nabla \cdot \vec{\mathbf{B}}_{eff} = 0 \tag{2.1.15}$$

$$\nabla \cdot \vec{\mathbf{D}}_{eff} = \bar{\rho}_F \tag{2.1.16}$$

where $\vec{\mathbf{E}}_{eff} = \bar{\vec{\mathbf{e}}}$, $\vec{\mathbf{D}}_{eff} = \bar{\vec{\mathbf{d}}}$, $\vec{\mathbf{B}}_{eff} = \bar{\vec{\mathbf{b}}}$ and $\vec{\mathbf{H}}_{eff} = \bar{\vec{\mathbf{h}}}$ denote the effective electromagnetic fields obtained by averaging the microscopic fields over the volume of interest containing the matter.

By expanding the convolution kernel $w(\vec{\mathbf{x}}')$, where $\vec{\mathbf{x}}' = (\vec{\mathbf{x}}_1', \vec{\mathbf{x}}_2', \vec{\mathbf{x}}_3')$, into a Taylor series in the integration region and subsequently using multipole expansions, the average charge density is found to be [7]

$$\bar{\rho}(\vec{\mathbf{x}}, t) \approx \bar{\rho}_F(\vec{\mathbf{x}}, t) - \nabla \cdot \vec{\mathbf{P}}(\vec{\mathbf{x}}, t) + \sum_{\alpha\beta} \frac{\partial^2}{\partial x_\alpha \, \partial x_\beta} Q'_{\alpha\beta}(\vec{\mathbf{x}}, t) + \ldots \ , \tag{2.1.17}$$

where $\vec{\mathbf{P}}$ and $Q'_{\alpha\beta}(\vec{\mathbf{x}}, t)$ denote the averaged dipole moment and the averaged molecular quadrupole density, respectively. $\rho(\vec{\mathbf{x}}, t)$ is the averaged charge density which is a superposition of free (electron) and bound (molecule) charge densities. If in the latter equation all terms higher than second are neglected and the definition of the microscopic current density is:

$$\vec{\mathbf{j}}(\vec{\mathbf{x}}, t) = \sum_{j} \rho_F \frac{d\vec{\mathbf{x}}}{dt} \delta(\vec{\mathbf{x}} - \vec{\mathbf{x}}_j) \ . \tag{2.1.18}$$

After averaging, the average current density $\bar{\bar{\mathbf{j}}}(\vec{\mathbf{x}}, t)$ is found to be of the following form:

$$\bar{\bar{\mathbf{j}}} \approx \vec{\mathbf{J}}_F(\vec{\mathbf{x}}, t) + \frac{\partial \vec{\mathbf{P}}(\vec{\mathbf{x}}, t)}{\partial t} + \nabla \times \mathbf{M}(\vec{\mathbf{x}}, t) . \tag{2.1.19}$$

When (2.1.17) is substituted into (2.1.16) and (2.1.19) into (2.1.13), the following relations are obtained which are valid within the material media:

$$\vec{\mathbf{D}} \approx \vec{\mathbf{D}}_o + \vec{\mathbf{P}} = \epsilon_0 \vec{\mathbf{E}} + \vec{\mathbf{P}} \tag{2.1.20}$$

$$\vec{\mathbf{B}} \approx \vec{\mathbf{B}}_o + \mu_0 \vec{\mathbf{M}} = \mu_0 \vec{\mathbf{H}} + \mu_0 \vec{\mathbf{M}} . \tag{2.1.21}$$

These approximations are satisfactory for most practical applications. Nevertheless the relationships between $\vec{\mathbf{E}}$ and $\vec{\mathbf{D}}$ and $\vec{\mathbf{H}}$ and $\vec{\mathbf{B}}$ are not revealed yet. The theoretical value of these equations is that they are the leading terms of the analytically derived equations from the fundamental microscopic quantities. Equations (2.1.20) and (2.1.21) indicate that total electric or magnetic flux densities consist of free space ones and polarization or magnetization due to a medium. The former equation is consistent with the model in [10], [11], [12], [13] and [14].

The fundamental requirement, i.e. that eqs. (2.1.1)-(2.1.2) be valid both in vacuum and in matter, allows us to substitute these results into (2.1.1) and (2.1.2). That way, we obtain a model of Maxwell's equations within a medium:

$$\frac{1}{\epsilon_0}\nabla \times \vec{\mathbf{D}} = -\mu_0 \frac{\partial \vec{\mathbf{H}}}{\partial t} + \frac{1}{\epsilon_0}\nabla \times \vec{\mathbf{P}} - \mu_0 \frac{\partial \vec{\mathbf{M}}}{\partial t} \tag{2.1.22}$$

$$\frac{1}{\mu_0}\nabla \times \vec{\mathbf{B}} = \vec{\mathbf{J}}_F(\vec{\mathbf{x}}, t) + \epsilon_0 \frac{\partial \vec{\mathbf{E}}}{\partial t} + \frac{\partial \vec{\mathbf{P}}}{\partial t} + \nabla \times \vec{\mathbf{M}} \tag{2.1.23}$$

where $\vec{\mathbf{E}}$, $\vec{\mathbf{H}}$, $\vec{\mathbf{D}}$ and $\vec{\mathbf{B}}$ correspond to total fields while the remaining quantities $\vec{\mathbf{M}}$, $\vec{\mathbf{P}}$ and $\vec{\mathbf{J}}_F$ correspond to partial fields due to matter. It is easy to identify the last two equations

[10] A C Eringen, "On the Foundations of Electroelastostatics", International Journal of Engineering Science, V 1, pp 127-153 1963

[11] J Van Bladel, "Relativity and Engineering", Springer Verlag, Berlin, 1984 pp 106-109

[12] R M Fano, L J Chu and R B Adler, "Electromagnetic Fields, Energy and Forces", John Wiley & Sohns, 1960, pp 269-316

[13] J A Stratton, *op cit*, pp 464-470

[14] N Marcuvitz and J Schwinger, 'On the Representation of the Electric and Magnetic Fields Produced by Currents and Discontinuities in Waveguides" Journal of Applied Physics, V 22, No 6, June 1951, pp 806-819

as *the mixed form of Maxwell's equations.* The use of polarization $\vec{\mathbf{P}}$ and magnetization $\vec{\mathbf{M}}$ vectors permitts an extension of the first equation by term $(\nabla \times \vec{\mathbf{P}})/\epsilon_0$.

Defining the total electric current by

$$\vec{\mathbf{J}}_e = \vec{\vec{\mathbf{J}}}_F + \frac{\partial \vec{\mathbf{P}}}{\partial t} + \nabla \times \vec{\mathbf{M}} \tag{2.1.24}$$

and the total magnetic current by

$$\vec{\mathbf{J}}_m = -\frac{1}{\epsilon_0}\nabla \times \vec{\mathbf{P}} + \mu_0 \frac{\partial \vec{\mathbf{M}}}{\partial t}\ , \tag{2.1.25}$$

the symmetric form of Maxwell's equations is obtained:

$$\frac{1}{\epsilon_0}\nabla \times \vec{\mathbf{D}} = -\mu_0 \frac{\partial \vec{\mathbf{H}}}{\partial t} - \vec{\mathbf{J}}_m \qquad \text{Faraday's Law} \tag{2.1.26}$$

$$\frac{1}{\mu_0}\nabla \times \vec{\mathbf{B}} = \epsilon_0 \frac{\partial \vec{\mathbf{E}}}{\partial t} + \vec{\mathbf{J}}_e \qquad \text{Maxwell} - \text{Ampere Law}\ . \tag{2.1.27}$$

The derived model of electromagnetic fields within matter is represented by all field components and secondary fields producing the magnetic and electric current densities $\vec{\mathbf{J}}_m$ and $\vec{\mathbf{J}}_e$, respectively. Therefore this representation may be called the mixed formulation as opposed to other formulations such as those in *, [15], [16] and [17]. This representation is useful to model the properties of the field within matter and in the vicinity of various discontinuities. Nevertheless, these equations, to the best of the author's knowledge, have not been earlier formulated in this manner. The validity of use of the magnetic current has also been proven in [18] and [19] to be correct for the general treatment of microwave antennas. Neglecting the magnetic current may lead to a discrepancy between calculations and experiment.

---

* [12], [13], [14] *op. cit.*

[15] H. Levine and J. Schwinger, "On the Theory of Electromagnetic Wave Diffraction by an Aperture in an Infinite Plane Conducting Screen", Communication on Pure and Applied Mathematics, No. 3, 1950, pp. 355-391.

[16] R.W.P. King, G. Smith, M.Owens and T.T. Wu, "Antennas in Matter", The MIT Press, Messachusetts, 1981, pp. 316-361.

[17] N.P. Zhuk and O.A. Tret'yakov, "Green's Functions for Maxwell's Equations for a Plane-Layered Medium", Raditekhnika i Elektronika, No. 5, 1985, pp. 76-81 (*English trans.*).

[18] B.W. Braude, "Ob Odnoj Oszibke pri Ispolzowanii Metoda Integralnych Urawnemy Teorii Antenn", Jurnal Technitcheskoy Fiziki *(in Russian)*, V. XXV, No. 10, 1955, pp. 1819-1824.

[19] A.Z Fradin, "Microwave Antennas", Pergamon Press, Oxford, 1961, pp. 48-58.

The electric current given in (2.1.24) consists of free and bound currents. The bound current is, in general, composed of the coulombian current resulting from temporal variations of polarization, i.e., equivalent to the polarization current, and the amperian current caused by spatial variation of magnetization, i.e., equivalent to the magnetization current. The magnetic counterpart of bound electric current is the *total* magnetic current (2.1.25), a notion resulting from the spatial and temporal variations of the polarization and the magnetization, respectively. Thus, the existence of a magnetic monopole is not required to use the notion of magnetic currents. It is straightforward to show from (2.1.22) that the magnetic charge density is the nonvanishing divergence of magnetization, namely

$$\rho_m = -\mu_0 \nabla \cdot \vec{\mathbf{M}} \ . \tag{2.1.28}$$

The presented equations also show that the induced magnetic charge results from the field concept, i.e., the spatial variation (divergence) of magnetization within the medium and there is no free magnetic charge density. The latter equation is also necessary to preserve the conservation of magnetic flux within the medium.

From presented mixed formulation of Maxwell's equations in matter, (2.1.22-23) allows a theoretical definition for a dielectric medium can be defined as a medium that satisfies the following condition:

$$\frac{1}{\epsilon_0} \nabla \times \vec{\mathbf{P}} - \mu_0 \frac{\partial \vec{\mathbf{M}}}{\partial t} = \vec{\mathbf{J}}_m = 0 \ . \tag{2.1.29}$$

This equation provides the internal balance of the magnetic current in a medium.

2.2 Conservation Equations

That electric charge can be neither created nor destroyed is expressed by the continuity equation (2.1.3), which provides the first conservation equation. Further conservation equations may be deduced. Repeating the standard procedure to derive electromagnetic momentum density $\vec{\mathbf{D}} \times \vec{\mathbf{B}}$ from the mixed formulation of Maxwell's equations (2.1.22-23) by premultiplying* the first by total magnetic flux $\vec{\mathbf{B}}$, and the second by total electric flux $\vec{\mathbf{D}}$ and subtracting the second from the first we obtain:

$$\nabla \cdot (\vec{\mathbf{D}} \times \vec{\mathbf{B}}) = -\mu_0(\vec{\mathbf{D}} - \vec{\mathbf{P}}) \cdot \left(\vec{\mathbf{j}}_F + \epsilon_0 \frac{\partial \vec{\mathbf{E}}}{\partial t} + \frac{\partial \vec{\mathbf{P}}}{\partial t}\right) - \epsilon_0(\vec{\mathbf{B}} - \mu_0 \vec{\mathbf{H}}) \cdot \left(\mu_0 \frac{\partial \vec{\mathbf{H}}}{\partial t} + \mu_0 \frac{\partial \vec{\mathbf{M}}}{\partial t}\right) +$$

$$\underbrace{+\epsilon_0\mu_0 \nabla \cdot (\vec{\mathbf{E}} \times \vec{\mathbf{M}}) + \mu_0 \nabla \cdot (\vec{\mathbf{P}} \times \vec{\mathbf{H}}) + \mu_0 \nabla \cdot (\vec{\mathbf{P}} \times \vec{\mathbf{M}})}_{\textit{interaction terms}} \tag{2.2.1}$$

The last three divergence terms represent interaction between field and matter. These terms have not been revealed in the literature known to the author. They indicate the advantage of the mixed formulation of electromagnetic fields in matter by explicit separation of interaction terms. A significant difference between (2.2.1) and conventional forms of the electromagnetic momentum density is that the interaction terms are expressed in terms of secondary field vectors: $\vec{\mathbf{M}}$ and $\vec{\mathbf{P}}$. Their properties depend on the constitution of matter no assumption about the relations between $\vec{\mathbf{M}}$ and $\vec{\mathbf{B}}$, and between $\vec{\mathbf{P}}$ and $\vec{\mathbf{D}}$ are made. Therefore, this form is valid both for linear and nonlinear relations between relevant vector magnitudes.

Equation (2.2.1) may be transformed into a general macroscopic form of Poynting's Theorem (local in time and space) by grouping divergence terms in its LHS, using (2.1.20-21) and dividing both sides of the equation by the factor $1/c^2 = \epsilon_0\mu_0$. The familiar Poynting's theorem is thus obtained

$$\nabla \ (\vec{\mathbf{E}} \times \vec{\mathbf{H}}) = -\vec{\mathbf{E}} \cdot \vec{\mathbf{J}}_F - \vec{\mathbf{E}} \cdot \frac{\partial}{\partial t}(\epsilon_0 \vec{\mathbf{E}} + \vec{\mathbf{P}}) - \mu_0 \vec{\mathbf{H}} \cdot \frac{\partial}{\partial t}(\vec{\mathbf{H}} + \vec{\mathbf{M}}) \tag{2.2.2}$$

This equation proves that the applied form of Maxwell's equations (2.1.22-23). is equivalent to the form in which only total fields appear, i.e. (2.1.1-3). The interpretation of this relation depends on the property that the scalar product $-\vec{\mathbf{E}} \ \vec{\mathbf{J}}_F$ represents the

* It is meant as multiplying vectorially on the left of both sides of an vector equation

work done by the electric forces per unit time on the moving charges which constitute the current $\vec{\mathbf{J}}_F$ and are contained in a unit volume element. In the case of a source, this term may be interpreted as the energy delivered by the charges to the surrounding field. However, in the case of a sink it corresponds to the energy dissipated into heat. The two remaining dot products on the right-hand side of (2.2.2) express electric and magnetic energy, respectively, stored in a unit volume both for a source and a sink. These are locally distributed motionless energies. The right-hand side of (2.2.2) represents the energy flow of the field moving at the group velocity in the direction of Poynting vector $\vec{\mathbf{S}} = \vec{\mathbf{E}} \times \vec{\mathbf{H}}$.

Energy density $\vec{\mathbf{E}} \times \vec{\mathbf{H}}$, momentum density $\vec{\mathbf{D}} \times \vec{\mathbf{B}}$, and angular momentum density $\vec{\mathbf{x}} \times (\vec{\mathbf{D}} \times \vec{\mathbf{B}})$ together with charge conservation equation (2.1.3), represent the fundamental set of conservation equations.

2.3 Dispersion Relation for the Permittivity - Foundations

A medium in which the phase velocity v_p is dependent on the propagation vector $\vec{\mathbf{k}}$, namely $v_p = f(\vec{\mathbf{k}})$, is called dispersive [20]. In general, it is impossible to treat a refractive medium without dispersion. The electromagnetic properties of a dispersive medium depend on frequency, ω, density, ρ, and temperature T. Sommerfeld and Brillouin [20], [21] proved that in an idealized dielectric no signal travels faster than the speed of light c, although there may be frequencies at which both the phase velocity and the group velocity exceed c.

The dispersion relation is traditionally best known in the theory of dispersion of light in a dielectric [22], [23]. Kramers [24] originally used the notion of the complex refractive

[20] A.Sommerfeld, "Über die Fortpflanzug des Lichtes in dispergierenden Medien", Annalen der Physik, B 44, 1914, pp 177-203
[21] L.Brillouin, "Uber die Fortpflanzug des Lichtes in dispergierenden Medien', Annalen der Physik, B 44, 1914, pp 204-240
[22] R W Ditchburn, "Light", Interscience Publishers, New York, 1963, pp 772-776
[23] M Born and E Wolf, "Principles of Optics" Pergamon Press, Oxford, 1980, pp 494-499
[24] H.A. Kramers, "Estratto dagli Atti del Congresso Internationale de Fisici Como", Nicolo Zanichelli, Bologna, V 2, 1928, p 545

index defined by an analytic continuation in the complex frequency plane to show that a signal cannot travel faster than light in any medium. Krönig [25] proved the equivalence of causality and dispersion. He also showed that the dispersion relation is the necessary and sufficient condition for strict causality to be satisfied. The classical derivation of the dispersion relation contains only three major assumptions: boundedness, linearity and causality.

A dispersion relation is a simple integral formula relating a dispersion process to an absorption process. For the steady state of the electromagnetic stimulus [26], the most general, spatially local, linear and causal relation between $\vec{\mathbf{D}}$ and $\vec{\mathbf{E}}$ in a homogeneous isotropic medium is

$$\vec{\mathbf{D}}(\vec{\mathbf{x}},t) = \epsilon_o \vec{\mathbf{E}}(\vec{\mathbf{x}},t) + \int_0^\infty P(t')\,\vec{\mathbf{E}}(\vec{\mathbf{x}},\, t-t')dt' \ , \tag{2.3.1}$$

where the kernel $P(t')$ is a characteristic function and is represented by

$$P(t') = \epsilon_o \int_{-\infty}^{\infty} e^{-j\omega t'} d\phi(\omega) \tag{2.3.2}$$

The function $\phi(\omega)$ is a spectral function in $0 \le \omega < \infty$ which by odd continuation to negative ω satisfies the following conditions [27] [28]:

1. $\phi(\omega)$ is defined in $-\infty < \omega < \infty$;
2. $\phi(\omega)$ is nowhere decreasing;
3. $\phi(\omega)$ is bounded, namely $\phi(\infty) - \phi(-\infty) < \infty$;
4. $\phi(\omega)$ is continuous and zero at $\omega = 0$, i.e. $\phi(0^+) = \phi(0^-) = 0$;
5. $\phi(\omega) = [\phi(\omega^+) + \phi(\omega^-)]/2$ at points of discontinuity;
6. $\phi(\omega) = \lim_{\tilde{z}\to\omega+j\eta} f(\tilde{z})$, i.e., it represents a complex function of real argument and is a limiting case of a function of complex argument $f(\tilde{z})$.

---

[25] R Kronig, Ned Tijdschr Natuurk, No 9, 1942, p 402
[26] J Meixner, "Impedanz and Lagrange Funktion linearen dissipativen Systeme', Zeitschrift der Physik, 156, 1959, pp 200-210
[27] E C Titchmarsh, "Introduction to the Theory of Fourier Integrals", Oxford at the Clarendon Press, 1948, pp 119-151
[28] J D Jackson, *op cit.*, pp 307-309

It can be shown for dielectric materials that the spectral function $\phi(\omega)$ is identical with the susceptibility function $\tilde{\epsilon}(\omega)-1$, where $\tilde{\epsilon}(\omega)$ is the complex permittivity. Therefore the inverse of (2.3.2) may be written as [28]:

$$\tilde{\epsilon}(\omega) - 1 = \int_{-\infty}^{+\infty} P(t')e^{j\omega t'}dt' \ . \tag{2.3.3}$$

From the requirement $P(t') = 0$ for $t' < 0$, i.e., $P(t')$ is causal, it follows that $\tilde{\epsilon}(\omega)$ is an analytic function regular in the upper half plane, since only positive t' contribute to the integral. Therefore the value of $\tilde{\epsilon}(\omega)$ for $\Im\omega > 0$ is given as

$$\tilde{\epsilon}(\omega) - 1 = \frac{1}{2\pi j}\int_C \frac{\tilde{\epsilon}(\omega') - 1}{\omega' - \omega}d\omega' + \frac{1}{2\pi j}\int_{C'} \frac{\tilde{\epsilon}(\omega') - 1}{\omega' - \omega}d\omega' \ , \tag{2.3.4}$$

where C and C' are properly chosen contours of integration. Application of Cauchy's theorem to the latter integral leads to the following form

$$\tilde{\epsilon}(\omega) - 1 = \frac{1}{j\pi}⨍_{-\infty}^{+\infty} \frac{\tilde{\epsilon}(\omega') - 1}{\omega' - \omega}d\omega' \ , \tag{2.3.5}$$

where ⨍ denotes the Cauchy principal value integral. By writing $\tilde{\epsilon}(\omega) = \epsilon'(\omega)+1+j\epsilon''(\omega)$, one obtains a pair of Hilbert transforms:

$$\epsilon'(\omega) = 1 + \frac{1}{\pi}⨍_{-\infty}^{+\infty} \frac{\epsilon'(\omega')}{\omega' - \omega}d\omega' \tag{2.3.6}$$

and

$$\epsilon''(\omega) = -\frac{1}{\pi}⨍_{-\infty}^{+\infty} \frac{\epsilon'(\omega') - 1}{\omega' - \omega}d\omega' \ . \tag{2.3.7}$$

The real and imaginary parts of the complex permittivity $\tilde{\epsilon}(\omega)$ have different physical meanings. Since $\epsilon(t - t')$ is a causal function, it follows that $\epsilon(\omega) - 1$ is analytic for $\Im\omega > 0$.

Thus dispersion relation, a general property of a causal system, serves as a tool to investigate phenomenological models of the permittivity. The dispersion relation usually can be used for the following purposes:

a. The dispersion relation allows us to calculate the real or imaginary part of the permittivity when one of them is known.

b. To test the causality of mathematical models of the permittivity.

c. To verify whether the experimental results of a system are causal.

2.4 Boundary Conditions

For instantaneous time harmonic and linear electromagnetic fields, boundary conditions are deduced from the general form of Maxwell's equations (2.1.1-2.1.5), which may be cast into integral form by the use of Stokes' theorem and the divergence theorem. The usual procedure (shown elsewhere [29]) leads to two pairs of boundary conditions between two media where the boundary is time-independent:

$$\vec{\mathbf{n}} \times (\vec{\mathbf{E}}_+ - \vec{\mathbf{E}}_-) = 0 \ , \tag{2.4.1}$$

$$\vec{\mathbf{n}} \times (\vec{\mathbf{H}}_+ - \vec{\mathbf{H}}_-) = \vec{\mathbf{K}} \tag{2.4.2}$$

for field components tangential to the interface, and

$$\vec{\mathbf{n}} \cdot (\vec{\mathbf{D}}_+ - \vec{\mathbf{D}}_-) = \sigma \ , \tag{2.4.3}$$

$$\vec{\mathbf{n}} \cdot (\vec{\mathbf{B}}_+ - \vec{\mathbf{B}}_-) = 0 \tag{2.4.4}$$

for field components normal to the interface. The connection between the surface current $\vec{\mathbf{K}}$ and the surface charge σ is inferred from continuity equation (2.4.3) which leads to [30]

$$\nabla_t \cdot \vec{\mathbf{K}} + \vec{\mathbf{n}} \cdot (\vec{\mathbf{J}}_+ - \vec{\mathbf{J}}_-) = \frac{\partial \sigma}{\partial t} \tag{2.4.5}$$

Continuity of the tangential electric field components may be inferred from (2.4.1) and (2.4.2), respectively. In spite of many "proofs" of the continuity of the tangential magnetic

[29] J D Jackson, *op cit.*, pp 17-25
[30] C T Tai, *op cit*, pp 20-23

field component, e.g, (2.4.2), as shown in [31], they are all based on the invalid assumption of validity of Maxwell-Ampere's equation (2.1.2) across the separation surface between two different media. More precisely, they are based on the assumption of differentiability of field components at the discontinuity points. It is for this reason that we can question the validity of these boundary condition in the general case. The concept of discontinuity of the tangential field components is also used in [32] and [33] with the provision that the surface current $\vec{\mathbf{K}}$ is due to the "impressed" currents or fields usually identified with a source attached to the discontinuity. In [34] both magnetic and electric surface currents are considered as those corresponding to "current sheets", which are also assumed to be mathematical abstractions due to spatially limited forms of electromagnetic objects.

Summarizing this chapter, a known material is presented in a form convenient for applications that follows.

[31] S.A. Schelkunoff, "On Teaching the Undergraduate Electromagnetic Theory", IEEE Transactions on Education Vol 15, 1972, pp 15-25

[32] F N H Robinson, "Macroscopic Electromagnetism", Pergamon Press, 1973, pp 71-72

[33] Ch. Hafner, "Numerische Berechnung electromagnetischer Felder", Springer Verlag, New York, 1987, pp 63-66

[34] Ch H. Papas, "Theory of Electromagnetic Wave Propagation", McGraw-Hill, 1965, pp 8-9

III. Representation of Electromagnetic Fields at Dielectric Discontinuities

3.1 Past Work

As was pointed out in the preceeding chapter, the field singularities lead to the conventional boundary conditions (3.1.1-3.1.4) on the basis of possibly invalid assumptions of the continuity of both tangential components ($\vec{\mathbf{E}}_t$ and $\vec{\mathbf{H}}_t$) across the boundaries, i.e., when components of a field or their derivatives are discontinuous. These boundary conditions are considered in [35] as an essential postulate of electromagnetic theory, and the agreement between theory and experiment then provides the evidence in favour of their validity. For these reasons various techniques were developed to find alternative approaches. The best known one, called the Leontovitch boundary condition [36], [37], has the form:

$$\frac{\partial \psi}{\partial n} + jk\alpha\psi \Big|_S = 0 \ . \tag{3.1.1}$$

where ψ is the attenuation factor which satisfies the following equation:

$$|\vec{\mathbf{E}}| = \frac{e^{jk_o\rho}}{\rho}\psi(\vec{\mathbf{x}}) \tag{3.1.2}$$

and is evaluated at surface S, while α is a function of medium and surface properties. This condition is the time harmonic form of the more general impedance boundary condition:

$$\frac{\partial \psi}{\partial n} + k\frac{\partial \psi}{\partial t}\Big|_S = 0 \tag{3.1.3}$$

When (3.1.1) is applied to a curved surface such that ψ is equal to E_n, $\alpha = \mathcal{Y}$ and $\psi = H_n$, $\alpha = \mathcal{Z}$ for magnetic and electric normal field components, respectively, the two equations

[35] T.B.A. Senior, "Impedance Boundary Conditions for Imperfectly Conducting Surfaces", Appl. Sci. Research, Sec. B, Vol. 8, 1960, pp. 418-436.

[36] G. Boudouris, "Une Nouvelle Solution du Problème de Propagation au-dessus d'une Terre Plane", Supplemento Del Nuovo Cimento, V. X, No. 1, 1957, pp. 71-91.

[37] E.L. Feinberg, "Propagation of Radio Waves along an Inhomogeneous Surface", Supplemento Del Nuovo Cimento, V. XI, No. 1, 1959, pp. 147-170.

are obtained which may be conveniently cast into the following approximate single vector equation:

$$\vec{\mathbf{E}} - (\vec{\mathbf{E}} \cdot \vec{\mathbf{n}})\vec{\mathbf{n}} = \tilde{Z}_s \vec{\mathbf{n}} \times \vec{\mathbf{H}} \,. \tag{3.1.4}$$

This approximate condition also transforms a classical diffraction problem to a reflection one. In [38], it is shown that for a compact surface * confining a conducting body, the surface impedance permits uncoupling of the well known magnetic field (MFIE) and electric field (EFIE) integral equations [39]. However, this analysis is limited to conducting scatterers in free space and is based on a phenomenological approach. Therefore, it is not suitable for the rigorous dielectric spectroscopy.

Statistical analysis was initiated for a flat mean surface in [40] where the field perturbation technique was applied to the scattering from rough surfaces with surface roughness much smaller than wavelength.

When a rough conducting surface is considered [41], the boundary condition may be replaced by a form of the impedance boundary condition applied to a neighboring fictitious mean surface which is modelled as perfectly conducting. The effective surface impedance is a tensor function of the statistical properties of the irregularities and of the direction at which the field is incident.

Another approach is based on physical reasoning. The analysis of the dielectric response of a semi-infinite solid is established by the phase perturbation theory [42], [43]. The Random Phase Approximation technique (RPA) is a fundamental tool for self-consistent fields and currents investigation at an interface of different media. This

[38] I.J. Ciric and L. Shafai, "Comparison of Surface Impedance Models for quasistationary Electromagnetic Field Scatterers", IEEE Symposium on Antenna Technology and Applied Electromagnetics, Winnipeg, Canada, 1986.

* A compact surface is a closed and bounded surface.

[39] A.J. Poggio and E.K. Miller, "Integral Equation Solutions of Three-Dimensional Scattering Problems", Chapter 4 in "Computer Techniques for Electromagnetics", edited by R. Mittra, Pergamon Press, Oxford, 1973, pp.159-261.

[40] S.O. Rice, "Reflection of Electromagnetic Wave From Slightly Rough Surfaces", Commun. on Pure and Applied Math., No. 40, 1951, pp. 351-378.

[41] T.B.A. Senior, "Impedance Boundary Conditions for Statistically Rough Surfaces", Appl. Sci. Research, Sec. B, Vol. 8, 1960, pp. 437-462.

[42] R. Del Sole, "Response Functions at Surfaces", in "Electromagnetic Surface Excitations", Proceedings of an International Summer School at the Ettore Majorana Centre, Erice, Italy, edited by R.F. Wallis and G.I. Stegman, Springer-Verlag, 1985, pp. 162-179.

[43] D. Winebrenner and A. Ishimaru, "Investigation of a Surface Field Phase Perturbation Technique for Scattering from Rough Surfaces", Radio Science, V. 20, No. 2, 1985, pp. 161-170.

approach uses the microscopic viewpoint which is beyond the scope of this thesis.

The idea of surface impedance enabled obtaining solutions to various practical problems. This helped to form some qualitative picture of the process of wave propagation sometimes permitting to estimate a solution without rigorous detailed calculations. Nevertheless, the form of the boundary conditions (3.1.1.) may also lead to erroneous solutions as reported elsewhere [44].

3.2 New Formulation of Boundary Condition

Consider an arbitrary generalized open surface (Lyapunov's surface) S separating two dielectric media, as shown in Fig.3.1. Properties of this system are defined as follows:

$$\tilde{\epsilon}(\omega) = \begin{cases} \tilde{\epsilon}_1(\omega)H(\zeta - \zeta_o) \\ \\ \tilde{\epsilon}_2(\omega)[1 - H(\zeta - \zeta_o)] \end{cases} \tag{3.2.1}$$

and

$$\tilde{\sigma}(\omega) = \begin{cases} \tilde{\sigma}_1(\omega)H(\zeta - \zeta_o) \\ \\ \tilde{\sigma}_2(\omega)[1 - H(\zeta - \zeta_o)] \end{cases} \tag{3.2.2}$$

where $H(\zeta - \zeta_o)$ and ζ denote Heaviside's unit step function and the coordinate along normal direction pointed outside the surface, respectively. ζ_o coincides with the boundary surface.

Any arbitrary wave may be decomposed into **E** and **H** polarized components [45], [46]. When the wavefront of an incident wave does not coincide with boundaries of an electromagnetic object the concept of the transverse-longitudinal decomposition of the arbitrary fields may be applied [47], [48]. The classical technique of dealing with field singularities uses the integration of the field equations over infinitesimal surfaces

[44] N G Alexopoulos, "Accuracy of the Leontovich boundary condition for continuous and discontinuous surface impedances", Journal of Applied Physics, V 46, No 8, 1975, pp 3326-3332

[45] R E Collin, *op cit.*, pp 43-47

[46] J Fritz, "Plane Waves and Spherical Means", Interscience Publishers, New York, 1955, pp 7-13

[47] N Marcuvitz and J Schwinger, *op cit*, p 810

[48] K S H Lee and C E Baum, "Application of Modal Analysis to Braided-Shield Cables", IEEE Trans on Electromagnetic Compatibility, V 17, No 3, August 1975, pp 159-169

perpendicular to the direction currents. From the viewpoint of boundary value problems, the tangential fields at the boundary are sufficient for determination of fields everywhere and hence these boundary conditions are very important. The explicit determination of surface current in (3.1.2) has not been considered yet.

Consider the following decomposition of the field equations at two fictitious, auxiliary surfaces lying in the media of interest close to the discontinuity:

$$\begin{aligned}\frac{\partial}{\partial\zeta}\vec{\mathbf{H}}_t^+ - \frac{1}{j\omega\mu_0}\nabla_t J_{m\zeta}^+ - \vec{\mathbf{n}}\times\vec{\mathbf{J}}_e^+ =& j\omega\tilde{\epsilon}_1(\omega)H(\zeta-\zeta_o)\vec{\mathbf{n}}\times\vec{\mathbf{E}}^+ \\ &- \frac{1}{j\omega\mu_o}\nabla_t\nabla_t\cdot(\vec{\mathbf{n}}\times\vec{\mathbf{E}}^+)\end{aligned} \tag{3.2.3}$$

and

$$\begin{aligned}\frac{\partial}{\partial\zeta}\vec{\mathbf{H}}_t^- - \frac{1}{j\omega\mu_o}\nabla_t J_{m\zeta}^- - \vec{\mathbf{n}}\times\vec{\mathbf{J}}_e^- =& j\omega\tilde{\epsilon}_2(\omega)[1-H(\zeta-\zeta_o)]\vec{\mathbf{n}}\times\vec{\mathbf{E}}^- \\ &- \frac{1}{j\omega\mu_o}\nabla_t\nabla_t\cdot(\vec{\mathbf{n}}\times\vec{\mathbf{E}}^-)\end{aligned} \tag{3.2.4}$$

where the subscripts + and − represent field quantities at positive and negative parts of the discontinuity in question. Define the positive side of the discontinuity surface as that adjacent to its convex side as depicted in Fig. 3.1. The region $\zeta > \zeta_o$ will be called the external region, from which the electromagnetic perturbations (radiation) are applied.

The question may then be posed: "What is the limiting procedure for finding an explicit formula for the tangential field component $\vec{\mathbf{H}}_t$ as the field passes through the discontinuity ?". This is investigated in the next section.

3.3 Solution of the Posed Problem

The tangential component of magnetic field density vector $\vec{\mathbf{H}}_t(\zeta)$ on the positive side of the discontinuity may be expressed by its value at the boundary when the "forward" Taylor series expansion is used

$$\vec{\mathbf{H}}_t(\zeta) = \vec{\mathbf{H}}_t(\zeta_o^+) + \frac{\partial \vec{\mathbf{H}}_t(\zeta_o^+)}{\partial \zeta}(\zeta - \zeta_o^+) + \frac{1}{2}\frac{\partial^2 \vec{\mathbf{H}}_t(\zeta_o^+)}{\partial \zeta^2}(\zeta - \zeta_o^+)^2 + \cdots \tag{3.3.1}$$

which is valid for real values $\zeta > \zeta_o^+$. The Heaviside unit function $H(\zeta - \zeta_o)$ is omitted for brevity. Differentiating this equation with respect to ζ. Using the well known constitutive equation

$$\vec{\mathbf{J}}_e = \tilde{\sigma}(\omega)\vec{\mathbf{E}} \tag{3.3.2}$$

and substituting the results into (3.2.3) we obtain

$$\frac{\partial \vec{\mathbf{H}}_t(\zeta_o^+)}{\partial \zeta} + \frac{\partial^2 \vec{\mathbf{H}}_t(\zeta_o^+)}{\partial \zeta^2}(\zeta - \zeta_o^+) + \cdots + \frac{\partial^n \vec{\mathbf{H}}_t(\zeta_o^+)}{\partial \zeta^n}\frac{(\zeta - \zeta_o^+)^{n-1}}{(n-1)!} + \cdots =$$
$$\left[\tilde{\sigma}_1(\omega) + j\omega\tilde{\epsilon}_1(\omega)\right][\vec{\mathbf{n}} \times \vec{\mathbf{E}}(\zeta)] - \frac{1}{j\omega\mu_o}\nabla_t\nabla_t \cdot [\vec{\mathbf{n}} \times \vec{\mathbf{E}}(\zeta)] + \frac{1}{j\omega\mu_o}\nabla_t J_{m\zeta}^+ \tag{3.3.3}$$

Using the relation for homogeneous matter [49] to express the tangential component of the magnetic field, namely

$$\tilde{\mathcal{Z}}_{o1}\vec{\mathbf{H}}_t(\zeta) = \vec{\mathbf{n}} \times \vec{\mathbf{E}}(\zeta) \ , \tag{3.3.4}$$

where $\mathcal{Z}_{o1}$ denotes the intrinsic impedance of medium 1, and eliminating the electric field from (3.3.3), we obtain

$$\frac{\partial \vec{\mathbf{H}}_t(\zeta_o^+)}{\partial \zeta} + \frac{\partial^2 \vec{\mathbf{H}}_t(\zeta_o^+)}{\partial \zeta^2}(\zeta - \zeta_o^+) + \cdots + \frac{\partial^n \vec{\mathbf{H}}_t(\zeta_o^+)}{\partial \zeta^n}\frac{(\zeta - \zeta_o^+)^{n-1}}{(n-1)!} + \cdots$$
$$- jk_o\sqrt{\frac{\tilde{\epsilon}_1(\omega)}{\epsilon_o} - j\frac{\tilde{\sigma}_1(\omega)}{\omega\epsilon_o}}\sum_{n=0}^{N}\frac{\partial^n \vec{\mathbf{H}}_t(\zeta_o^+)}{\partial \zeta^n}\frac{(\zeta - \zeta_o^+)^n}{n!} +$$
$$- j\frac{1}{k_o\sqrt{\frac{\tilde{\epsilon}_1(\omega)}{\epsilon_o} - j\frac{\tilde{\sigma}_1(\omega)}{\omega\epsilon_o}}}\nabla_t\nabla_t \cdot \sum_{n=0}^{N}\frac{\partial^n \vec{\mathbf{H}}_t(\zeta_o^+)}{\partial \zeta^n}\frac{(\zeta - \zeta_o^+)^n}{n!} = \frac{1}{j\omega\mu_o}\nabla_t J_{m\zeta}^+ \tag{3.3.5}$$

[49] S.A Schelkunoff, "Electromagnetic Waves", Van Nostrand Company, New York, 1956, Sec. 4.5, pp. 74-75.

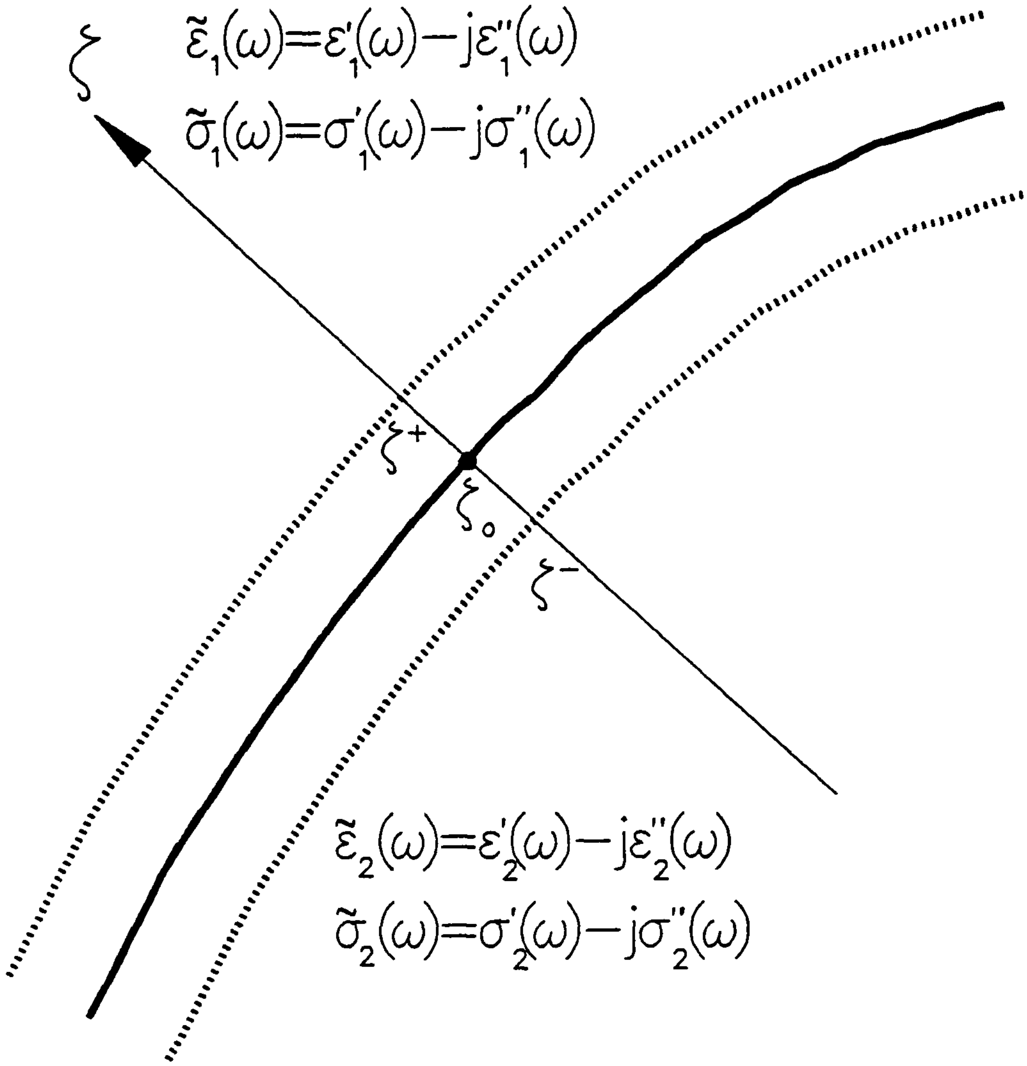

Fig. 3.1

Boundary separating two different media. ζ denotes the axis of the local coordinate system along the normal to the mean surface at an arbitrary point ζ_o.

Considering ζ and ζ_o^+ as points on real axis where ζ_o^+ is fixed and ζ is moving such that $\zeta \rightarrow \zeta_o^+$, we find the right hand limit of (3.3.5) as

$$\frac{\partial \vec{\mathbf{H}}_t(\zeta_o^+)}{\partial \zeta} - jk_o\sqrt{\frac{\tilde{\epsilon}_1(\omega)}{\epsilon_o} - j\frac{\tilde{\sigma}_1(\omega)}{\omega\epsilon_o}}\vec{\mathbf{H}}_t(\zeta_o^+)$$
$$-j\frac{1}{k_o\sqrt{\frac{\tilde{\epsilon}_1(\omega)}{\epsilon_o} - j\frac{\tilde{\sigma}_1(\omega)}{\omega\epsilon_o}}}\nabla_t\nabla_t \cdot \vec{\mathbf{H}}_t(\zeta_o^+) = \frac{1}{j\omega\mu_o}\nabla_t J_{m\zeta}(\zeta_o^+)\ . \qquad (3.3.6)$$

By repeating a similar procedure for the concave part of the discontinuity, i.e., $\zeta < \zeta_o'$, using "backward" Taylor expansion, the following equation is obtained:

$$\frac{\partial \vec{\mathbf{H}}_t(\zeta_o^-)}{\partial \zeta} - jk_o\sqrt{\frac{\tilde{\epsilon}_2(\omega)}{\epsilon_o} - j\frac{\tilde{\sigma}_2(\omega)}{\omega\epsilon_o}}\vec{\mathbf{H}}_t(\zeta_o^-)$$
$$-j\frac{1}{k_o\sqrt{\frac{\tilde{\epsilon}_2(\omega)}{\epsilon_o} - j\frac{\tilde{\sigma}_2(\omega)}{\omega\epsilon_o}}}\nabla_t\nabla_t \cdot \vec{\mathbf{H}}_t(\zeta_o^-) = \frac{1}{j\omega\mu_o}\nabla_t J_{m\zeta}(\zeta_o^-)\ . \qquad (3.3.7)$$

By imposing the Dirichlet boundary conditions $J_{m\zeta}(\zeta^+) = J_{m\zeta}(\zeta_o^-)$ i.e., continuity of normal component of magnetic current (corresponding to surface layer of magnetic flux), the most general formula for the tangential magnetic field at the discontinuity is in the form:

$$\left\{\frac{\partial \vec{\mathbf{H}}_t(\zeta_o^+)}{\partial \zeta} - \frac{\partial \vec{\mathbf{H}}_t(\zeta_o^-)}{\partial \zeta}\right\} + jk_o\left\{\sqrt{\frac{\tilde{\epsilon}_1(\omega)}{\epsilon_o} - j\frac{\tilde{\sigma}_1(\omega)}{\omega\epsilon_o}}\vec{\mathbf{H}}_t(\zeta_o^+) - \sqrt{\frac{\tilde{\epsilon}_2(\omega)}{\epsilon_o} - j\frac{\tilde{\sigma}_2(\omega)}{\omega\epsilon_o}}\vec{\mathbf{H}}_t(\zeta_o^+)\right\}$$
$$+\frac{j}{k_o}\left\{\frac{1}{\sqrt{\frac{\tilde{\epsilon}_1(\omega)}{\epsilon_o} - j\frac{\tilde{\sigma}_1(\omega)}{\omega\epsilon_o}}}\nabla_t\nabla_t \cdot \vec{\mathbf{H}}_t(\zeta_o^+) - \frac{1}{\sqrt{\frac{\tilde{\epsilon}_2(\omega)}{\epsilon_o} - j\frac{\tilde{\sigma}_2(\omega)}{\omega\epsilon_o}}}\nabla_t\nabla_t \cdot \vec{\mathbf{H}}_t(\zeta_o^-)\right\} = 0\ .$$

(3.3.8)

At high frequencies, k_o is large. Therefore, the last term in (3.3.8) becomes very small (if radius of curvature R is sufficiently large). It is trivial to show that this condition is equivalent the rigorous condition in the spherical coordinate system that $k_oR >> 1$. It also permitts elimination of the surface curvature from consideration.

Defining the surface current density as [50], [51]

$$\frac{1}{jk_o}\left\{\frac{\partial \vec{\mathbf{H}}_t(\zeta_o^+)}{\partial \zeta} - \frac{\partial \vec{\mathbf{H}}_t(\zeta_o^-)}{\partial \zeta}\right\} \stackrel{\text{def}}{=} -\vec{\mathbf{n}} \times \vec{\mathbf{K}}(\zeta_o) \; , \tag{3.3.9}$$

we can write the approximate boundary condition in the following form:

$$\vec{\mathbf{n}} \times \vec{\mathbf{K}}(\zeta_o) \approx \sqrt{\frac{\tilde{\epsilon}_2(\omega)}{\epsilon_o} - j\frac{\tilde{\sigma}_2(\omega)}{\omega\epsilon_o}}\vec{\mathbf{H}}_t(\zeta_o^-) \; - \; \sqrt{\frac{\tilde{\epsilon}_1(\omega)}{\epsilon_o} - j\frac{\tilde{\sigma}_1(\omega)}{\omega\epsilon_o}}\vec{\mathbf{H}}_t(\zeta_o^+) \; . \tag{3.3.10}$$

This is a new form of the quasi-stationary boundary condition for tangential magnetic field components, which can be compared with the classical boundary conditions.

Definition (3.3.9) corresponds to 2D model in which the surface current is represented as the sheet current [52].

When relation (2.1.29) holds, i.e., a medium is considered a dielectric, it is implied that (3.3.6) and (3.3.7) have the homogeneous right hand side. By dividing these equations by the complex coefficients of $\vec{\mathbf{H}}_t(\zeta_o^+)$ and $\vec{\mathbf{H}}_t(\zeta_o^-)$, respectively, the following pair of equations is obtained:

$$\frac{1}{jk_o\sqrt{\frac{\tilde{\epsilon}_1(\omega)}{\epsilon_o} - j\frac{\tilde{\sigma}_1(\omega)}{\omega\epsilon_o}}}\frac{\partial \vec{\mathbf{H}}_t(\zeta_o^+)}{\partial \zeta} - \vec{\mathbf{H}}_t(\zeta_o^+) - \frac{1}{k_o^2\left(\frac{\tilde{\epsilon}_1(\omega)}{\epsilon_o} - j\frac{\tilde{\sigma}_1(\omega)}{\omega\epsilon_o}\right)}\nabla_t\nabla_t \cdot \vec{\mathbf{H}}_t(\zeta_o^+) = 0 \tag{3.3.11}$$

and

$$\frac{1}{jk_o\sqrt{\frac{\tilde{\epsilon}_2(\omega)}{\epsilon_o} - j\frac{\tilde{\sigma}_2(\omega)}{\omega\epsilon_o}}}\frac{\partial \vec{\mathbf{H}}_t(\zeta_o^-)}{\partial \zeta} - \vec{\mathbf{H}}_t(\zeta_o^-) - \frac{1}{k_o^2\left(\frac{\tilde{\epsilon}_2(\omega)}{\epsilon_o} - j\frac{\tilde{\sigma}_2(\omega)}{\omega\epsilon_o}\right)}\nabla_t\nabla_t \cdot \vec{\mathbf{H}}_t(\zeta_o^-) = 0 \tag{3.3.12}$$

Subtracting (3.3.12) form (3.3.11) and repeating the same argumentation as that when (3.3.10) was derived, we obtain

$$\frac{1}{jk_o}\left\{\frac{1}{\sqrt{\frac{\tilde{\epsilon}_1(\omega)}{\epsilon_o} - j\frac{\tilde{\sigma}_1(\omega)}{\omega\epsilon_o}}}\frac{\partial \vec{\mathbf{H}}_t(\zeta_o^+)}{\partial \zeta} - \frac{1}{\sqrt{\frac{\tilde{\epsilon}_2(\omega)}{\epsilon_o} - j\frac{\tilde{\sigma}_2(\omega)}{\omega\epsilon_o}}}\frac{\partial \vec{\mathbf{H}}_t(\zeta_o^-)}{\partial \zeta}\right\} \stackrel{\text{def}}{=} -\vec{\mathbf{n}} \times \vec{\mathbf{K}}(\zeta_o)$$
$$= \vec{\mathbf{H}}_t(\zeta_o^+) - \vec{\mathbf{H}}_t(\zeta_o^-)$$

[50] V Fock, "Generalization of the Reflection Formulae to the Case of Reflection of an Arbitrary Wave from a Surface of Arbitrary Form", Chapter 8 in "Electromagnetic Diffraction and Propagation Problems", Pergamon Press, Oxford, 1965, pp 147-170

[51] J N Feld, "Difraktiya Skalarnoy Volny na Nyezamknutoy Poverkhnosti s Krayevym Uslovyem Dirichle" (in *Russian*), Doklady Akademii Nauk USSR, 1972, No 6 ,pp 1321-1323

[52] M Nakayama, "Theory of Electromagnetic Response of Solid Surface", Journal of the Physical Society of Japan, Vol 39 No 2, August, 1975, pp 265-273

(3.3.13)

Differentiating (3.3.4) with respect to ζ, expanding the electric and magnetic field density into "forward" Taylor series within the region $\zeta^+ < \zeta < \zeta_o^+$ and evaluating the right hand limit, the following relationship is obtained:

$$\frac{\partial \vec{\mathbf{H}}_t(\zeta_o^+)}{\partial \zeta} = -\vec{\mathbf{n}} \times \frac{1}{\tilde{\mathcal{Z}}_{o1}} \frac{\partial \vec{\mathbf{E}}_t(\zeta_o^+)}{\partial \zeta} . \tag{3.3.14}$$

The transverse-longitudinal decomposition of the Maxwell-Faraday equation gives the following approximate formula for this region:

$$-\frac{\partial \vec{\mathbf{E}}_t(\zeta_o^+)}{\partial \zeta} \approx \frac{j\omega\mu_o}{\tilde{\mathcal{Z}}_{o1}} \vec{\mathbf{E}}_t(\zeta_o^+) . \tag{3.3.15}$$

The meaning "approximate" is subject to the same constraints as those leading to (3.3.10). This equation allows us to replace the value of the derivative of the electric field by the value of this field multiplied by an operator. When (3.3.15) is substituted into (3.3.14) and the latter into (3.3.13), the left hand side is expressed in terms of the electric field $\vec{\mathbf{E}}_t(\zeta_o^+)$.

Repeating the same procedure for the region $\zeta_o^- < \zeta < \zeta^-$, (3.3.13) may be rewritten as

$$-\vec{\mathbf{n}} \times \sqrt{\frac{\epsilon_o}{\mu_o}} \left(\sqrt{\frac{\tilde{\epsilon}_2(\omega)}{\epsilon_o} - j\frac{\tilde{\sigma}_2(\omega)}{\omega\epsilon_o}} - \sqrt{\frac{\tilde{\epsilon}_1(\omega)}{\epsilon_o} - j\frac{\tilde{\sigma}_1(\omega)}{\omega\epsilon_o}} \right) \vec{\mathbf{E}}_t(\zeta_o) = -\vec{\mathbf{n}} \times \tilde{Y}_s \vec{\mathbf{E}}_t(\zeta_o)$$
$$= \vec{\mathbf{H}}_t(\zeta_o^+) - \vec{\mathbf{H}}_t(\zeta_o^-) , \tag{3.3.16}$$

where continuity of the tangential electric field density $\vec{\mathbf{E}}_t(\zeta_o^+) = \vec{\mathbf{E}}_t(\zeta_o^-) = \vec{\mathbf{E}}_t(\zeta_o)$ is assumed. Equation (3.3.16) implies that

$$\tilde{Y}_s(\omega) = \sqrt{\frac{\epsilon_o}{\mu_o}} \left(\sqrt{\frac{\tilde{\epsilon}_2(\omega)}{\epsilon_o} - j\frac{\tilde{\sigma}_2(\omega)}{\omega\epsilon_o}} - \sqrt{\frac{\tilde{\epsilon}_1(\omega)}{\epsilon_o} - j\frac{\tilde{\sigma}_1(\omega)}{\omega\epsilon_o}} \right) \tag{3.3.17}$$

is an explicit form of the surface impedance. The surface current is simply

$$\vec{\mathbf{K}}(\zeta_o) = \tilde{Y}_s \vec{\mathbf{E}}_t(\zeta_o) \tag{3.3.18}$$

The operator $\tilde{Y}_s(\omega)$ represents the surface admittance. It is derived for the first time for the interface between two dielectric media. Equation (3.3.16) implies that the tangential electric field component is continuous across the discontinuity surface. However, the tangential magnetic field intensity can, in general, be discontinuous. The surface current is an essential consequence of this discontinuity.

3.4 Surface Impedance of a Dielectric Discontinuity

Consider TM_{on}-waves at a coaxial waveguide aperture attached to a dielectric medium at $z = z_o$. A comparison of two equations (3.3.10) and (3.3.16) is of interest. The three nonvanishing electromagnetic field components are:

$$E_\rho = -\frac{1}{j\omega\tilde{\epsilon}(\omega)} \frac{\partial H_\phi}{\partial z} \tag{3.4.1}$$

$$E_z = \frac{1}{j\omega\tilde{\epsilon}(\omega)} \Big(\frac{H_\phi}{\rho} + \frac{\partial H_\phi}{\partial \rho} \Big) \tag{3.4.2}$$

$$H_\phi = -\frac{\partial \Psi}{\partial \rho} \tag{3.4.3}$$

where Ψ is a solution of a scalar Helmholtz equation corresponding to the vector Helmholtz equation for the magnetic field density. Finding the differentials from (3.4.1) for both sides of the discontinuity surface and substituting them into defining equation (3.3.9) and subsequently the result into (3.3.10) we obtain

$$\frac{\omega\epsilon_o}{k_o}\Big\{\tilde{\varepsilon}(\omega)E_\rho(z_o^+) + \tilde{\varepsilon}_c(\omega)E_\rho(z_o^-)\Big\} = \sqrt{\tilde{\varepsilon}(\omega)}H_\phi(z_o^+) \; - \; \sqrt{\tilde{\varepsilon}_c(\omega)}H_\phi(z_o^-) \tag{3.4.4}$$

where

$$\tilde{\varepsilon}(\omega) = \frac{\tilde{\epsilon}_2(\omega)}{\epsilon_o} - j\frac{\tilde{\sigma}_2(\omega)}{\omega\epsilon_o} \tag{3.4.5}$$

and

$$\tilde{\varepsilon}_c(\omega) = \frac{\tilde{\epsilon}_1(\omega)}{\epsilon_o} - j\frac{\tilde{\sigma}_1(\omega)}{\omega\epsilon_o} \tag{3.4.6}$$

are the relative permittivities of the external medium and the line interior, respectively. The complex relative permittivity $\tilde{\varepsilon}$ incorporates both dielectric and conduction losses. For a coaxial line, the dielectric inside it has negligibly small losses, thus it is assumed to be a real function, i.e. $\tilde{\varepsilon}_c(\omega) \approx \varepsilon_c(\omega)$.

Dirichlet boundary condition can be imposed for tangential electric field components as $E_\phi(z_o^-) = E_\phi(z_o^+)$. Imposing a similar condition on tangential magnetic fields, i.e. $H_\rho(z_o^-) = H_\rho(z_o^+)$, and noting that TM-impedance is defined as $\tilde{Z}_{TM} = E_\rho/H_\phi$, it is easily found that

$$\tilde{Z}_{TM} = z_o\frac{\sqrt{\tilde{\varepsilon}(\omega)} - \sqrt{\varepsilon_c(\omega)}}{\tilde{\varepsilon}(\omega) + \varepsilon_c(\omega)} \tag{3.4.7}$$

where z_o is the characteristic impedance of free space. This impedance vanishes as $\epsilon_c(\omega) \rightarrow \tilde{\epsilon}_r(\omega)|_{\omega=const}$. Thus, (3.4.7) represents the surface contribution and is here called the surface impedance for TM_{on} waves.

When (3.3.16) is applied, then the assumption of the continuity of the magnetic field density is invalid. Therefore, it is possible to determine the magnetic field at right hand side of the discontinuity in terms of both fields on its left hand side, namely

$$\vec{\mathbf{H}}_\phi(z_o^+) = (-\hat{\mathbf{e}}_z \times \hat{\mathbf{e}}_\rho)\tilde{Y}_s\vec{\mathbf{E}}_\rho(z_o) + \vec{\mathbf{H}}_\phi(z_o^-)\ . \tag{3.4.8}$$

When relations (3.4.1-3) are used, this equation is transformed into

$$\frac{\partial\Psi^+}{\partial\rho}\hat{\mathbf{e}}_\phi = \frac{\partial}{\partial\rho}\left\{\frac{1}{jk_o\sqrt{\frac{\tilde{\epsilon}_1(\omega)}{\epsilon_o} - j\frac{\tilde{\sigma}_1(\omega)}{\omega\epsilon_o}}}\left[\tilde{\vartheta}(\omega) - 1\right]\frac{\partial\Psi^-}{\partial z} - \Psi^-\right\}\hat{\mathbf{e}}_\phi \tag{3.4.9}$$

where

$$\tilde{\vartheta}(\omega) = \sqrt{\frac{\frac{\tilde{\epsilon}_2(\omega)}{\epsilon_o} - j\frac{\tilde{\sigma}_2(\omega)}{\omega\epsilon_o}}{\frac{\tilde{\epsilon}_1(\omega)}{\epsilon_o} - j\frac{\tilde{\sigma}_1(\omega)}{\omega\epsilon_o}}} \tag{3.4.10}$$

is the discontinuity operator. This operator represents correction to the Leontovitch boundary condition for the flat surface.

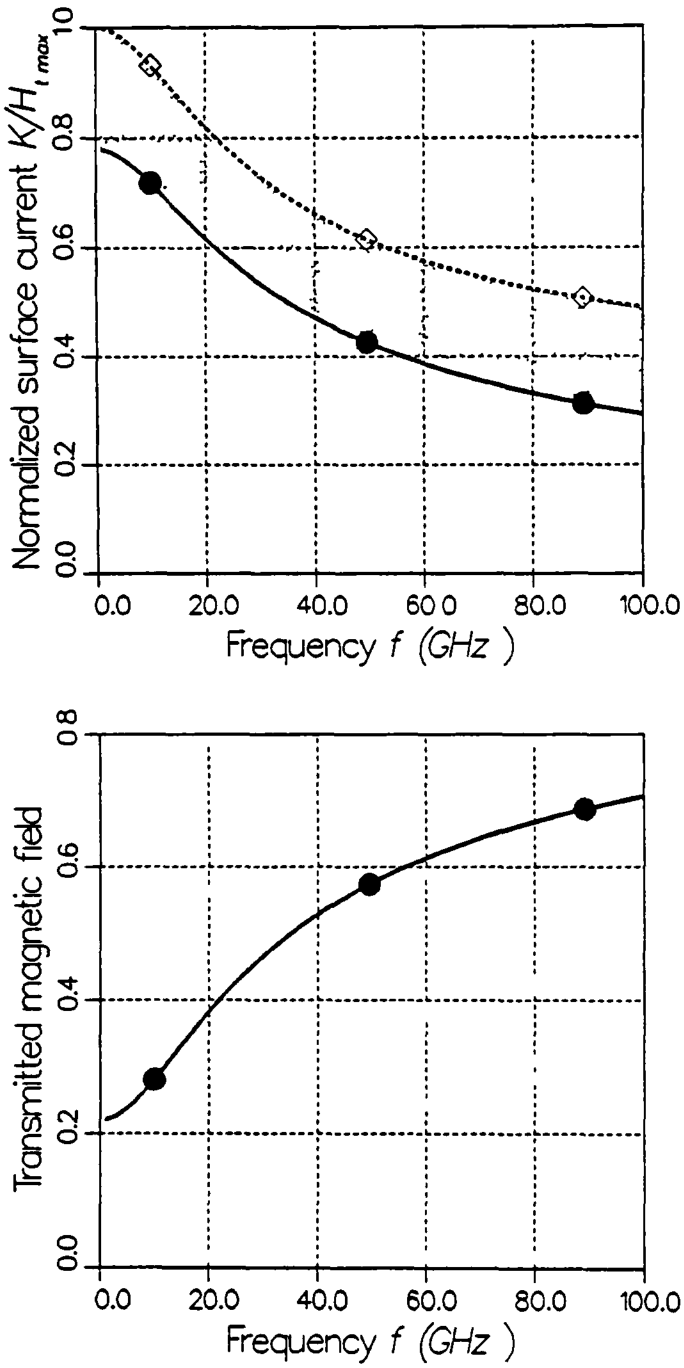

Fig. 3.2

Upper graph: Comparison of magnitudes of magnetic field density given by (3.4.7) ◇ and surface current density given by (3.4.8) • for the air-distilled water interface at 25^oC. The shaded area difference between results obtained by (3.4.7) and (3.4.8)
Lower graph: Magnitude of the transmitted magnetic field density according to (3.4.8). All magnitudes are normalized to the maximum value of the magnetic field density magnitude at the side of the wave incidence (air).

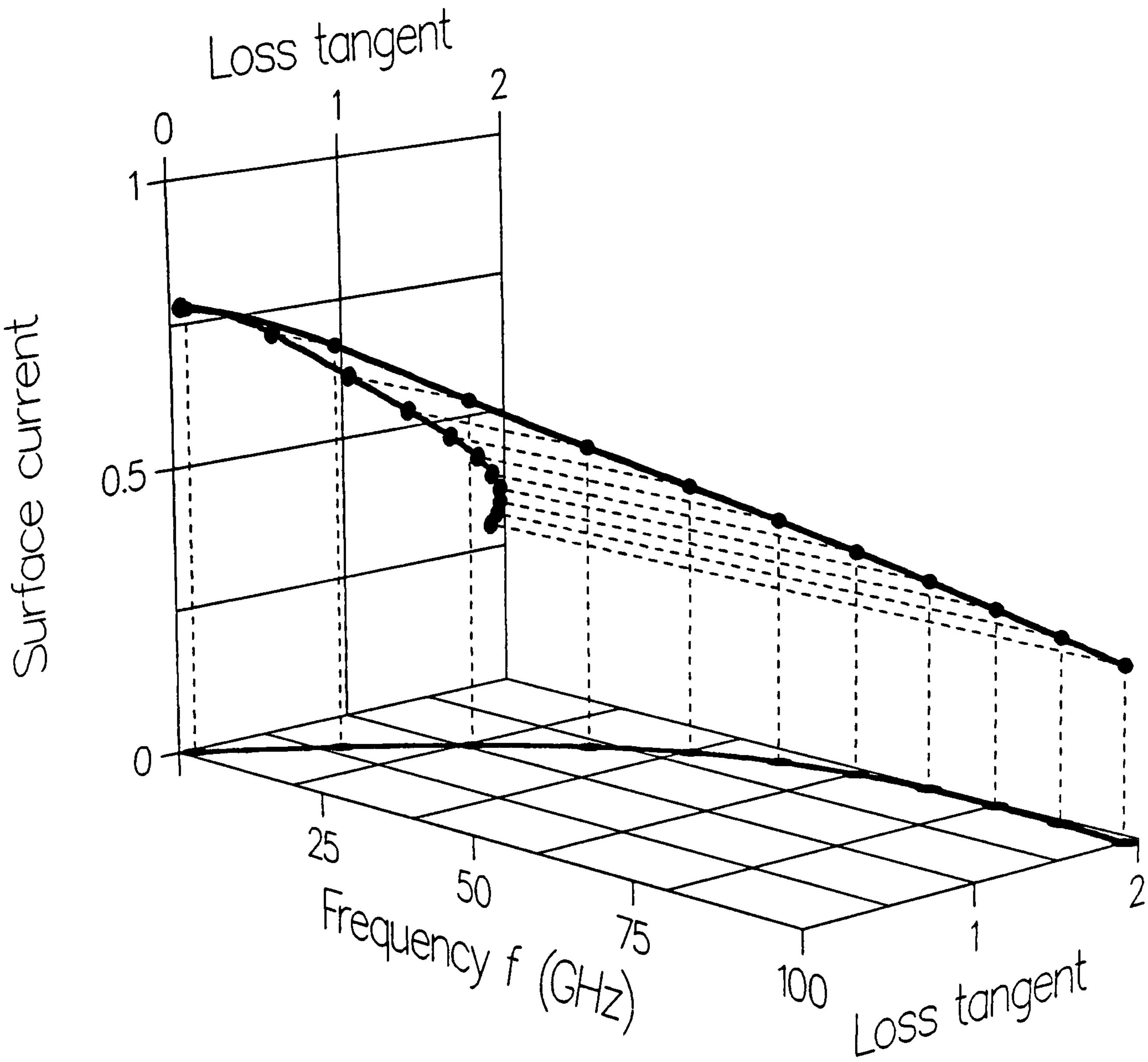

Fig. 3.3

Three-dimensional presentation of the surface current at the magnitude of the air-distilled water interface versus frequency and loss tangent at $25^{o}C$ according to (3.3.18). The magnitude is normalized to the maximum value of the magnetic field density magnitude at the side of the wave incidence (air).

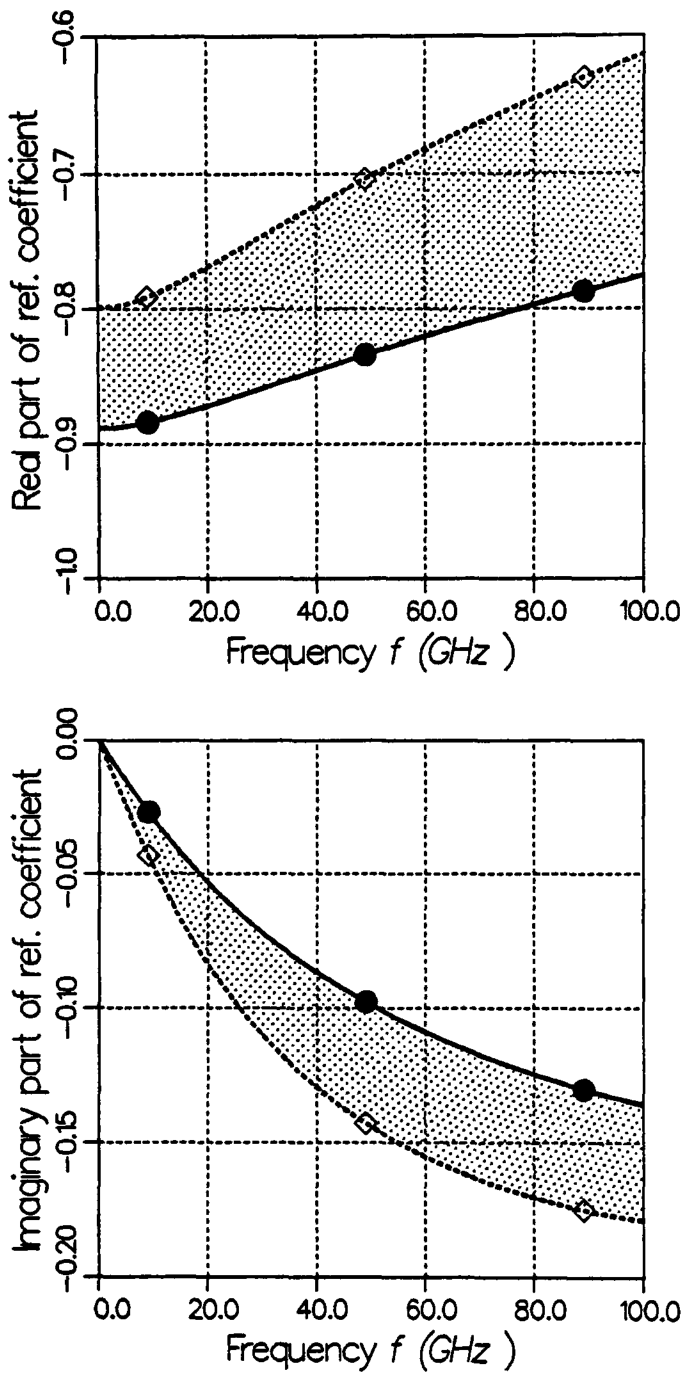

Fig. 3.4

Comparison of reflection coefficients evaluated by the equation (3.4.12), dashed line ◇, and by the equation (3.4.13), solid line •, at the air-distilled water discontinuity interface for the normally incident plane wave. The shaded areas correspond to discrepancies in real and imaginary parts depicted above and below, respectively.

When medium 1 and medium 2 are air and a perfect conductor, respectively, then both (3.3.10) and (3.3.16) reduce to the well known form, namely

$$\vec{\mathbf{n}} \times \vec{\mathbf{K}}(\zeta_o) \approx -\vec{\mathbf{H}}(\zeta_o^+) \,. \tag{3.4.11}$$

However, the simplest presentation of the influence of the boundary condition (3.4.8) on the reflection coefficient is when one considers reflection of the normally incident plane wave at the air-distilled water discontinuity interface. The standard procedure [53] gives

$$\tilde{\Gamma}(\omega) = \frac{1 - \tilde{\vartheta}(\omega)}{1 + \tilde{\vartheta}(\omega)} \,. \tag{3.4.12}$$

The same procedure with continuity condition for the transverse magnetic field density replaced by (3.4.8) gives

$$\tilde{\Gamma}(\omega) = \frac{1 - \tilde{\vartheta}(\omega)}{\tilde{\vartheta}(\omega)} \,. \tag{3.4.13}$$

$\tilde{\vartheta}$ is defined by (3.4.10) and for this case

$$\tilde{\vartheta}(\omega) = \sqrt{\frac{\tilde{\epsilon}_2(\omega)}{\epsilon_o} - j\frac{\tilde{\sigma}_2(\omega)}{\omega\epsilon_o}} \,. \tag{3.4.14}$$

A computer simulation of the new equations derived in this chapter was carried out. The results are depicted in Figs. 3.2, 3.3 and 3.4. The experimental verification of (3.4.13) is shown in Appendix F. A detailed discussion follows in the next section.

3.5 Discussion

Two formulas were derived for the surface admittance, namely (3.3.10) and (3.3.16). The consequences of these equations to the electromagnetic boundary value problems in regions consisting of at least one dielectric are:

1 The magnetic field component transverse to the discontinuity surface is discontinuous (3.4.8). The surface impedance given by (3.4.7) is not correct value, since it is derived

[53] R.E. Collin, "Field Theory of Guided Waves", McGraw-Hill Book Company, New York, 1960, pp. 76-77.

from the assumption of the continuity both electric and magnetic field components. The differences between both equations are shown in Fig. 3.2 for an air-distlled water interface.

2 The surface current shown in Figs. 3.2 and 3.3 is a measure of discontinuity of the tangential magnetic field density. The value of the transmitted magnetic field varies for distilled water varies from about 20 % at 1 GHz to about 70 % at 100 GHz of the incident field density.

3 The higher the discontinuity operator $\tilde{\vartheta}(\omega)$ the higher is the surface current $\vec{\mathbf{K}}(\tilde{\vartheta})$. The value of the loss tangent of distilled water does not influence this surface phenomenon as shown in Fig. 3.3.

4 The reflection coefficient is modified by existence of the surface current as shown in Fig. 3.4. The real part of the modified reflection coefficient (3.4.13) increases from about 10 % at 1 GHz to about 18 % at 100 GHz with respect to the value given by (3.4.12). The imaginary part of the modified reflection coefficient is lower than that given by (3.4.13), and varies from 0 % at low frequencies to about 5 % at 100 GHz.

In summary, the following may be stated:

- Equation (3.3.16) is important for the dielectric reflection spectroscopy;
- The reflection coefficient is modified by the existence of the surface current $\vec{\mathbf{K}}$ on the discontinuity as shown in Fig. 3.4.
- The important engineering implication is that the inverse problem of dielectric reflection spectroscopy must be reformulated in order to obtain lower uncertainties than in the conventional approach where the surface current is neglected. This implies that boundary value problems must take into account the form of continuity condition given by (3.3.16).
- In problems involving dielectric materials, the surface current may be transformed to the tangential magnetic field components multiplied by operators being a function of material properties, thus linking internal and external fields for solving the surface

integral equation corresponding to aperture antennas, e.g., open-ended coaxial line or microstrip antenna.

Therefore, this approach offers an alternative formula for this boundary condition and paves the way to a variety of applications.

The procedure, computer simulation presented in this chapter and experiment in Appendix F provide evidence for the hypothesis that the surface current causes the screening effect of the dielectric body from the incident field.

IV. Analysis of the Open-ended Coaxial Line Sensors

4.1. Introduction

The open-ended coaxial sensor consists of a truncated coaxial line in contact with or immersed in a dielectric medium. This structure can be seen as an aperture radiating into semi-infinite dielectric medium. However, at lower frequencies the radiation losses are very small and a static model of the line termination is valid. Thus, it permits these lines to be used for measurements, both *in vivo* and *in vitro*, over a very broad range of frequencies (10 kHz 10 GHz). The development of the high accuracy microwave automated network analyzer (ANA) has made a sensor of this type a very attractive research tool which is now commonly used in dielectric spectroscopy [54], [55] and [56]. Nevertheless, the use of the open-ended coaxial sensor has some disadvantages: a complicated mathematical procedure is needed to relate the measured reflection coefficient to the properties of a medium with an exact model, and an increase in the uncertainty occurs when a simple model is assumed for the boundary between the aperture and the dielectric medium.

The theoretical analysis of this class of structures was undertaken as early as 1951 [57] with a variational approach leading to an integral equation approximation of an unknown field distribution on the aperture. However, the numerical calculation was only carried out for the principal mode of the coaxial line. This solution was also only valid if the aperture was in an infinite ground plane and the ambient medium, $\tilde{\epsilon}_m = \epsilon_0$ was free

[54] M A Stuchly and S S Stuchly, "Coaxial Line Reflection Methods for Measuring Dielectric Properties of Biological Substances at Radio and Microwave Frequencies - A Review", IEEE Trans on Instr and Measur ,Vol IM-29, No 3, 1980, pp 176-183

[55] Athey,T W , Stuchly,M A and Stuchly,S S "Measurement of Radiofrequency Permittivity of Biological Tissues With an Open-Ended Coaxial Line Part I", IEEE Trans M.T T vol 30, 1982, pp 82-86

[56] T W Athey, M A. Stuchly, and S S Stuchly, "Measurement of Radiofrequency Permittivity of Biological Tissue with an Open Ended Coaxial Line Part II Experimental Results ", IEEE Trans M T T , vol 30, pp 87-92, 1982

[57] H Levine and C H Papas, "Theory of Circular Diffraction Antenna", Journal of Applied Physics, V 22, No 1, 1951 pp 29-43

space: The theory was modified to take into account higher order modes in the aperture in [58] with the assumption a certain idealized behavior of the electric field within the aperture. The analysis considered only radiation into the free space. Hence, it is not directly applicable to the material media. The modal matching technique was used in [59] with the limitation of an incident field to the principal mode and a simplified boundary condition for the azimuthal magnetic field component (both tangential electric field $\vec{\mathbf{E}}_t$ and $\vec{\mathbf{H}}_t$ continuous across boundary), equivalent to the assumption of lack of surface current at the interface. The problem was solved numerically in [60] with limitation to quasi-electrostatic conditions by applying the finite element method. Recently, the problem was attacked in [61] following the method of [58] where an approximate evaluation of integrals was carried out. These integrals resulted from a three term Taylor series expansion of the free space kernel of the final integral formula for the load admittance. Except for [60], all the analytical approaches assume an aperture in an infinitely large flange (screen) and consider rotationally symmetric fields, i.e., all field components are independent on the azimuthal angle ϕ and subsequently their number is limited to three.

If the ground plane to is infinite, then the limiting case is represented by the finite cross-section of the outer conductor. The restriction on the rotational symmetry of the fields is severe, because it corresponds to assumption that only TM_{on} modes exist in the vicinity of the junction between the line and the medium [62]. This simplifies the calculations but neglects the physically possible TM_{mn} and TE_{mn} modes in the transitional region. A discussion of these modes is given in Appendix C. When these

[58] J Galejs, "Antennas in Inhomogeneous Media", Pergamon Press, Oxford, 1969, pp 39-44

[59] J R Mosig, J E Besson, M Gex-Fabry and F Gardiol, "Reflection of an Open-Ended Coaxial Line and Application to Nondestructive Measurement of Materials", IEEE Trans Microw Theory Techn , V IM-30, 1981, pp 46-51

[60] G Gajda and S S Stuchly, "Numerical Analysis of Open-ended Coaxial Lines", IEEE Trans M T T , V IM-32, 1983, pp 380-384

[61] D K Misra, "A Quasi-static Analysis of Open-Ended Coaxial Lines", IEEE Trans Microwave Theory and Tech , V IM-35, No 10, 1987, pp 925-928

[62] E W Risley, "Discontinuity Capacitance of a Coaxial Line a Circular Waveguide", IEEE Trans M T T , V IM-17, 1969, pp 86-92

types of modes are included, the analysis must be carried out for the 3-dimensional case for all six components of the field, equivalent to hybrid modes.

Open-ended coaxial line sensors have a significant advantage over their waveguide counterparts in their size and frequency coverage. However, they have also a drawback, namely it is difficult to obtain a good contact between the center conductor and the dielectric material. This also appears in waveguide sensor, where windows are used to separate the sample from the waveguide interior. A critical study of coaxial line sensors is given in [63]. The possibility of application of open-ended coxial line sensors above 10 GHz and in the millimeter wave region necessitates an analysis which includes the complete set of modes.

The goals of the study of the open-ended sensor are as follows:

- to find a complete equivalent circuit for the input admittance;
- to determine the relation between the reflection coefficient and dielectric properties of the external medium;
- to investigate relation between reflection and diffraction at the aperture of the sensor;
- to separate conduction and radiation losses at higher frequencies.

4.2. Formulation

Consider the structure depicted in Fig.4.1. The coaxial line extends in z direction $-\infty < z < 0$ and has inner and outer radii a and b, respectively. A circular flange of radius d is mounted at $z = 0$. If $d \to \infty$ then the flange becomes an infinite ground plane. This finite flange is a realistic element which has not yet been considered for this type of problem. The line is filled with a lossless medium characterized by permittivity ϵ_c. A medium of unknown permittivity $\tilde{\epsilon}_m(\omega)$ completely fills the space $0 < z < \infty$.

[63] J P Grant, R N Clarke, G T Symm and N M Spyrou, "A Critical Study of the Open-Ended Coaxial Line Sensor Technique for RF and Microwave Complex Permittivity Determination", unpublished, Department of Physics, University of Surrey, Guildford, England, GU2 5XH

4.2.1 Green's Function for Semi-infinite Coaxial Line

The construction of Green's function of the second-order differential equation, e.g., the wave equation, can be carried out by a well-established mathematical formalism. The first step involves solution of the homogeneous Helmholtz equation. When the domain is finite, the spectrum of $\nabla^2 + k^2$ is completely discrete, i.e., consists of eigenfunctions of finite multiplicity. However, when the coaxial line is infinitely long, $z \in (-\infty, \infty)$, the scalar wave function Ψ, according to representation theorem for Helmholtz equation*, [64] satisfies the homogeneous Helmholtz equation $(\nabla^2 + k^2)\Psi(\rho) = 0$ in the waveguide region, and homogeneous boundary condition $\Psi\,|_S = 0$ or $\partial\Psi/\partial\rho\,|_S = 0$ at the cylindrical surfaces S at $\rho = a$ and $\rho = b$.

If the cylindrical system of coordinates is used, the scalar wave function Ψ satisfies the following equation

$$\frac{1}{\rho}\frac{\partial}{\partial\rho}\left(\rho\frac{\partial\Psi}{\partial\rho}\right) + \frac{1}{\rho^2}\frac{\partial^2\Psi}{\partial\phi^2} + \frac{\partial^2\Psi}{\partial z^2} + k^2\Psi = 0 \ . \tag{4.2.1}$$

The separation of variables leads to Bessel's equation with the solution:

$$\Psi(\vec{\mathbf{x}}) = \sum_{m=0}^{\infty}\sum_{n=1}^{\infty}\Psi_{m\,n}(\rho,\,\phi)e^{j\gamma_{m\,n}z} \ , \tag{4.2.2}$$

where $\Psi_{m\,n}$ is scalar mode function which satisfies the fourth boundary value problem with respect to azimuthal dependence, i.e., the periodicity condition

$$\Psi_{m\,n}(\rho,\,\phi) = \Psi_{m\,n}(\rho, \phi + 2\pi m) \ . \tag{4.2.3}$$

This function has real and positive eigenvalues $\kappa_{m\,n}$.

When the boundary condition at $\rho = a$ is applied, the transverse eigenfunction of the first boundary value problem is found:

$$\Psi_{Em\,n}(\rho,\,\phi) = A_E\left[J_m(\kappa_{m\,n}\rho) - \frac{J_m(\kappa_{m\,n}a)}{Y_m(\kappa_{m\,n}a)}Y_m(\kappa_{m\,n}\rho)\right]\begin{pmatrix}\cos\\ \sin\end{pmatrix} m\phi \ , \tag{4.2.4}$$

* For any solenoidal vector field, a solution of its vector Helmholtz equation is a function of the solution of the corresponding scalar Helmholtz equation (Representation Theorem for Helmholtz Equation)

[64] P M Morse and H Feshbach, "Methods of Theoretical Physics", McGraw-Hill, New York, Part II, 1953, pp 1764-1767

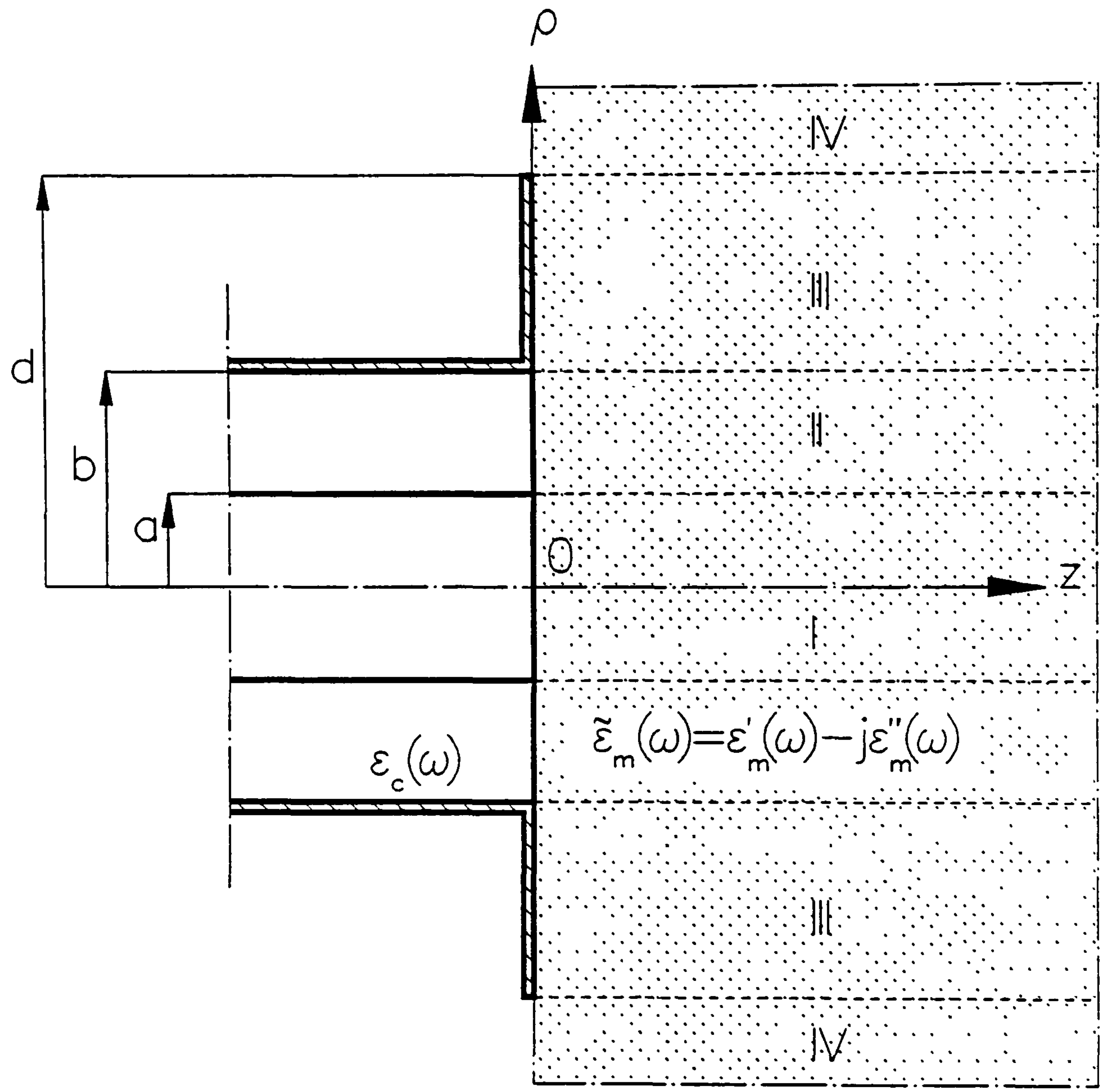

Fig. 4.1

Geometry and dimensions of the open-ended coaxial probe.

while the transverse eigenfunction of the second boundary value problem is:

$$\Psi_{Hmn}(\rho,\phi) = A_H\left[J_m(\kappa_{mn}\rho) - \frac{J_m'(\kappa_{mn}a)}{Y_m'(\kappa_{mn}a)}Y_m(\kappa_{mn}\rho)\right]\binom{\cos}{\sin} m\phi\ . \tag{4.2.5}$$

A_E and A_H are the constants which may be eliminated by the standard normalization procedure [65]. Introducing scaled (normalized) eigenvalues χ_{mn} which, according to usual substitution are given as $\chi_{mn} = \kappa_{mn}b$, $\ell = a/b$ such that $0 \le \ell \le 1$, normalization constants are found to be

$$A_E = \sqrt{\frac{\pi}{2}}\frac{\chi_{mn}J_m(\chi_{mn})}{b\sqrt{1+\delta_{m0}}\sqrt{J_m^2(\chi_{mn}\ell) - J_m^2(\chi_{mn})}} \tag{4.2.6}$$

and

$$A_H = \sqrt{\frac{\pi}{2}}\frac{\chi_{mn}}{b\sqrt{1+\delta_{m0}}}\frac{1}{\sqrt{\left(1-\frac{m^2}{\chi_{mn}^2}\right)\left(\frac{J_m'(\chi_{mn}\ell)}{J_m'(\chi_{mn})}\right)^2 - \left(1-\frac{m^2}{\chi_{mn}^2\ell^2}\right)}}\ . \tag{4.2.7}$$

By applying boundary condition at $\rho = b$, the following transcendental equations are implied:

$$J_m(\chi_{mn})Y_m(\chi_{mn}\ell) - J_m(\chi_{mn}\ell)Y_m(\chi_{mn}) = 0 \tag{4.2.8}$$

for the first boundary value problem ($TM-$waves) and

$$J_m'(\chi_{mn})Y_m'(\chi_{mn}\ell) - J_m'(\chi_{mn}\ell)Y_m'(\chi_{mn}) = 0 \tag{4.2.9}$$

for the second boundary value problem ($TE-$waves). Prime $'$ denotes derivative with respect to the argument and δ_{m0} is defined as:

$$\delta_{m0} = \begin{cases} 1, & \text{if } m = 0; \\ 0, & \text{otherwise.} \end{cases}$$

The eigenvalues are tabulated in various sources, e.g., [66]. Their approximate values may be derived from McMahon's formulas [66] which are adopted here to the notation as

$$\chi_{E,mn} = \frac{n\pi}{1-\ell} + \frac{1}{8\pi}\frac{4m^2-1}{n}\frac{1-\ell}{\ell} + O\left(\left[\frac{1}{n\pi}\frac{1-\ell}{\ell^2}\right]^3\right) \tag{4.2.10}$$

[65] N. Marcuvitz, "Waveguide Handbook", Boston Technical Publishers, Lexington, 1964, pp 72-80

[66] M Abramovitz and I Stegun, "Handbook of Mathematical Functions", Dover Publications, 1972, pp 371-373

and

$$\chi_{H,mn} = \frac{n\pi}{1-\ell} + \frac{1}{8\pi}\frac{4m^2+3}{n}\frac{1-\ell}{\ell} + O\left(\left[\frac{1}{n\pi}\frac{1-\ell}{\ell^2}\right]^3\right) , \tag{4.2.11}$$

where $O(\ )$ denotes "order of".

However, no complete tabulation of roots of (4.2.8-4.2.9) is presently available [67].

The method of separation of variables implies the following form of Green's function

$$G^{(-)}(\rho , z ; \rho' , z') = \sum_{m=0}^{\infty}\sum_{n=1}^{\infty} \Psi_{mn}(\rho, \phi)\Psi^*_{mn}(\rho', \phi')g_{m\,n}(z, z') . \tag{4.2.12}$$

By substituting (4.2.12) to (4.2.1) for Ψ and adding the δ-function to its right hand side, one obtains:

$$\sum_{m=0}^{\infty}\sum_{n=1}^{\infty}\left(-\kappa^2_{mn} + k^2 + \frac{\partial^2}{\partial z^2}\right)\Psi_{mn}(\rho, \phi)\Psi^*_{mn}(\rho', \phi')g_{mn}(z, z') \ = -\delta(z-z')\frac{\delta(\rho-\rho')}{\rho}\delta(\phi-\phi') . \tag{4.2.13}$$

Upon multiplying both sides of this equation by $\Psi_{mn}(\rho, \phi)\rho\cos\phi$ and integrating from a to b with respect to ρ and from 0 to 2π with respect to ϕ, and using the orthogonality relations we obtain the following equation for a single mode:

$$\left(-\kappa^2_{mn} + k^2 + \frac{\partial^2}{\partial z^2}\right)g_{m\,n}(z, z') \ = -\delta(z-z') \tag{4.2.14}$$

where $-\infty < z \le 0$.

The problem is thus reduced to that of finding the solution of (4.2.14) in the semi-infinite domain. In a semi-infinite domain the problem of finding Green's function is not an easy task. It is well known that for the infinite domain and bounded only internally by a finite boundary, the spectrum of Helmholtz operator $(\nabla^2 + k^2)$ is continuous (Rellich theorem [68]). The general solution of (4.2.13) is

$$G^{(-)}(\rho , \phi, z ; \rho' \phi', z') = \sum_{m=0}^{\infty}\sum_{n=1}^{\infty}\frac{\Psi_{mn}(\rho, \phi)\Psi_{mn}(\rho', \phi')}{k^2 - \kappa^2_{mn}}$$

[67] Chen-To Tai, "Dyadic Green's Function for a Coaxial Line", IEEE Trans on Antennas & Propag , V AP-31, No 2, 1983, pp 355-358

[68] I. N Vekua, "New Methods for Solving Elliptic Equations", John Wiley & Sons, New York, 1968, pp 315-339

$$\times \left[e^{j\sqrt{k^2-\kappa_{m\,n}^2}|z-z'|} + \Gamma_{m\,n}(0,z')e^{-j\sqrt{k^2-\kappa_{m\,n}^2}|z-z'|} \right] , \tag{4.2.15}$$

where $z \leq 0$ and $z' \leq 0$.

Green's function is composed of an "incident" wave appropriate to an infinite region with wave numbers $\sqrt{k^2 - \kappa_{m\,n}^2}$ and a "reflected" wave whose amplitude dependence $\Gamma_{m\,n}(0,z')$ is determined by details of the configuration in the half space $z > 0$ [69].

4.2.2 Inadequacy of Green's Function for the Dielectric Region

When $d \to \infty$, the flange becomes an infinite screen and the Green's function of the region $z > 0$ is related to the free space Green's function by [57]

$$G^{(+)}(\rho\,,\,z\,;\,\rho'\,,\,z') = \frac{1}{4\pi}\int_0^{2\pi} G_o(\rho\,,\,z\,;\,\rho'\,,\,z')\cos(\phi-\phi')d\phi \tag{4.2.16}$$

where

$$G_o(\rho\,,\,z\,;\,\rho'\,,\,z') = \frac{e^{jk\sqrt{\rho^2+\rho'^2-2\rho\rho'\cos\phi+(z-z')^2}}}{\sqrt{\rho^2+\rho'^2-2\rho\rho'\cos\phi+(z-z')^2}} \tag{4.2.17}$$

is the free space Green's function.

This Green's function was used in all previous approaches to find the field in the region $z > 0$. The finite size of the screen has not yet been taken into account. The effect of a circular ground-plane on antenna radiation was considered in [70], where a solution of the wave equation in the oblate spherical coordinates for the quarter-wave-length monopole antenna was obtained. This method was restricted to the groundplane of a small radius with respect to the wavelength. The computation becomes tedious for planes whose radii are large compared to the length of the antenna. In [71], the analysis of a

[69] L.B. Felsen and N. Marcuvitz, "Radiation and Scattering of Waves", Prentice-Hall, New Jersey, 1973, pp. 278-361.

[70] A. Leitner and R.D. Spence, "Effect of a Circular Groundplane on Antenna Radiation", Journal of Applied Physics, V. 21, No. 10, 1950, pp. 1001-1006.

[71] J.E. Storer, "The Impedance of an Antenna over a Large Circular Screen", Journal of Applied Physics, V. 22, No 8, 1951, pp. 1058-1066.

similar problem is based on the Green's function given by (4.2.16-17) so it follows the method developed in [57]. Both approaches are also relevant to free space. Next section deals with a study to find the solution appropriate to the problem posed.

4.3. A Method of Field Evaluation for Semi-infinite Dielectric Space with Mixed Boundary Conditions at z=0.

4.3.1 Method of Partial Regions

The central problem of this section consists of constructing a Green's function to calculate the field at any point of the region $z > 0$ in terms of the field distribution at the coaxial line aperture and current on the flange. The greatest difficulty lies in the mixed boundary condition applied to the Helmholtz equation. Therefore, the region is partitioned into subregions for which the boundary condition at $z = 0$ belongs to one of the three classes: Dirichlet, Neumann or Cauchy (Robin). This means, that the Green's function must be constructed in such a way that all the boundary conditions with respect to electric and magnetic fields $\vec{\mathbf{E}}$ and $\vec{\mathbf{H}}$ are satisfied on the center conductor $\rho < a$, on the flange (ground plane) $b > \rho > d$ and regions: $a < \rho < b$ and $d < \rho < \infty$. The homogeneous scalar Helmholtz equation must be solved first.

Consider the most general wave equation (4.1.1) in the dielectric region $0 < z < +\infty$ characterized by $\tilde{k}^2(\omega) = k_o^2\tilde{\epsilon}(\omega)$. This equation may be separated into:

$$\frac{1}{\rho}\frac{\partial}{\partial\rho}\left(\rho\frac{\partial\Psi^+(\rho,z)}{\partial\rho}\right) - \frac{m^2}{\rho^2}\Psi^+(\rho,z) + \frac{\partial^2\Psi^+(\rho,z)}{\partial z^2} + k_o^2\tilde{\epsilon}(\omega)\Psi^+(\rho,z) = 0 \qquad (4.3.1)$$

and

$$\frac{\partial^2\Phi^+}{\partial\phi^2} + m^2\Phi^+ = 0 \qquad (4.3.2)$$

This decomposition separates the rotational symmetry and azimuthal problems and is equivalent to the postulate that the total field Ψ^+_{tot} may be factored as [72]

$$\Psi^+_{tot}(\rho,\, z,\, \phi) = \Psi^+(\rho,\, z)\Phi^+(\phi)\ , \tag{4.3.3}$$

where

$$\Phi^+(\phi) = \begin{pmatrix} \cos \\ \sin \end{pmatrix} m\phi\ . \tag{4.3.3.1}$$

Equation (4.3.1) is the subject to the following boundary conditions at $z = 0$:

Region I*

$$\frac{\partial \Psi^+}{\partial z} = 0 \qquad \text{for} \qquad 0 < \rho < a\ . \tag{4.3.4}$$

Region II

$$\Psi^+ = f_1(\rho) \qquad\qquad \text{for} \qquad a < \rho < b\ , \tag{4.3.5}$$

where $f_1(\rho)$ is assumed to be a known function which is determined by the proper matching procedure at the aperture. This function depends on the field distribution on the aperture of the coaxial waveguide, or alternatively on the field in the coaxial waveguide region. The general form of this function is given as

$$f_1(\rho) = \sum_m^{\infty} \sum_n^{\infty} \Theta_{mn} \Psi_{Emn}(\xi_{mn}\rho)\ , \tag{4.3.5.1}$$

where Θ_{mn} is the transmission coefficient matrix to be determined and $\Psi_{Emn}(\xi_{mn}\rho)$ is the eigenfunction of the scalar Helmholtz equation for TM-waves, respectively. This also bears the assumption that the total field is sought as superposition of TM-modes.

- Region III*

$$\frac{\partial \Psi^+}{\partial z} = 0 \qquad\qquad \text{for} \qquad b < \rho < d\ . \tag{4.3.6}$$

Region IV

$$\frac{\partial^2 \Psi^+}{\partial \rho \partial z} + \tilde{h}\frac{\partial \Psi^+}{\partial \rho} \approx 0 \qquad\qquad \text{for} \qquad d < \rho < \infty \tag{4.3.7}$$

[72] E.C. Titchmarsh, "Eigenfunction Expansions Associated with Second-Order Differential Equations", Part II, Oxford at the Clarendon Press, 1958, pp 123-126.

* Justification for this choice is given in Appendix C

The complex operator $\tilde{h}$ is given by

$$\tilde{h} = \frac{-jk_o\sqrt{\tilde{\varepsilon}(\omega)}}{\tilde{\vartheta} - 1} , \tag{4.3.7.1}$$

where $\tilde{\vartheta}$ is defined by (3.4.10) with $\tilde{\varepsilon}_2 = 1$. If $\tilde{\varepsilon}(\omega)$ is large then $\tilde{h} = jk_o\sqrt{\tilde{\varepsilon}(\omega)}$, and then (4.3.7) represents the Leontovitch boundary condition with respect to z-variable.

Solutions to equations (4.3.1-2) have to be found in each of regions I, II, III and IV with the associated boundary conditions and the continuity conditions derived at the imposed boundaries, which consist of circular surfaces and separate regions.

4.3.2 Representation in Partial Regions

To facilitate solution of the problem, an integral transform has been selected appropriate to geometry of the problem. The Finite Hankel Transform (FHT) was formulated in [73], [74] and later developed in [75] and [76]. Mathematical details of the FHT and restrictions associated with application to Helmholtz equation in composite regions are described in Appendix A. This transform reduces (4.3.1) to a well known nonhomogeneous transmission line type equation in a semi-infinite domain.

By multiplying (4.3.1) in region I by a transformation kernel $\rho\mathcal{K}(\kappa)$ proper for the domain boundary (see (A.5) in Appendix A) and integrating both its sides from 0 to a, one obtains the following equation in the FHT domain

$$\frac{\partial^2\mathcal{P}^+}{\partial z^2} + [k_o^2\tilde{\varepsilon}(\omega) - \kappa^2]\mathcal{P}^+ = \kappa a \Psi^+(a) J_m'(\kappa a) , \tag{4.3.8}$$

where $\mathcal{P}^+$ is the Finite Hankel Transform of Ψ^+. Equation (4.3.8) is subject to the following transformed boundary conditions

$$\mathcal{P}^+ = 0 \qquad \text{for} \quad 0 < \rho < a . \tag{4.3.9}$$

[73] G.N. Watson, "A Treatise on the Theory of Bessel Functions", Cambridge University Press, 1966, pp. 576-582.

[74] I.N. Sneddon, "Finite Hankel Transforms", Philosophical Magazine, V. 37, No.264, 1946, pp. 17-24.

[75] G. Cinnelli, "An Extension of the Finite Hankel Transform and Applications", International Journal of Engineering Science, Vol. 3, 1965, pp. 539-559.

[76] I. N. Sneddon, "The Use of Integral Transforms", McGraw-Hill, New York, 1972, pp. 446-454.

In order to distinguish this region from the others, the FHT domain is called κ-space.

By a similar procedure, with the kernel given by (A.8), and integration from a to b, one obtains the following transformed equation in region II

$$\frac{\partial^2 \mathcal{P}^+}{\partial z^2} + [k_o^2 \tilde{\varepsilon}(\omega) - \xi^2]\mathcal{P}^+ = \frac{2}{\pi}\Psi^+(a) - \frac{2}{\pi}\frac{J_m(\xi a)}{J_m(\xi b)}\Psi^+(b) \ , \tag{4.3.10}$$

with the boundary condition at $z = 0$

$$\mathcal{P}^+|_{z=0^+} = \mathcal{F}_1 = \int_a^b f_1(\rho)\mathcal{K}_m(\xi\rho)\rho d\rho \qquad \text{for} \quad a < \rho < b \ , \tag{4.3.11}$$

where $f_1(\rho)$ is defined by (4.3.5.1). This domain is called ξ-space.

The transformed equation in region III, called here χ-space, is given as

$$\frac{\partial^2 \mathcal{P}^+}{\partial z^2} + [k_o^2 \tilde{\varepsilon}(\omega) - \chi^2]\mathcal{P}^+ = \frac{2}{\pi}\Psi^+(b) - \frac{2}{\pi}\frac{J_m(\chi b)}{J_m(\chi d)}\Psi^+(d) \ , \tag{4.3.12}$$

subject to the following transformed boundary condition* at $z = 0$

$$\mathcal{P}^+ = 0 \qquad\qquad \text{for} \quad b < \rho < d \ . \tag{4.3.13}$$

In Appendix C, it is shown that the Neumann boundary conditions applied in regions I and III instead of (4.3.9) and (4.3.13), respectively, make the problems ill-posed. One consequence of this is that the solutions of (4.3.8) and (4.3.12) are nonunique.

In the semi-infinite region IV two transformations may be applied:

- Finite Hankel transform over region $d < \rho < d_m$, where d_m is the finite penetration distance which is a function of medium parameters [77].
- Hankel-Weber transform, for the region $d < \rho < \infty$, as shown in Appendix B.

From the first transformation, it can be found that power density for the nonvanishing radial component is given by

$$\bar{S}(\rho) = \frac{D_1}{\rho} e^{\frac{-2\alpha}{\sqrt{\tan^2\delta + 1}}\rho} \cos\left(\frac{2\alpha \tan\delta}{\sqrt{\tan^2\delta + 1}}\rho\right) \ . \tag{4.3.14}$$

---

* Appendix B

[77] Z A Delecki and S S Stuchly, "Electromagnetic Power Propagation in Dielectric Lossy Media' in press, J of Microwave Power, 1989

Applying the Finite Hankel Transform to the equation (4.3.1), one obtains

$$\frac{\partial^2 \mathcal{P}^+}{\partial z^2} + [k_o^2 \tilde{\epsilon}(\omega) - \nu^2]\mathcal{P}^+ = \frac{2}{\pi}\mathcal{P}^+(d) \tag{4.3.15}$$

with the boundary condition

$$\frac{\partial \mathcal{P}^+}{\partial z} + \tilde{h}\mathcal{P}^+ = 0 \qquad \text{for} \qquad d < \rho < d_p \ , \tag{4.3.16}$$

where constant $\tilde{h}$ is given by (4.3.7.1).

The Hankel-Weber transform applied to the (4.3.1) gives

$$\frac{\partial^2 \mathcal{P}^+}{\partial z^2} + [k_o^2 \tilde{\epsilon}(\omega) - \nu^2]\mathcal{P}^+ = -\frac{\pi}{2}\frac{\Psi^+(d)}{\nu\sqrt{J_m^2(\nu d) + Y_m^2(\nu d)}} \tag{4.3.17}$$

subject to the transformed continuity condition at $\rho = d$, as shown in Appendix B, the radiation boundary condition at infinity and the boundary condition (4.3.16) at $z = 0$ with operator $\tilde{h}$ given by (4.3.7.1).

The use of the FHT has a distinct advantage over classical methods which often require great ingenuity in establishing *a priori* form for the solution. Another significant advantage of this transform over the Laplace transform is that the difficult contour integral of the inversion formula for the Laplace transform is avoided. However, the method has one important drawback: namely, eigenvalues of both kernels of the transformation $\mathcal{K}(a, b, \lambda)$ have not been tabulated to the extent required for practical applications.

4.3.3. Determination of Eigenvalues of FHT Kernels

The use of the Finite Hankel Transform offers a conceptually simple tool for solving mixed boundary value problem of Helmholtz equation for problems expressed in cylindrical coordinate systems. Despite this, it has not obtained dissemination largely due to a lack of tabulated values of roots of a key transcendental equation. There is no application to the author's knowledge of this method to the solution of practical problems in electromagnetics. Outside electromagnetics, its applications have been few [78].

[78] H.S. Carslaw and J C. Jaeger, "Conduction of Heat in Solids", Oxford at Clarendon Press, 1959, pp 188-229

For region I, the roots κ_{mn} of the following transcendental equation

$$J_m(\kappa_k a) = 0 \tag{4.3.18}$$

are of interest. In regions II and III, the kernels of the FHT become:

$$J_m(\chi_k)Y_m(\chi_k \ell) - Y_m(\chi_k)J_m(\chi_k \ell) = 0 \ , \tag{4.3.19}$$

where $\chi_k = \kappa_k b$, while $\ell = a/b$ in region II and $\ell = b/d$ in region III, respectively.

The most extensive table of roots of (4.3.19) had been published in [79]. However, as shown in [86], there is lack of the complete tabulation of (4.3.19). In fact, (4.3.19) is tabulated only up to the order $m = 3$ of Bessel functions involved and up to the 5-th root for limited number of parameters ℓ. This is not sufficient for application of the FHT. When $\ell \to 0$, the roots of (4.3.19) approach the corresponding roots of (4.3.18) for the same order m.

Therefore, to be able to apply the FHT, the existing tables had to be confirmed and extended. Only that part of the work which coincides with its main objective, i.e., finding the solution of the problem posed is included in the thesis. The particulars of the root computation technique are described in Appendix D. The transcendental function (4.3.19) and its zero contours projected onto $\chi - \ell$-plane for $m = 0$ is shown in Fig. 4.2. The 2-D representation of zero-contour for $m = 0$, depicted in Fig. 4.3, serves as a pictorial representation of the domain spanned by eigenvalues.

4.3.4. Solutions in Different Regions

Equations (4.3.8), (4.3.10), (4.3.12), (4.3.15) and (4.3.17) are of the nonhomogeneous "transmission line" type. Their solutions are found as:

[79] H.B. Dwight, "Table of Roots for Natural Frequencies in Coaxial Type Cavities", Journal of Mathematical and Applied Physics, v. 27, No. 1, 1949, pp. 84-89.

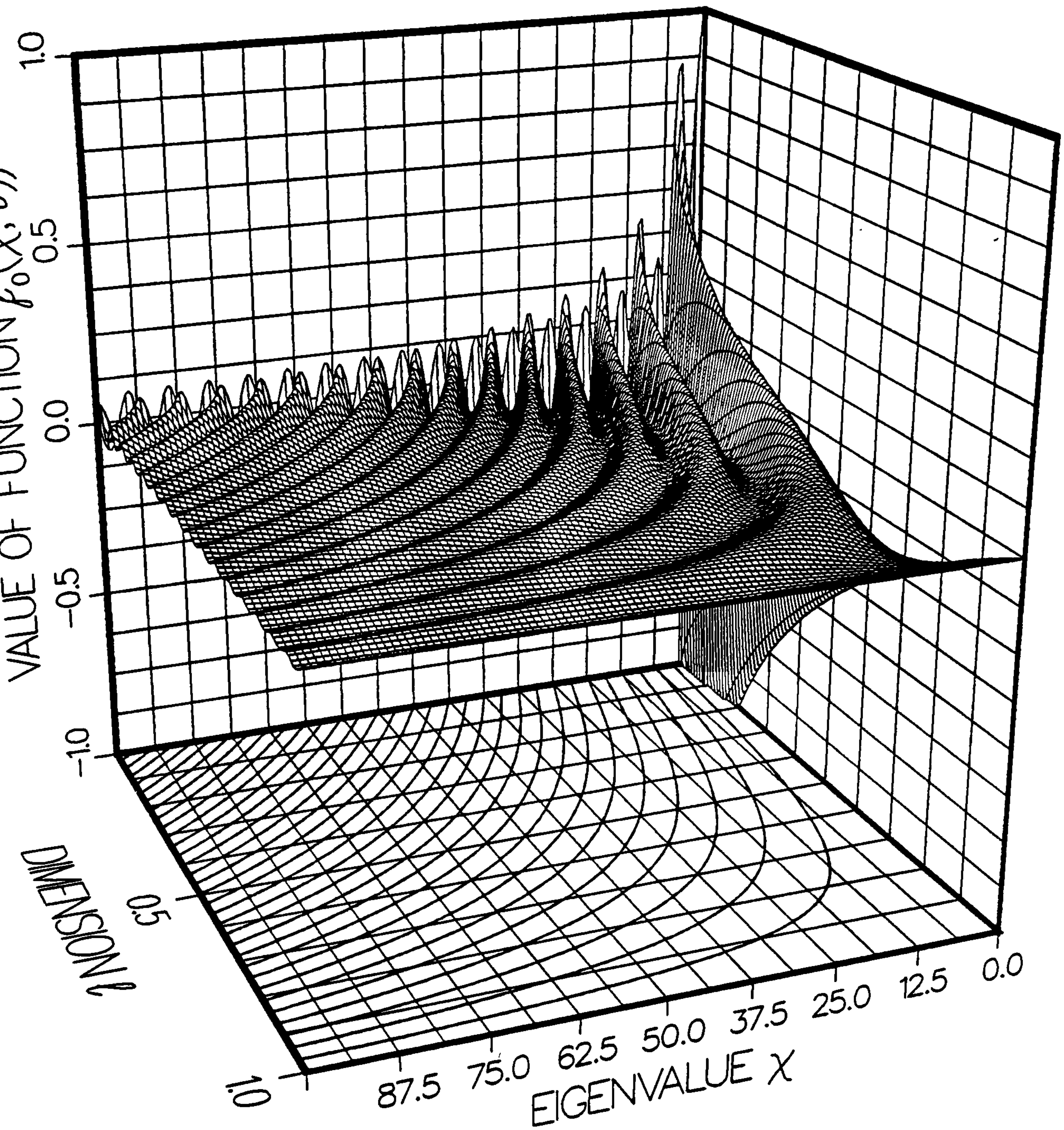

Fig. 4.2

Transcendental function $\mathcal{K}_o(\chi\,,\ell)$ and its zero-contour projected onto $\chi\, -\ell$ plane.

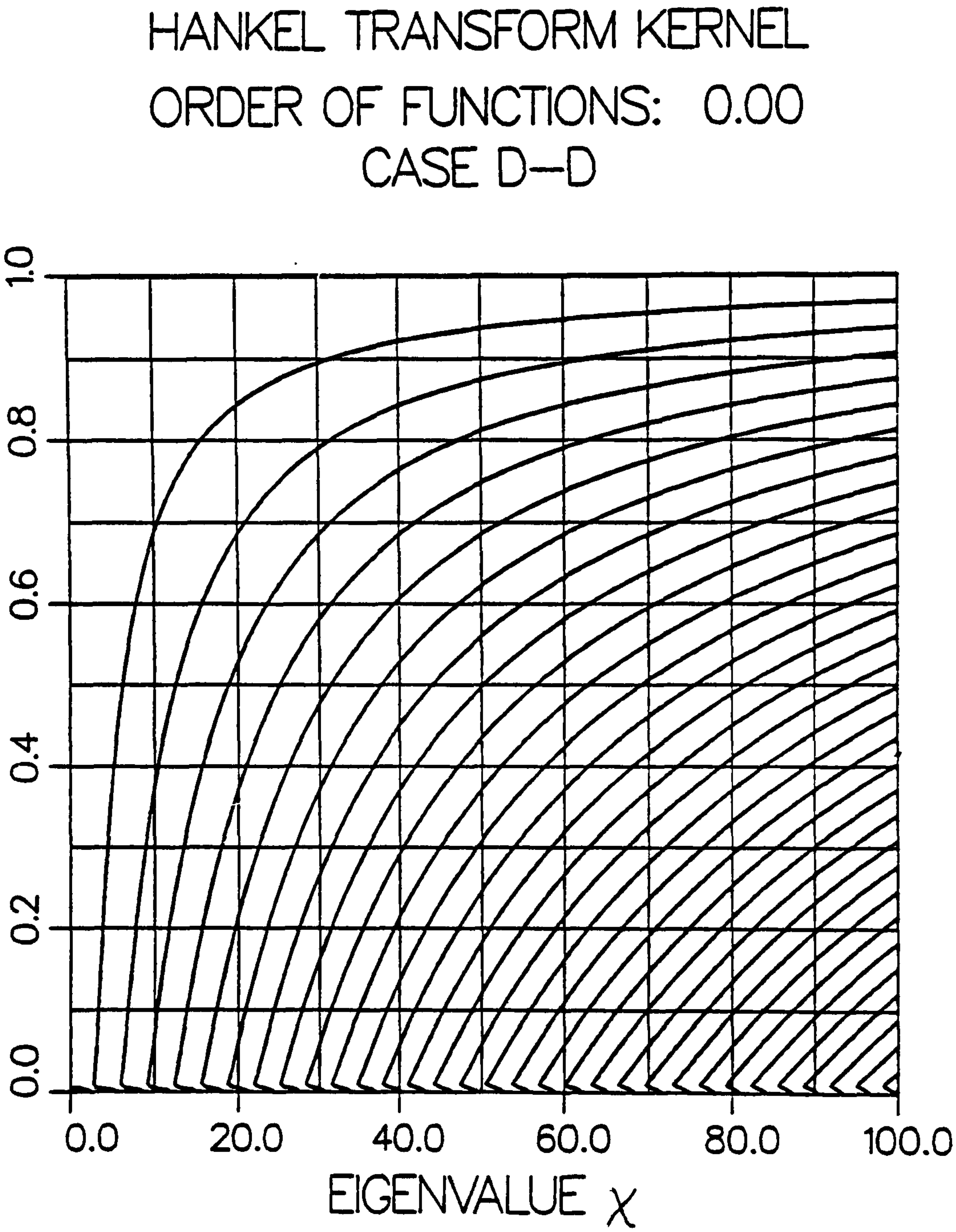

Fig. 4.3

2-D representation of the solution of transcendental equation $\mathcal{K}_o(\chi, \ell) = 0$.

- for κ-space

$$\mathcal{P}_I^+(\kappa, z) = \Psi^+(a)\frac{\kappa a}{k_o^2\tilde{\epsilon}(\omega) - \kappa^2}J_m'(\kappa a)\left\{1 - e^{-\jmath\sqrt{k_o^2\tilde{\epsilon}(\omega)-\kappa^2}z}\right\} \tag{4.3.20}$$

in region I and $\rho \in [0, a]$;

- for ξ-space

$$\mathcal{P}_{II}^+(\xi, z) = \frac{\left\{\frac{2}{\pi}\Psi^+(a) - \frac{2}{\pi}\frac{J_m(\xi a)}{J_m(\xi b)}\Psi^+(b)\right\}}{k_o^2\tilde{\epsilon}(\omega) - \xi^2}\left(1 - e^{-\jmath\sqrt{k_o^2\tilde{\epsilon}(\omega)-\xi^2}z}\right) + \mathcal{F}_1(\xi, 0)e^{-\jmath\sqrt{k_o^2\tilde{\epsilon}(\omega)-\xi^2}z} \tag{4.3.21}$$

where $\mathcal{F}_1(\xi, 0)$ denotes the boundary condition at $z = 0$ and $\rho \in [a, b]$ in region II;

- for χ-space

$$\mathcal{P}_{III}^+(\chi, z) = \frac{\left\{\frac{2}{\pi}\Psi^+(b) - \frac{2}{\pi}\frac{J_m(\chi b)}{J_m(\chi d)}\Psi^+(d)\right\}}{k_o^2\tilde{\epsilon}(\omega) - \chi^2}\left\{1 - e^{-\jmath\sqrt{k_o^2\tilde{\epsilon}(\omega)-\chi^2}z}\right\} \tag{4.3.22}$$

in region III, $\rho \in [b, d]$;

- for ν-space

$$\mathcal{P}_{IV}^+(\nu, z) = -\frac{2}{\pi}\frac{\Psi^+(d)}{\nu\sqrt{J_m^2(\nu d) + Y_m^2(\nu d)}(k_o^2\tilde{\epsilon}(\omega) - \nu^2)}\left\{1 + \frac{1}{\frac{\jmath\sqrt{k_o^2\tilde{\epsilon}(\omega)-\nu^2}}{\tilde{h}} - 1}e^{-\jmath\sqrt{k_o^2\tilde{\epsilon}(\omega)-\nu^2}z}\right\} \tag{4.3.23}$$

in region IV, $\rho \in [b, \infty)$, where

$$\frac{j\sqrt{k_o^2\tilde{\epsilon}(\omega) - \nu^2}}{\tilde{h}} = \{\tilde{\vartheta}(\omega) - 1\}\sqrt{1 - \frac{\nu^2}{k_o^2\tilde{\epsilon}(\omega)}}\,. \tag{4.3.23.1}$$

When solutions are obtained in all finite Hankel transform domains, it is necessary to use the appropriate inversion formulas pertaining to regions of interest as is shown in Appendix A. Applying the FHT inversion formulas to solutions (4.3.20-23), one obtains:

- In region I, $\rho \in [0, a]$:

$$\Psi_I^+(\rho, z) = \frac{2\Psi^+(a)}{a}\sum_{k=1}^{K}\frac{-1}{\kappa_k\left\{\left(\frac{k_o}{\kappa_k}\right)^2\tilde{\epsilon}(\omega) - 1\right\}}\frac{J_m(\kappa_k\rho)}{J_{m+1}(\kappa_k a)}\left\{1 - e^{-\jmath\sqrt{k_o^2\tilde{\epsilon}(\omega)-\kappa_k^2}z}\right\}\,.$$

(4.3.24)

where κ_k is the $k-th$ root of

$$J_m(\kappa_k a) = 0\ . \tag{4.3.24.1}$$

- In region II, $\rho \in [a,b]$:

$$\begin{aligned}
\Psi^+_{II}(\rho,z) =& \pi\Psi^+(a)\sum_{k=1}^{K}\frac{1-e^{-j\sqrt{k_o^2\tilde{\epsilon}(\omega)-\xi_k^2}z}}{\left(\frac{k_o}{\xi_k}\right)^2\tilde{\epsilon}(\omega)-1}\frac{J_m^2(\xi_k b)}{J_m^2(\xi_k a)-J_m^2(\xi_k b)}B_m(\xi_k,a,\rho)- \\
&-\pi\Psi^+(b)\sum_{k=1}^{K}\frac{1-e^{-j\sqrt{k_o^2\tilde{\epsilon}(\omega)-\xi_k^2}z}}{\left(\frac{k_o}{\xi_k}\right)^2\tilde{\epsilon}(\omega)-1}\frac{J_m(\xi_k a)J_m(\xi_k b}{J_m^2(\xi_k a)-J_m^2(\xi_k b)}B_m(\xi_k,a,\rho)+ \\
&+\frac{\pi^2}{2}\sum_{k=1}^{K}\mathcal{F}(\xi_k,0)e^{-j\sqrt{k_o^2\tilde{\epsilon}(\omega)-\xi_k^2}z}\frac{\xi_k^2 J_m^2(\xi_k b)}{J_m^2(\xi_k a)-J_m^2(\xi_k b)}B_m(\xi_k,a,\rho)
\end{aligned} \tag{4.3.25}$$

where

$$B_m(\xi_k,a,\rho) = J_m(\xi_k\rho)Y_m(\xi_k a) - Y_m(\xi_k\rho)J_m(\xi_k a) \tag{4.3.25.1}$$

and ξ_k is the $k-th$ root of

$$J_m(\xi_k b)Y_m(\xi_k a) - Y_m(\xi_k b)J_m(\xi_k a) = 0. \tag{4.3.25.2}$$

- In region III, $\rho \in [b,d]$:

$$\begin{aligned}
\Psi^+_{III}(\rho,z) =& \pi\Psi^+(b)\sum_{k=1}^{K}\frac{1-e^{-j\sqrt{k_o^2\tilde{\epsilon}(\omega)-\chi_k^2}z}}{\left(\frac{k_o}{\chi_k}\right)^2\tilde{\epsilon}(\omega)-1}\frac{J_m^2(\chi_k d)}{J_m^2(\chi_k b)-J_m^2(\chi_k d)}C_m(\chi_k,b,\rho) \\
&-\pi\Psi^+(d)\sum_{k=1}^{K}\frac{1-e^{-j\sqrt{k_o^2\tilde{\epsilon}(\omega)-\chi_k^2}z}}{\left(\frac{k_o}{\chi_k}\right)^2\tilde{\epsilon}(\omega)-1}\frac{J_m(\chi_k b)J_m(\chi_k d}{J_m^2(\chi_k b)-J_m^2(\chi_k d)}C_m(\chi_k,b,\rho)
\end{aligned} \tag{4.3.26}$$

where

$$C_m(\chi_k,b,\rho) = J_m(\chi_k\rho)Y_m(\chi_k b) - Y_m(\chi_k\rho)J_m(\chi_k b). \tag{4.3.26.1}$$

and χ_k is the $k-th$ root of

$$J_m(\chi_k d)Y_m(\chi_k b) - Y_m(\chi_k d)J_m(\chi_k b) = 0. \qquad (4.3.26.2)$$

When the inverse Weber-Hankel transform is evaluated from (4.3.17), the wave function in region IV is found as:

$$\Psi^+_{IV}(\rho) = -\frac{2}{\pi}\Psi^+(d)\int_0^\infty \frac{J_m(\nu\rho)Y_m(\nu d) - Y_m(\nu\rho)J_m(\nu d)}{\{J^2_m(\nu d) + Y^2_m(\nu d)\}\{k_o^2\tilde{\epsilon}(\omega) - \nu^2\}}d\nu$$

$$+\frac{2}{\pi}\Psi^+(d)\int_0^\infty \frac{[J_m(\nu\rho)Y_m(\nu d) - Y_m(\nu\rho)J_m(\nu d)]e^{-j\sqrt{k_o^2\tilde{\epsilon}(\omega)-\nu^2}z}}{\{\tilde{\vartheta}(\omega) - 1\}\sqrt{1-\frac{\nu^2}{k_o^2\tilde{\epsilon}(\omega)}}\{J^2_m(\nu d) + Y^2_m(\nu d)\}\{(k_o^2\tilde{\epsilon}(\omega) - \nu^2\}}d\nu \qquad (4.3.27)$$

4.3.5. Construction of the Global Solution

The scalar wave function Ψ^+ in a dielectric medium represents magnitude and phase of the magnetic vector potential. The considerations in chapter II show that only the magnetic flux vector $\vec{\mathbf{B}}$ is a solenoidal field. When the magnetic vector potential $\vec{\mathbf{A}} = \hat{a}_z\Psi^+$ in external region*, the TM_{mn} field is implied in the dielectric region. Therefore, the B_ϕ field is continuous across separating "boundaries" of the partial regions and the following conditions are satisfied [79]:

$$\left\{\begin{array}{c} \left.\frac{\partial\Psi^+_I(\rho,z)}{\partial\rho}\right|_{\rho=a^-} = \left.\frac{\partial\Psi^+_{II}(\rho,z)}{\partial\rho}\right|_{\rho=a^+} \\ \left.\frac{\partial\Psi^+_{II}(\rho,z)}{\partial\rho}\right|_{\rho=b^-} = \left.\frac{\partial\Psi^+_{III}(\rho,z)}{\partial\rho}\right|_{\rho=b^+} \\ \left.\frac{\partial\Psi^+_{III}(\rho,z)}{\partial\rho}\right|_{\rho=d^-} = \left.\frac{\partial\Psi^+_{IV}(\rho,z)}{\partial\rho}\right|_{\rho=d^+} \end{array}\right\} \qquad (4.3.28)$$

* See the discussion in Appendix C for other possibilities

[79] R F Harrington, "Time-harmonic Electromagnetic Fields", Mc-Graw-Hill, 1961, p 202

This leads to the following system of equations:

$$\begin{bmatrix} a_{11} & a_{12} & 0 \\ a_{21} & a_{22} & a_{23} \\ 0 & a_{32} & a_{33} \end{bmatrix} \begin{bmatrix} \Psi^{+}(a) \\ \Psi^{+}(b) \\ \Psi^{+}(d) \end{bmatrix} = \begin{bmatrix} b_1 \\ b_2 \\ b_3 \end{bmatrix}, \tag{4.3.29}$$

where parametric coefficients with respect to the $z-$ variable are given:

$$a_{11} = \sum_{k=1}^{K} \frac{1 - e^{-j\sqrt{k_o^2\tilde{\epsilon}(\omega) - \kappa_k^2}z}}{\left(\frac{k_o}{\kappa_k}\right)^2 \tilde{\epsilon}(\omega) - 1} - \frac{1 - e^{-j\sqrt{k_o^2\tilde{\epsilon}(\omega) - \xi_k^2}z}}{\xi_k \left\{\left(\frac{k_o}{\xi_k}\right)^2 \tilde{\epsilon}(\omega) - 1\right\}} \frac{J_m(\xi_k b)}{J_m^2(\xi_k a) - J_m^2(\xi_k b)}, \tag{4.3.30}$$

$$a_{12} = \sum_{k=1}^{K} \frac{1 - e^{-j\sqrt{k_o^2\tilde{\epsilon}(\omega) - \xi_k^2}z}}{\xi_k \left\{\left(\frac{k_o}{\xi_k}\right)^2 \tilde{\epsilon}(\omega) - 1\right\}} \frac{J_m(\xi_k a)}{J_m^2(\xi_k a) - J_m^2(\xi_k b)}, \tag{4.3.31}$$

$$a_{13} = 0, \tag{4.3.32}$$

and

$$a_{21} = a_{12} \tag{4.3.33}$$

$$a_{22} = -\sum_{k=1}^{K} \frac{1 - e^{-j\sqrt{k_o^2\tilde{\epsilon}(\omega) - \xi_k^2}z}}{\xi_k \left\{\left(\frac{k_o}{\xi_k}\right)^2 \tilde{\epsilon}(\omega) - 1\right\}} \frac{J_m^2(\xi_k a)}{[J_m^2(\xi_k a) - J_m^2(\xi_k b)] J_m(\zeta_k b)} + \frac{1 - e^{-j\sqrt{k_o^2\tilde{\epsilon}(\omega) - \chi_k^2}z}}{\chi_k \left\{\left(\frac{k_o}{\chi_k}\right)^2 \tilde{\epsilon}(\omega) - 1\right\}} \frac{J_m(\chi_k d)}{J_m^2(\chi_k b) - J_m^2(\chi_k d)}, \tag{4.3.34}$$

$$a_{23} = \sum_{k=1}^{K} \frac{1 - e^{-j\sqrt{k_o^2\tilde{\epsilon}(\omega) - \chi_k^2}z}}{\chi_k \left\{\left(\frac{k_o}{\chi_k}\right)^2 \tilde{\epsilon}(\omega) - 1\right\}} \frac{J_m(\chi_k b)}{J_m^2(\chi_k b) - J_m^2(\chi_k d)} \tag{4.3.35}$$

and

$$a_{31} = 0, \tag{4.3.36}$$

$$a_{32} = a_{23}, \tag{4.3.37}$$

$$a_{33} = -\sum_{k=1}^{K} \frac{1 - e^{-j\sqrt{k_o^2\tilde{\epsilon}(\omega) - \chi_k^2}z}}{\chi_k \left\{\left(\frac{k_o}{\chi_k}\right)^2 \tilde{\epsilon}(\omega) - 1\right\}} \frac{J_m^2(\chi_k b)}{[J_m^2(\chi_k b) - J_m^2(\chi_k d)] J_m(\zeta_k d)} + \frac{2}{\pi} \int_0^{\infty} \frac{J_m'(\nu\rho) Y_m(\nu d) - Y_m'(\nu\rho) J_m(\nu d)}{\{J_m^2(\nu d) + Y_m^2(\nu d)\}\{k_o^2 \tilde{\epsilon}(\omega) - \nu^2\}} d\nu$$

$$-\frac{2}{\pi}\int_0^\infty \frac{[J_m'(\nu\rho)Y_m(\nu d) - Y_m'(\nu\rho)J_m(\nu d)]e^{-j\sqrt{k_o^2\tilde{\epsilon}(\omega)-\nu^2}z}}{\{\tilde{\vartheta}(\omega)-1\}\sqrt{1-\frac{\nu^2}{k_o^2\tilde{\epsilon}(\omega)}}\{J_m^2(\nu d)+Y_m^2(\nu d)\}\{k_o^2\tilde{\epsilon}(\omega)-\nu^2\}}d\nu \tag{4.3.38}$$

where differentiation is with respect to ρ-variable, and

$$b_1 = \frac{\pi}{2}\sum_{k=1}^{K}\mathcal{F}(\xi_k, 0^+)e^{-j\sqrt{k_o^2\tilde{\epsilon}(\omega)-\xi_k^2}z}\frac{\xi_k J_m(\xi_k b)}{J_m^2(\xi_k a) - J_m^2(\xi_k b)}, \tag{4.3.39}$$

$$b_2 = -b_1, \tag{4.3.40}$$

$$b_3 = 0. \tag{4.3.41}$$

$[\mathbf{A}_{i,j}]$ is a symmetric, banded, tridiagonal matrix. Function $\mathcal{F}_1(\xi_k, 0^+)$ is given by (E.4) in Appendix E.

By solving the system of equations (4.3.29), the values of functions $\Psi^+(a)$, $\Psi^+(b)$ and $\Psi^+(d)$ are given as

$$\Psi^+(a) = b_1\frac{a_{22}a_{33} - a_{23}^2 + a_{12}a_{33}}{a_{11}a_{22}a_{33} - a_{11}a_{23}^2 - a_{12}^2a_{33}}, \tag{4.3.42}$$

$$\Psi^+(b) = -b_1a_{33}\frac{a_{11} + a_{12}}{a_{11}a_{22}a_{33} - a_{11}a_{23}^2 - a_{12}^2a_{33}} \tag{4.3.43}$$

and

$$\Psi^+(d) = b_1a_{23}\frac{a_{11} + a_{12}}{a_{11}a_{22}a_{33} - a_{11}a_{23}^2 - a_{12}^2a_{33}}. \tag{4.3.44}$$

Coefficient functions $a_{11}\cdots a_{33}$ and b_1 are defined by (4.3.30)...(4.3.41).

Once the homogeneous Helmholtz equation is solved for this region, the Green's function may be found by standard procedures, i.e., the use of:

$$G^+(\vec{\mathrm{x}}, \vec{\mathrm{x}}') = \sum_m\sum_n\frac{\Psi_{mn}^{+*}(\vec{\mathrm{x}}')\Psi_{mn}^+(\vec{\mathrm{x}})}{\lambda_{mn} - \lambda}, \tag{4.3.45}$$

where λ_{mn} represents eigenvalues and primed variables to the source distribution. The function Ψ_{mn}^+ must possess well-behaved (e.g., finite and continuous) solutions.

4.4. The Reflection Coefficient

The Green's function (4.2.15) becomes unique when the appropriate matching is carried over the aperture of the line. The reflection coefficient Γ_{mn} can then be determined.

By considering the tangential component of the magnetic field at the aperture, one finds upon applying Green's Theorem to the coaxial waveguide region that

$$H_\phi^-(\rho,z) = \int_{A_o} G^{(-)}(\rho,0;\rho',z')\left[\frac{\partial}{\partial z'}H_\phi^-(\rho',z')\right]_{z=0} \rho' d\rho' \ . \tag{4.4.1}$$

By a similar procedure, the tangential component of magnetic field H_ϕ^+ on the dielectric space side can be found. The matching of these two fields at the aperture is the basis for the determination of the reflection coefficient in (4.1.15. The same method is used by others [81]. This procedure leads to the stationary value of the input admittance. The stationary form of the input admittance, found in [81], is an approximate solution based on a variational expression utilizing the detailed field distribution on the discontinuity. By "stationary" it is meant that the variation in $\tilde{Y}_{00}$ is minimum for an arbitrary first order variation in the surface current distribution in the plane of discontinuity.

However, this method requires knowledge of the Green's function which satisfies boundary conditions on the ground plane and dielectric interface. The method of the previous section leads to a very complicated solution for the the scalar wave function Ψ^+. Various assumptions have been made with respect to the type of boundary condition at the aperture. The most common one is the Neumann boundary condition [81]. Therefore, another method is developed here utilizing results formulated in Chapter III and limiting form of the solution for Ψ_{II}^+ as $z \to 0^+$.

[81] F.E. Borgnis and C.H. Papas, "Randwertprobleme der Mikrowellenphysik", Springer-Verlag, Berlin, 1955, pp. 88-101.

4.4.1 The Surface Impedance Method

Consider (3.4.8) at the aperture which is also an interface between a known lossless dielectric material of relative real dielectric constant $\varepsilon_c(\omega)$ and an unknown dielectric half space whose properties are described by the complex relative permittvity $\tilde{\varepsilon}(\omega)$. It is shown in Chapter III that (3.4.8) represents the surface impedance.

Equation (3.4.8) implies the following two equations

$$\tilde{Y}_s = \frac{H_\phi^+ - H_\phi^-}{E_\phi^-} = j\omega\epsilon_o\epsilon_c \frac{\lim_{z\to 0^-}\frac{\partial\Psi^-}{\partial\rho} - \lim_{z\to 0^+}\frac{\partial\Psi^+}{\partial\rho}}{\lim_{z\to 0^-}\frac{\partial^2\Psi^-}{\partial\rho\partial z}} \tag{4.4.2}$$

$$\tilde{Y}_s = \frac{H_\phi^+ - H_\phi^-}{E_\phi^+} = j\omega\epsilon_o\tilde{\epsilon}_m(\omega) \frac{\lim_{z\to 0^-}\frac{\partial\Psi^-}{\partial\rho} - \lim_{z\to 0^+}\frac{\partial\Psi^+}{\partial\rho}}{\lim_{z\to 0^+}\frac{\partial^2\Psi^+}{\partial\rho\partial z}} \tag{4.4.3}$$

In these two equations, the continuity of the tangential electric field is used, that is

$$\frac{1}{\epsilon_c}\lim_{z\to 0^-}\frac{\partial^2\Psi^-}{\partial\rho\partial z} = \frac{1}{\tilde{\epsilon}_m(\omega)}\lim_{z\to 0^+}\frac{\partial^2\Psi^+}{\partial\rho\partial z}\ . \tag{4.4.4}$$

The third condition is found from the discontinuity of the normal component of the electric flux density D_z across the aperture. From (2.4.4), (2.4.5) and (3.3.16), the following equation is obtained

$$\lim_{z\to 0^-}\left(\frac{\partial^2\Psi^-}{\partial z^2} + k_o^2\epsilon_o\varepsilon_c\Psi^-\right) - \lim_{z\to 0^+}\left(\frac{\partial^2\Psi^+}{\partial z^2} + k_o^2\tilde{\epsilon}(\omega)\Psi^+\right)$$
$$= \lim_{z\to 0^-}\frac{\tilde{Y}_s}{j\omega\epsilon_o\varepsilon_c}\frac{\partial}{\partial z}\left(\frac{\partial^2\Psi^-}{\partial z^2} + k_o^2\epsilon_o\varepsilon_c\Psi^-\right)\ . \tag{4.4.5}$$

Let us restrict for brevity the electromagnetic field to a superposition of TEM and TM_{on} modes. Three conditions are needed in order to determine unknown constants $\tilde{\Gamma}_o$, $\tilde{\Gamma}_n$ and $\tilde{\Theta}_n$ corresponding to magnitudes of TEM and TM_{on} backward scattered (or alternatively modal reflection coefficients) and TM_{on} forward scattered modes.

Using relations (3.4.1-3) to express the field components for the fields inside and outside the line, one obtains

$$H_\phi|_{z=0^-} = \frac{1}{\rho}(1+\tilde{\Gamma}_o) + \sum_{n=1}^{\infty}\tilde{\Gamma}_n\Psi'_{E_n}(\rho)\ , \tag{4.4.6}$$

$$E_\rho|_{z=0^-} = \frac{z_o}{\sqrt{\varepsilon_c}}\left\{\frac{1}{\rho}(1-\tilde{\Gamma}_o) - \sum_{n=1}^{\infty}\frac{\gamma_n}{\gamma_c}\tilde{\Gamma}_n \Psi'_{E_n}(\rho)\right\} , \tag{4.4.7}$$

$$\begin{aligned} H_\phi|_{z=0^+} &= \lim_{z\to 0^+}\frac{\partial \Psi^+}{\partial \rho} \\ &= \sum_{k=1}^{K}\left\{\sum_{n=k}^{\infty}\tilde{\Theta}_n \frac{1}{\xi_n^2}\left(\frac{J_o^2(\xi_n a)}{J_o^2(\xi_n b)}-1\right)\right\}\frac{\xi_k^2 J_o^2(\xi_k b)}{J_o^2(\xi_k a)-J_o^2(\xi_k b)}\frac{\partial B_o(\xi_k,a,\rho)}{\partial\rho} , \end{aligned} \tag{4.4.8}$$

$$\begin{aligned} E_\rho|_{z=0^+} &= -\frac{z_o}{\sqrt{\tilde{\epsilon}_m(\omega)}}\lim_{z\to 0^+}\frac{\partial^2\Psi^+}{\partial\rho\partial z} \\ &= -\frac{z_o}{\sqrt{\tilde{\epsilon}_m(\omega)}}\sum_{k=1}^{K}\tilde{\Theta}_n\sqrt{1-\frac{\xi_k^2}{k_o^2\tilde{\epsilon}(\omega)}}\frac{\partial B_o(\xi_k,a,\rho)}{\partial\rho} , \end{aligned} \tag{4.4.9}$$

where $\Psi_{E_n}(\rho)$ is given by (4.2.4) for $m\to 0$ while $B_o(\xi_k,a,\rho)$ is the eigenfunction of the Fourier-Bessel expansion as given by (A.8) in Appendix A. It is clear from (4.4.8) that the tangential component of the electric field density completely depends on the local properties of the space outside the sensor, namely the properties of its aperture. Equation (4.4.9) was simplified by using condition that for $n = k$

$$\begin{aligned} &\sum_{k=1}^{K}\left\{\sum_{n=k}^{\infty}\tilde{\Theta}_n \frac{1}{\xi_n^2}\left(\frac{J_o^2(\xi_n a)}{J_o^2(\xi_n b)}-1\right)\right\}\frac{\xi_k^2 J_o^2(\xi_k b)}{J_o^2(\xi_k a)-J_o^2(\xi_k b)}\frac{\partial B_o(\xi_k,a,\rho)}{\partial\rho} \\ &\qquad = \sum_{n=k}^{\infty}\tilde{\Theta}_n\frac{\partial B_o(\xi_k,a,\rho)}{\partial\rho} \end{aligned} \tag{4.4.10}$$

which says that the Fourier-Bessel expansion of a Fourier-Bessel series is equal to the original series.

Introducing a complex parameter

$$\tilde{\vartheta}(\omega) = \sqrt{\frac{\tilde{\varepsilon}_m(\omega)}{\varepsilon_c(\omega)}} \tag{4.4.11}$$

and substituting (4.4.6), (4.4.7) and (4.4.8) into (4.4.2) the following identity is obtained

$$\frac{1}{\rho}\{(\tilde{\vartheta}-2)-\tilde{\vartheta}\tilde{\Gamma}_o\} =$$
$$\sum_{n=1}^{\infty}\underbrace{\left\{\left(1-\frac{\gamma_n}{\gamma_c}(\tilde{\vartheta}-1)\right)\frac{2}{\pi^2\kappa_n^2}\left(\frac{J_o^2(\kappa_n a)}{J_o^2(\kappa_n b)}-1\right)\tilde{\Gamma}_n-\frac{2}{\pi^2\kappa_n^2}\left(\frac{J_o^2(\kappa_n a)}{J_o^2(\kappa_n b)}-1\right)\Theta_n\right\}}_{\tilde{A}_n}\times$$
$$\times\frac{\pi^2\kappa_n^2}{2}\frac{1}{\frac{J_o^2(\kappa_n a)}{J_o^2(\kappa_n b)}-1}\kappa_n B_o'(\kappa_n,\rho,a)\ . \tag{4.4.12}$$

The differentiability property of the Fourier-Bessel expansion results in the expression [82]

$$\tilde{A}_n = \{(\tilde{\vartheta}-2)-\tilde{\vartheta}\Gamma_o\}\int_a^b \ln\rho B_o(\kappa_n,\rho,a)\rho d\rho \tag{4.4.13}$$

where $\tilde{A}_n$ is defined in (4.4.12).

The integral is found as

$$I_1(\kappa_n) = \int_a^b B_o(\rho)\rho\ln\rho d\rho$$

$$= \int_a^b \{J_o(\kappa_n\rho)Y_m(\kappa_n a) - Y_m(\kappa_n\rho)J_o(\kappa_n a)\}\rho\ln\rho d\rho$$

$$=\frac{2}{\pi\kappa_n^2}\left(\ln b\frac{J_o(\kappa_n a)}{J_o(\kappa_n b)}-\ln a\right) \tag{4.4.14}$$

$$=\frac{2b^2}{\pi\chi_n^2}\left(\ln b\frac{J_o(\chi_n\ell)}{J_o(\chi_n)}-\ln a\right) \tag{4.4.15}$$

Substituting (4.4.14) into (4.4.13), the following equation is obtained

$$\tilde{\vartheta}f(\chi_n,\ell)\tilde{\Gamma}_o+\left\{1+(\tilde{\vartheta}-1)\sqrt{1-\frac{\chi_n^2}{k_o^2b^2\varepsilon_c}}\right\}\tilde{\Gamma}_n-\tilde{\Theta}_n=(\tilde{\vartheta}-2)f(\chi_n,\ell) \tag{4.4.16}$$

where

$$f(\chi_n,\ell)=\pi\frac{\ln b\frac{J_o(\chi_n\ell)}{J_o(\chi_n)}-\ln a}{\frac{J_o^2(\chi_n\ell)}{J_o^2(\chi_n)}-1}\ . \tag{4.4.17}$$

[82] G.N. Watson, *op. cit.*, pp. 605-606.

Similar procedures applied to equations (4.4.3) and (4.4.5) lead to a system of equations interrelating scattering coefficients $\tilde{\Gamma}_n$, $\tilde{\Theta}_n$ and the fundamental mode reflection coefficient $\tilde{\Gamma}_o$. The system has the following matrix form

$$\begin{pmatrix} \tilde{\vartheta} f(\chi_n,\ell) & 1+(\tilde{\vartheta}-1)\sqrt{1-\frac{\chi_n^2}{k_o^2 b^2 \varepsilon_c}} & -1 \\ f(\chi_n,\ell) & 1 & -(1-\frac{1}{\tilde{\vartheta}})\sqrt{1-\frac{\chi_n^2}{k_o^2 b^2 \tilde{\epsilon}_m(\omega)}}-1 \\ 0 & 1-(\tilde{\vartheta}-1)\sqrt{1-\frac{\chi_n^2}{k_o^2 b^2 \varepsilon_c}} & -1 \end{pmatrix}$$

$$\times \begin{pmatrix} \tilde{\Gamma}_o \\ \tilde{\Gamma}_n \\ \tilde{\Theta}_n \end{pmatrix} = \begin{pmatrix} (\tilde{\vartheta}-2) f(\chi_n,\ell) \\ -f(\chi_n,\ell) \\ 0 \end{pmatrix} \tag{4.4.18}$$

Members of the above matrices are dimensionless.

The system of equations (4.4.18) has the following solutions

$$\tilde{\Gamma}_o = \frac{(\tilde{\vartheta}-2)}{\tilde{\vartheta}}$$

$$\times \frac{\tilde{\vartheta}\sqrt{1-\frac{\chi_n^2}{k_o^2 b^2 \varepsilon_c}}\left\{\frac{2}{\tilde{\vartheta}-2}+(\tilde{\vartheta}-1)\sqrt{1-\frac{\chi_n^2}{k_o^2 b^2 \tilde{\epsilon}_m(\omega)}}\right\}-\sqrt{1-\frac{\chi_n^2}{k_o^2 b^2 \tilde{\epsilon}_m(\omega)}}}{(\tilde{\vartheta}-2)\sqrt{1-\frac{\chi_n^2}{k_o^2 b^2 \varepsilon_c}}+(\tilde{\vartheta}-1)\sqrt{\left(1-\frac{\chi_n^2}{k_o^2 b^2 \varepsilon_c}\right)\left(1-\frac{\chi_n^2}{k_o^2 b^2 \tilde{\epsilon}_m(\omega)}\right)}-\sqrt{1-\frac{\chi_n^2}{k_o^2 b^2 \tilde{\epsilon}_m(\omega)}}} \tag{4.4.19}$$

$$\tilde{\Gamma}_n = 2\pi \frac{\ln a - \ln b \frac{J_o(\chi_n \ell)}{J_o(\chi_n)}}{\frac{J_o^2(\chi_n \ell)}{J_o^2(\chi_n)}-1} \times$$

$$\frac{1}{(\tilde{\vartheta}-2)\sqrt{1-\frac{\chi_n^2}{k_o^2 b^2 \varepsilon_c}}+(\tilde{\vartheta}-1)\sqrt{\left(1-\frac{\chi_n^2}{k_o^2 b^2 \varepsilon_c}\right)\left(1-\frac{\chi_n^2}{k_o^2 b^2 \tilde{\epsilon}_m(\omega)}\right)}-\sqrt{1-\frac{\chi_n^2}{k_o^2 b^2 \tilde{\epsilon}_m(\omega)}}} \tag{4.4.20}$$

and

$$\tilde{\Theta}_n = \left(1 - (\tilde{\vartheta} - 1)\sqrt{1 - \frac{\chi_n^2}{k_o^2 b^2 \varepsilon_c}}\right)\tilde{\Gamma}_n \ . \tag{4.4.21}$$

In this section, the use of the Fourier-Bessel series theory and the surface impedance concept allowed us to merge the aperture diffraction and the reflection problems using a mathematically rigorous approach.

4.4.2 The Method of Internal Diffraction

This subsection represents an alternative solution for the reflection coefficient of the fundamental mode. Restricting for simplicity, as in the previous section, electromagnetic field to a superposition of TEM and TM_{on} modes and using relation (3.4.1) to express the tangential field component, we can obtain an expression for the surface impedance

$$\tilde{Z}_{TM}|_{z=0^-} = \frac{E_\rho^-}{H_\phi^-} \tag{4.4.22}$$

$$= z_o \frac{\sqrt{\tilde{\varepsilon}_m(\omega)} - \sqrt{\varepsilon_c(\omega)}}{\tilde{\varepsilon}_m(\omega) + \varepsilon_c(\omega)} \tag{4.4.23}$$

$$= - \frac{z_o}{\sqrt{\varepsilon_c}} \frac{1 - \tilde{\Gamma}_o - \sum_{n=1}^{\infty} \frac{\gamma_n}{\gamma_o} \tilde{\Gamma}_n \rho \Psi'_{E_n}(\rho)}{1 + \tilde{\Gamma}_o + \sum_{n=1}^{\infty} \tilde{\Gamma}_n \rho \Psi'_{E_n}(\rho)} \ , \tag{4.4.24}$$

where H_ϕ^- and E_ρ^- are given by (E.7) and (E.8) in Appendix E, and $\Psi_{E_n}(\rho)$ is given by (4.2.4). Comparing (4.4.23) and (4.4.24) and introducing a complex function

$$f(\tilde{\vartheta}) = \frac{\tilde{\vartheta} - 1}{\tilde{\vartheta}^2 + 1} \tag{4.4.25}$$

where

$$\tilde{\vartheta}(\omega) = \sqrt{\frac{\tilde{\varepsilon}_m(\omega)}{\varepsilon_c(\omega)}} \tag{4.4.26}$$

is a discontinuity operator, the following equation is obtained

$$\frac{1}{\rho}\{(f(\tilde{\vartheta}) + 1) + \tilde{\Gamma}_o(f(\tilde{\vartheta}) - 1)\} = \sum_{n=1}^{\infty} \tilde{\Gamma}_n \left\{\frac{\gamma_n}{\gamma_c} - f(\tilde{\vartheta})\right\} \kappa_n \Psi'_{E_n}(\rho) \tag{4.4.27}$$

From the differentiability of the Fourier-Bessel expansion

$$\left(\frac{\gamma_n}{\gamma_c} - f(\tilde{\vartheta})\right)\tilde{\Gamma}_n = \{(f(\tilde{\vartheta})+1) + \tilde{\Gamma}_o(f(\tilde{\vartheta})-1)\}\frac{\pi}{\sqrt{2}}\frac{\kappa_n}{\sqrt{\frac{J_o^2(\kappa_n a)}{J_o^2(\kappa_n b)} - 1}}\int_a^b \ln\rho\Psi_{E_n}(\rho)\rho d\rho \tag{4.4.28}$$

where Ψ_{E_n} is normalized by the constant given by (4.2.6). The term involving integral of Bessel functions is found as

$$I_1 = \frac{\pi}{\sqrt{2}}\frac{\kappa_n}{\sqrt{\frac{J_o^2(\kappa_n a)}{J_o^2(\kappa_n b)} - 1}}\int_a^b \Psi_{E_{mn}}(\rho')\rho' \ln\rho' d\rho'$$

$$= \frac{\pi^2}{2}\frac{\kappa_n^2}{\frac{J_o^2(\kappa_n a)}{J_o^2(\kappa_n b)} - 1}\int_a^b \{J_o(\kappa_n\rho')Y_o(\kappa_n a) - Y_o(\kappa_n\rho')J_o(\kappa_n a)\}\rho'\ln\rho' d\rho'$$

$$= \pi\frac{\ln b\frac{J_o(\kappa_n a)}{J_o(\kappa_n b)} - \ln a}{\frac{J_o^2(\kappa_n a)}{J_o^2(\kappa_n b)} - 1} \tag{4.4.29}$$

$$= \pi\frac{\ln b\frac{J_o(\chi_n \ell)}{J_o(\chi_n)} - \ln a}{\frac{J_o^2(\chi_n \ell)}{J_o^2(\chi_n)} - 1} \tag{4.4.30}$$

The modal reflection coefficient is found from (4.4.28) as

$$\tilde{\Gamma}_n = I_1\frac{\{(f(\tilde{\vartheta})+1) + \tilde{\Gamma}_o(f(\tilde{\vartheta})-1)\}}{\left(\frac{\beta_n}{\beta_o} - f(\tilde{\vartheta})\right)} \tag{4.4.31}$$

Substituting (4.4.31) into (4.2.15), (4.4.6) and (4.4.7), respectively, and subsequently the last three equations into (4.4.1), equation (4.4.1) is dependent on reflection coefficient $\tilde{\Gamma}_o$ of the fundamental mode. After some manipulations, (4.4.1) becomes

$$\frac{1}{\rho}(1+\tilde{\Gamma}_o) + \sum_{n=1}^{\infty} I_1\frac{\{(f(\tilde{\vartheta})+1) + \tilde{\Gamma}_o(f(\tilde{\vartheta})-1)\}}{\left(\frac{\gamma_n}{\gamma_o} - f(\tilde{\vartheta})\right)}\Psi'_{E_n}(\kappa_n\rho) =$$

$$= 2\pi j k_o\sqrt{\varepsilon_c}\sum_{n=1}^{\infty}\left\{\frac{1}{\gamma_n^2} + I_1\frac{\{(f(\tilde{\vartheta})+1) + \tilde{\Gamma}_o(f(\tilde{\vartheta})-1)\}}{\gamma_n^2\left(\frac{\gamma_n}{\gamma_o} - f(\tilde{\vartheta})\right)}\right\}\frac{I_1\{(f(\tilde{\vartheta})+1) + \tilde{\Gamma}_o(f(\tilde{\vartheta})-1)\}}{\left(\frac{\gamma_n}{\gamma_o} - f(\tilde{\vartheta})\right)}\Psi_{E_n}(\kappa_n\rho) \tag{4.4.32}$$

Multiplying (4.4.32) by ρ and integrating from a to b, a second order algebraic equation for the reflection coefficient $\tilde{\Gamma}_o$ is obtained in the following form

$$a(n)\tilde{\Gamma}_o^2 + b(n)\tilde{\Gamma}_o^2 + c(n) = 0 \; . \tag{4.4.33}$$

The coefficients of (4.4.33) are

$$a(n) = \frac{2\pi j k_o\sqrt{\varepsilon_c}}{(b-a)}(f(\tilde{\vartheta})-1)\sum_{n=1}^{\infty}\frac{I_1^2 I_3}{\gamma_n^2\left(\frac{\gamma_n}{\gamma_o}-f(\tilde{\vartheta})\right)} \; , \tag{4.4.34}$$

and

$$\begin{aligned} b(n) =& \frac{4\pi j k_o\sqrt{\varepsilon_c}}{(b-a)}(f^2(\tilde{\vartheta})-1)\sum_{n=1}^{\infty}\frac{I_1^2 I_3}{\gamma_n^2\left(\frac{\gamma_n}{\gamma_o}-f(\tilde{\vartheta})\right)} \\ &+ \frac{2\pi j k_o\sqrt{\varepsilon_c}}{(b-a)}(f(\tilde{\vartheta})-1)\sum_{n=1}^{\infty}\frac{I_1 I_3}{\gamma_n^2\left(\frac{\gamma_n}{\gamma_o}-f(\tilde{\vartheta})\right)} \\ &- \frac{(f(\tilde{\vartheta})-1)}{(b-a)}\sum_{n=1}^{\infty}\frac{I_1 I_2}{\left(\frac{\gamma_n}{\gamma_o}-f(\tilde{\vartheta})\right)} \quad -1 \; , \end{aligned} \tag{4.4.35}$$

and

$$\begin{aligned} c(n) =& \frac{2\pi j k_o\sqrt{\varepsilon_c}}{(b-a)}(f^2(\tilde{\vartheta})+1)\sum_{n=1}^{\infty}\frac{I_1 I_3}{\gamma_n^2\left(\frac{\gamma_n}{\gamma_o}-f(\tilde{\vartheta})\right)} \\ &+ \frac{2\pi j k_o\sqrt{\varepsilon_c}}{(b-a)}(f^2(\tilde{\vartheta})+1)^2\sum_{n=1}^{\infty}\frac{I_1^2 I_3}{\gamma_n^2\left(\frac{\gamma_n}{\gamma_o}-f(\tilde{\vartheta})\right)} \\ &- \frac{(f^2(\tilde{\vartheta})+1)}{(b-a)}\sum_{n=1}^{\infty}\frac{I_1 I_2}{\left(\frac{\gamma_n}{\gamma_o}-f(\tilde{\vartheta})\right)} \quad -1 \end{aligned} \tag{4.4.36}$$

I_1, I_2, and I_3 denote integrals. I_1 is given by (4.4.30). I_2 is found as

$$I_2 = \int_a^b \Psi'_{E_{mn}}(\rho')\rho'\rho' d\rho'$$

$$= -\frac{\pi}{\sqrt{2}} \frac{\kappa_n^2}{\sqrt{\frac{J_o^2(\kappa_n a)}{J_o^2(\kappa_n b)} - 1}} \int_a^b \{J_1(\kappa_n \rho')Y_o(\kappa_n a) - Y_1(\kappa_n \rho')J_o(\kappa_n a)\}\rho' d\rho'$$

$$= \frac{\frac{1}{\ell} - \frac{J_o(\chi_n \ell)}{J_o(\chi_n)}}{\sqrt{2}\chi_n \sqrt{\frac{J_o^2(\chi_n \ell)}{J_o^2(\chi_n)} - 1}}, \tag{4.4.37}$$

while I_3 is equal to:

$$I_3 = \frac{\pi}{\sqrt{2}} \frac{\kappa_n}{\sqrt{\frac{J_o^2(\kappa_n a)}{J_o^2(\kappa_n b)} - 1}} \int_a^b \{J_o(\kappa_n \rho')Y_o(\kappa_n a) - Y_o(\kappa_n \rho')J_o(\kappa_n a)\}\rho' d\rho'$$

$$= \frac{b\sqrt{2}}{\chi_n} \sqrt{\frac{\frac{J_o(\chi_n \ell)}{J_o(\chi_n)} - 1}{\frac{J_o(\chi_n \ell)}{J_o(\chi_n)} + 1}}. \tag{4.4.38}$$

The coefficients of (4.4.33) are dimensionless. The solution of (4.4.34) was found by using a computer technique. Results of the computer simulation are presented in Chapter V

4.5 The Input Admittance

4.5.1 The Lumped Element Model in Coaxial Lines

The propagation and distribution of electromagnetic fields is considerably modified by the presence of spatial discontinuities. A detailed description of this modification, although formally possible, is frequently unnecessary in bounded or so-called waveguide regions where one is concerned primarily with the control and distribution of electromagnetic power. In these regions, it is necessary to describe the modification only in terms of the constituent modes of the electromagnetic fields that carry power. It is this simplifying feature that permits to use of equivalent circuits to describe the effects of discontinuities both at low and high frequencies.

At low frequencies, geometrical discontinuities on wires are generally "lumped" in the form of coils, condensers, etc., whose dimensions are small compared with the wavelength. The effects of such discontinuities on the distribution of electromagnetic fields along the wires may be described almost everywhere in terms of only a single mode and schematically represented by a lumped equivalent circuit. The evanescent modes excited by the aperture store reactive energy until they are attenuated at some finite distance from the aperture. This distance can be defined as that corresponding to the value of a modal reflection coefficient equal to the noise level of a typical network analyzer which is -80 dB. These distances (or penetration depths) for the coaxial sensors used in practice are illustrated in Fig. 4.4.

The use of circuit representation stems from the introduction of voltages and currents as measures of the electric and magnetic fields of this single mode at "terminals" far from the discontinuity (i.e., far in terms of penetration distance defined above). These terminal voltages and currents characterize completely the flow of power into and out of the given structure, but are rather inadequate measures of the detailed fields within the discontinuities. The circuit picture provides a schematic representation of the relations among the terminal voltages and currents in terms of impedance parameters characteristic to the discontinuities. The wires connecting the discontinuities play nonessential role in this circuit model, since the voltages and currents do not vary along the wires. The quantitative derivation of these circuit relations from the fundamental field equations (Maxwell's equations $\rightarrow$ Kirchhoff's laws), requires that expressions for the electromagnetic fields at every point of the discontinuity are obtained in terms of the densities of the actual currents and charges flowing in and on it. Since at low frequencies a discontinuity is regarded as situated in free space, the desired field expressions may be obtained classically from the vector and scalar potentials produced by the unknown currents and charges on the discontinuities. The imposition of the boundary conditions to be satisfied by the fields on the discontinuities, leads to integral equations for the actual current and charge densities. By integrating and lumping the spatial dependence of these equations, one derives the desired circuit equations in terms of inductance or capacitance.

The presence of the aperture is seen from the terminal plane as a change in the input admittance of the fundamental, dominant wave. This change is in the amount of the additional energy stored within higher order modes. In bounded structures, it is generally difficult to solve field problems directly because of the complexities of geometry, i.e., the presence of the obstacle and aperture discontinuities. Therefore, it is convenient to replace the perturbing obstacle or aperture by equivalent distributions of electric and magnetic surface currents [14].

The convenient form of Maxwell's equations for solving this class of problems is obtained from (2.1.22-23) for steady state, time-harmonic fields provided that the steady state exists. Upon applying Fourier transform to (2.1.22-23) we obtain:

$$\nabla \times \vec{\mathbf{E}} = -j\omega\mu_0\vec{\mathbf{H}} - \vec{\mathbf{J}}_m \tag{4.5.1}$$

$$\nabla \times \vec{\mathbf{H}} = j\omega\epsilon_0\vec{\mathbf{E}} + \vec{\mathbf{J}}_e \ . \tag{4.5.2}$$

In this formulation $\vec{\mathbf{E}}$ and $\vec{\mathbf{H}}$ represent the Fourier transform of the total fields while

$$\vec{\mathbf{J}}_m = j\omega\mu_0\vec{\mathbf{M}} \tag{4.5.3}$$

and

$$\vec{\mathbf{J}}_e = \vec{\mathbf{j}}_F + j\omega\vec{\mathbf{P}} \ + \nabla \times \vec{\mathbf{J}}_m. \tag{4.5.4}$$

By comparing (2.1.22-23) and (4.5.1-4), it is evident that the meaning of electric and magnetic currents depends on the field quantities of interest. The full equivalence of both formulations is apparent when the wave equations are derived from (4.5.1-2), i.e.

$$(\nabla^2 + k^2)\vec{\mathbf{E}} = j\omega\mu_0(\vec{\mathbf{J}}_e + \nabla \times \vec{\mathbf{J}}_m) \tag{4.5.5}$$

$$(\nabla^2 + k^2)\vec{\mathbf{H}} = j\omega\epsilon_0\Big(\vec{\mathbf{J}}_m - \frac{1}{j\omega\epsilon_0}\nabla \times \vec{\mathbf{J}}_e\Big) \tag{4.5.6}$$

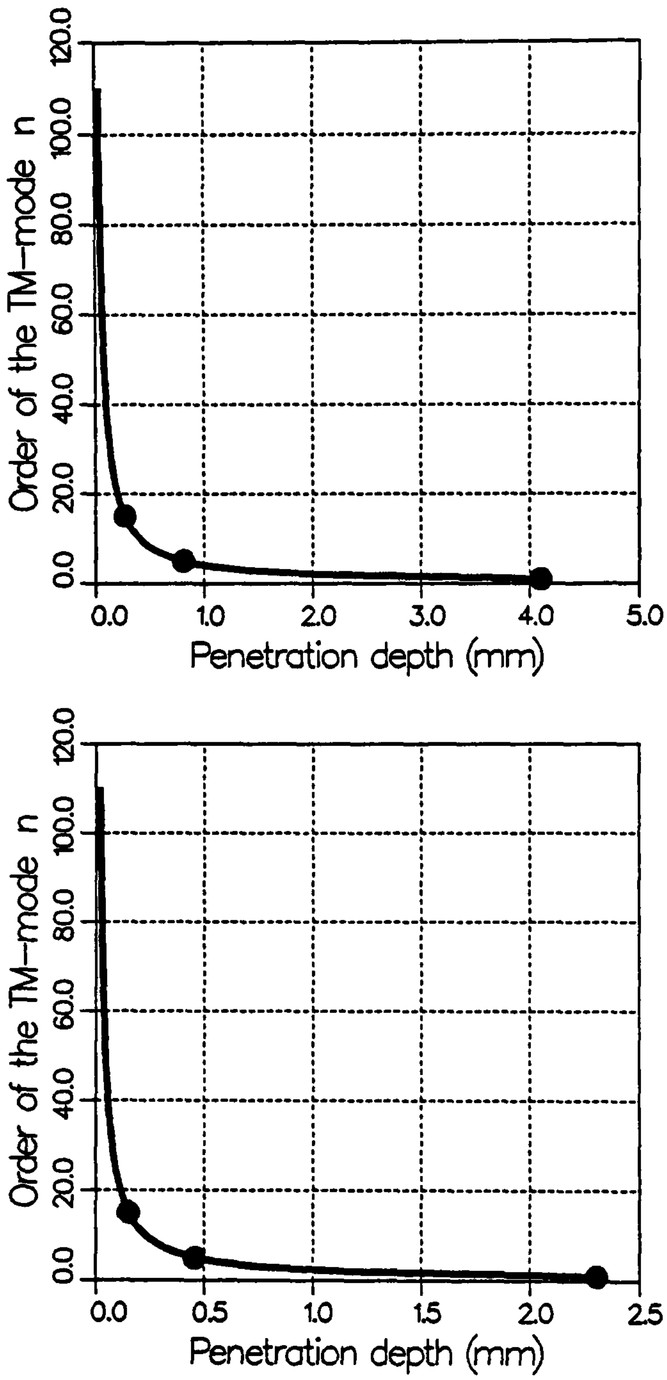

Fig. 4.4

Penetration depth of the evanescent TM-modes excited at the aperture of coaxial sensors used in precision measurements:
a: above: O.D. 6.35 mm, b: below: O.D. 3.58 mm.
• • • correspond to 1, 5 and 15 mode number, respectively.
Frequency: 2.69 GHz.

The term $\nabla \times \vec{\mathbf{J}}_m$ contributes to the total electric current and the term $\nabla \times \vec{\mathbf{J}}_e$ contributes to the total magnetic current.

There is a significant difference in the meaning of those terms. In bounded structures, the currents in the right hand side of (4.5.1-6) are regarded as surface currents such that obstacles and aperture discontinuities are replaced by surface currents according to the Schelkunoff equivalence principle [83]. The final results are

$$[\vec{\mathbf{H}}_t(\vec{\mathbf{x}}) \times \vec{\mathbf{n}}]_+^- = \vec{\mathbf{J}}_{et} + \frac{1}{j\omega\mu_0}\nabla_t \times \vec{\mathbf{J}}_{m\zeta}(\vec{\mathbf{x}}) \tag{4.5.7}$$

and

$$[\vec{\mathbf{n}} \times \vec{\mathbf{E}}_t(\vec{\mathbf{x}})]_+^- = \vec{\mathbf{J}}_{mt} + \frac{1}{j\omega\epsilon_0}\nabla_t \times \vec{\mathbf{J}}_{e\zeta}(\vec{\mathbf{x}}) \ , \tag{4.5.8}$$

where $[\ ]_+^-$ denotes the discontinuity in the field component in the left ζ_o^- and right ζ_o^+ sides of the discontinuity, $\vec{\mathbf{n}}$ denotes the unit vector normal to the surface and colinear with ζ axis in local coordinate system, while subscripts t and ζ denote the transverse and the normal components, respectively. The transverse (surface) operator ∇_t is described in coordinate free notation as:

$$\nabla_t = \nabla - \vec{\mathbf{n}}\frac{\partial}{\partial n} \ . \tag{4.5.9}$$

Equations (4.5.1.7-8) show that the field at a given surface is not necessarily tangential to this surface. However, right hand sides of these equations represent magnetic and electric current densities tangential to the given surface. These equations represent the Schwinger generalization of Schelkunoff's equivalence principle [14].

The fundamental advantage of the equivalent circuit is that the well developed circuit theory can be used. It also offers a powerful tool for fast solution of practical problems such as: calibration, matching, shielding, coupling, etc. From the point of view of the field theory, the equivalent circuit usually provides the means of verification of the theoretical derivation.

---

[83] S.A Schelkunoff, "Electromagnetic Waves", *op. cit.*, pp. 74-75.

4.5.2 The Lumped Element Model for the Coaxial Probe

When the complex reflection coefficient is known, the equivalent modal input admittance is given as [84]:

$$\tilde{Y}_{mn} = G_{mn} + jB_{mn} = \frac{1 - \tilde{\Gamma}_{mn}}{1 + \tilde{\Gamma}_{mn}}. \tag{4.5.10}$$

When non-rotationally symmetric modes are used, i.e., TM_{mn} modes (for $m > 0$), the important engineering implication is that this is equivalent to the analysis extended to 3-dimensions and, therefore, a correction to the equivalent input admittance is expected. Another method of evaluation of the aperture admittance is based on the following equation obtained from the total power at the aperture [85]

$$\tilde{Y}_a = \frac{1}{V_-^2} \int_{S_a} (\vec{\mathbf{E}}^- \times \vec{\mathbf{H}}^-) \cdot d\vec{S} \bigg|_{int} . \tag{4.5.12}$$

Defining the reference voltage at the aperture surface S_a as

$$V_- = \int_{S_a} \vec{\mathbf{E}}_\rho \cdot \hat{\mathbf{e}}_\rho dS, \tag{4.5.13}$$

the following equation is implied for the internal problem

$$\tilde{Y}_a^- = \frac{\int_{S_a} (\vec{\mathbf{E}}^- \times \vec{\mathbf{H}}^-) \cdot d\vec{S} \Big|_{int}}{\left\{ \int_{S_a} \vec{\mathbf{E}}_\rho \cdot \hat{\mathbf{e}}_\rho dS \right\}^2} \tag{4.5.14}$$

and for the external part of the aperture

$$\tilde{Y}_a^+ = \frac{1}{V^{2+}} \int_{S_a} (\vec{\mathbf{E}}_t^+ \times \vec{\mathbf{H}}^+) \cdot d\vec{S} . \tag{4.5.15}$$

The change in admittance level results in the coupling coefficient $c_c(\omega)$ which is defined as

$$c_c^2(\omega) = \frac{\tilde{Y}_a^+}{\tilde{Y}_a^-} \tag{4.5.16}$$

[84] C. Fray, N. Khayata and A. Papiernik, "TM_{01} Admittance and Radiation from Open-ended Waveguide into Layered Absorbing Media", Archiv für Elektronik und Übertragungtechnik, B 36, No 3, 1982, pp. 107-110

[85] R.F Harrington, *op. cit.*, pp. 420-422.

The coupling coefficient is modelled as an ideal transformer having a real turns ratio and a complex series impedance.

$$\tilde{Y}_a = \frac{y_o\sqrt{\varepsilon_c}}{2\pi} \times$$

$$\times \frac{(1-\tilde{\Gamma}_o^2)\ln\frac{b}{a} + (1+\tilde{\Gamma}_o)\sum_{n=1}^{\infty}\frac{\gamma_n}{\gamma_c}\tilde{\Gamma}_n\int_a^b \Psi'_{E_n}(\chi\frac{\rho}{b})d\rho}{(1-\tilde{\Gamma}_o)^2(b-a) - 2(1-\tilde{\Gamma}_n)(b-a)\sum_{n=1}^{\infty}\frac{\gamma_n}{\gamma_c}\tilde{\Gamma}_n\int_a^b \Psi'_{E_n}(\chi\frac{\rho}{b})\rho d\rho}\cdots$$

$$\cdots\frac{(1-\tilde{\Gamma}_o)\sum_{n=1}^{\infty}\tilde{\Gamma}_n\int_a^b \Psi'_{E_n}(\chi\frac{\rho}{b})d\rho - \sum_{n=1}^{\infty}\tilde{\Gamma}_n^2\frac{\gamma_n}{\gamma_c}}{+\left\{\sum_{n=1}^{\infty}\tilde{\Gamma}_n\frac{\gamma_n}{\gamma_c}\int_a^b \Psi'_{E_n}(\chi\frac{\rho}{b})\rho d\rho\right\}^2} \tag{4.5.17}$$

where $\tilde{\Gamma}_o$ and $\tilde{\Gamma}_n$are given by (4.4.19) and (4.4.20), respectively. In order to derive (4.5.17), the theory presented in Section 4.4.1 was used.

Although the expression (4.5.17) for the aperture admittance is rigorous, it is very difficult to separate real and imaginary parts of the aperture admittance. The complete picture of the input admittance also includes the contribution due to evanescent modes. The internal problem (the terminal region) contributes to the internal susceptance of the input admittance. Lumping of internal problem and aperture admittances leads to the complete equivalent circuit of the input admittance. The details of the model are described in the next chapter.

V. Numerical Results and Applied Aspects of Dielectric Reflection Spectroscopy

5.1 Numerical and Experimental Results for the Reflection Coefficient

Available experimental data* for the reflection coefficient are used for the comparison between experimental and theoretical curves.

Two types of lines: O.D. 3.58 mm and O.D. 6.35 mm were immersed in three different dielectrics: distilled water, formamide and methanol. The measurement of the complex reflection coefficient was performed with the HP8510A automatic network analyzer. The characteristic uncertainty in phase was 0.1^o at $|\Gamma| = 1$.

The method described in Section 4.4.2 was used to obtain the theoretical curves.

The comparison between theory and experiment is made for two coaxial lines immersed in distilled water (Fig. 5.1). Similar comparisons are made for the same lines for formamide and methanol in Figs. 5.2 and 5.3, respectively. The results show that the presence of the higher order modes has significant influence on the reflection coefficient. For the fundamental TEM-mode, they exhibit in the decrease of the magnitude of the reflection coefficient and in the increase of the phase shift with respect to the low frequency reference point as frequency increases. These occur for all dielectric materials investigated: distilled water, formamide and methanol. The same conclusion was drawn in [59]. The experimental and the theoretical values of reflection coefficient are within ± 10 % below 5 GHz. At frequencies above 5 GHz theoretical and experimental results diverge. The reason for this is due to the approximation in deriving (4.4.1) [80] being the basis for theoretical method of the reflection coefficient evaluation. Each of the figures 5.1-5.3 gives a good picture of the influence of the aperture size on the reflection coefficient and subsequently the input admittance, since properties of the medium are the same. This data may also serve as the basis for determination a regression model for the reflection coefficient.

* A. Kraszewski, private communication, 1986.

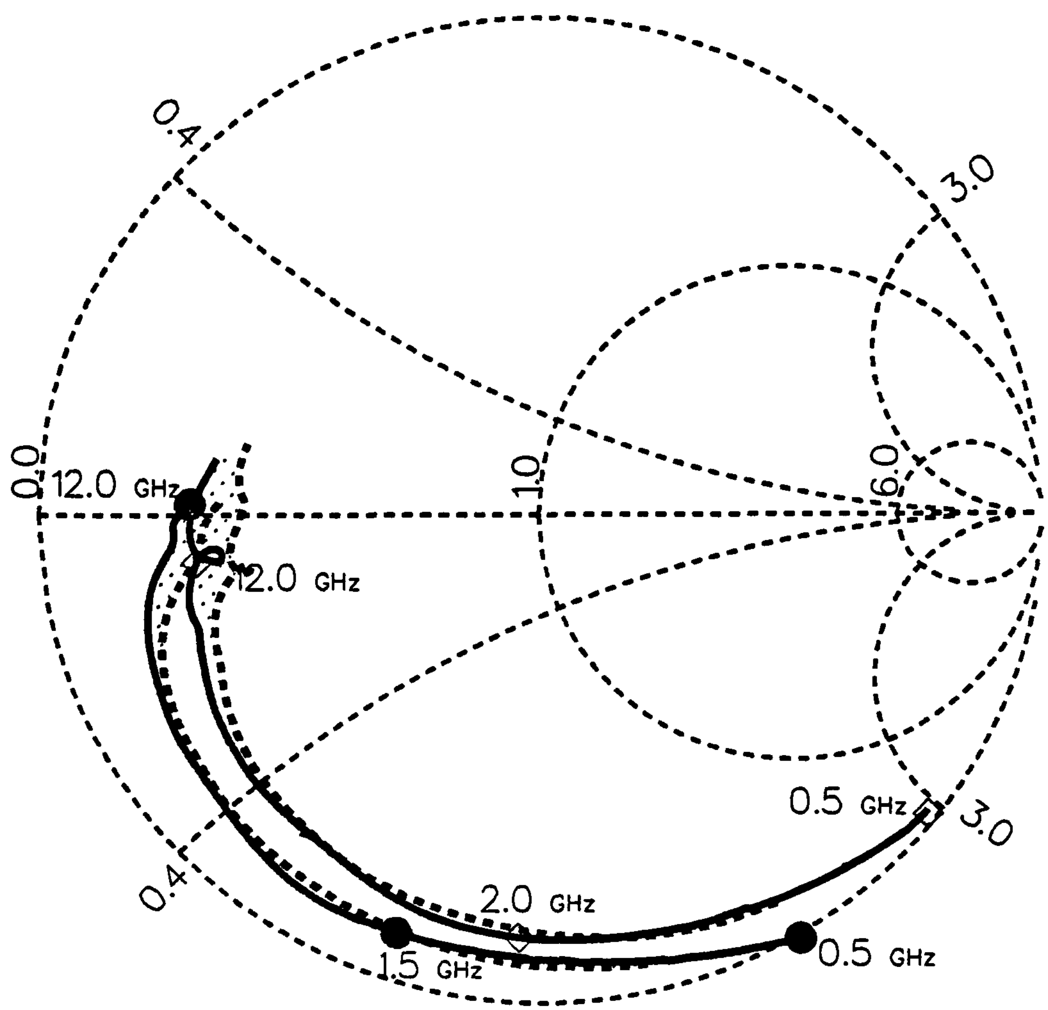

Fig. 5.1

The input impedance of open-ended coaxial lines having dimensions: O.D. 6.35 *mm* • and O.D. 3.58 *mm* ◇ and immersed in distilled water at 25°C. Solid lines - experimental curves; dashed lines theoretical model. Shaded areas show the difference between theoretical and experimental data.

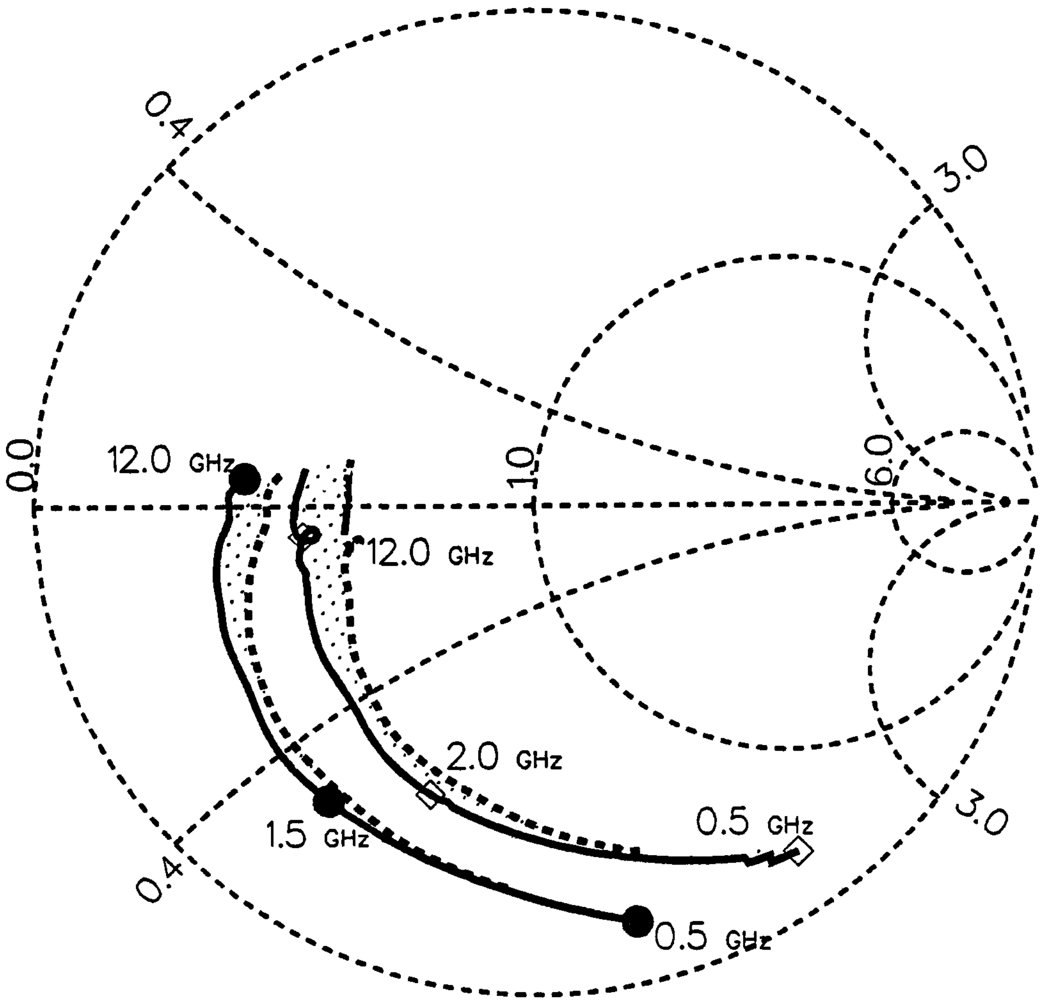

Fig. 5.2

The input impedance of open-ended coaxial lines having dimensions: O.D. 6.35 *mm*• and O.D. 3.58 *mm* ◇ and immersed in formamide at 25^oC. Solid lines - experimental curves; dashed lines theoretical model. Shaded areas show the difference between theoretical and experimental data.

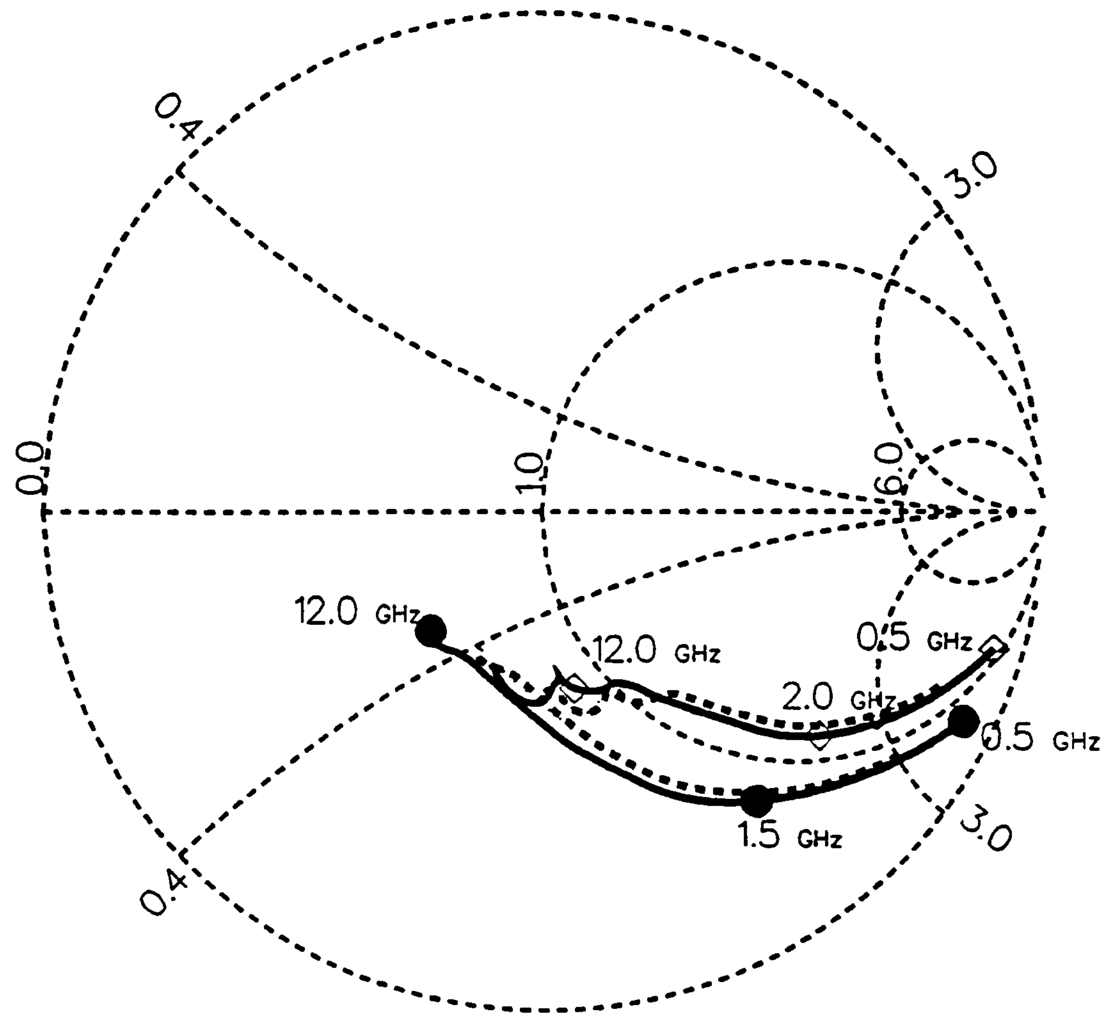

Fig. 5.3

The input impedance of open-ended coaxial lines having dimensions: O.D. 6.35 mm• and O.D. 3.58 mm ◇ and immersed in methanol at 25°C. Solid lines experimental curves; dashed lines theoretical model. Shaded areas show the difference between theoretical and experimental data.

5.2 Numerical Results for the Input Admittance

Because of the extreme complexity of the exact analysis in Chapter IV and other analysis of this type, e.g., [59] and subsequent considerable computational effort to obtain the permittivity of interest, most workers have used the approximate equivalent circuit model to provide a simpler, but less accurate, way to determine the permittivity from the sensor input admittance. The models used in the experiment and derived in this work are shown in Fig. 5.7-a. The reflection coefficient was transformed by (4.5.10) to the admittance plane, although the input admittance can be read directly from the Smith Chart of the reflection coefficient. The reason for that is to present it separately as a function of frequency for a given sensor. Fig. 5.4 shows the conductance and susceptance of the two probes in distilled water whose reflection coefficients are depicted in Fig. 5.1. Figures 5.5 and 5.6. shown the conductance and the susceptance of two probes immersed in formamide and methanol at 25 ^{o} C, respectively. Reflection coefficients for these probes are depicted in Figs. 5.2 and 5.3. In order to explain the behavior of the sensor in the vicinity of resonance, a new model is derived for the equivalent circuit. This model is depicted in Fig. 5.7-b. It appears to be reasonably adequate to describe the observed behavior of the sensor, as it predicts the parallel resonance in the terminal area.

The approximate method leading to the curves depicted in Figs. 5.1-5.3 does not allow us to determine explicitly the values of the elements of the equivalent circuit. Therefore, the method described in section 4.5.2 is utilized, and detailed derivations using this method are carried out in Section 5.3.

Another method of practical importance is the identification technique for determination of elements of the equivalent circuit, and this method is developed in Section 5.4.

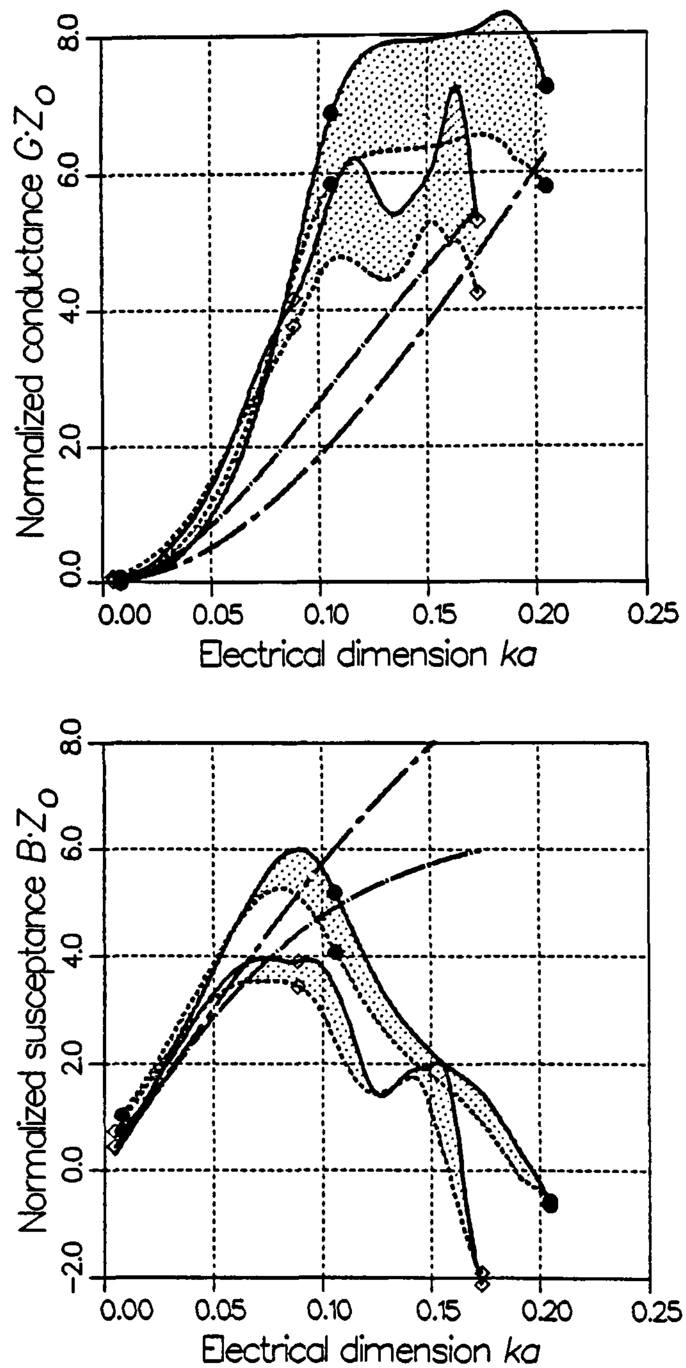

Fig. 5.4

Experimental and theoretical curves of normalized conductance and susceptance of open-ended coaxial lines: O.D. 6.35 *mm* • and O.D. 3.58 *mm* ◇ immersed in distilled water at 25°*C*. Solid lines: experimental curves dashed lines · theoretical model. Shaded areas show the difference between theoretical and experimental data. Uncertainty of experimental data: ±11.4% in GZ_o and ±0.6% in BZ_o at 1 GHz. Chain-dotted and chain-dashed lines correspond to the quasi-static model [60] for O.D. 6.35 *mm* and O.D. 3.58 *mm*, respectively.

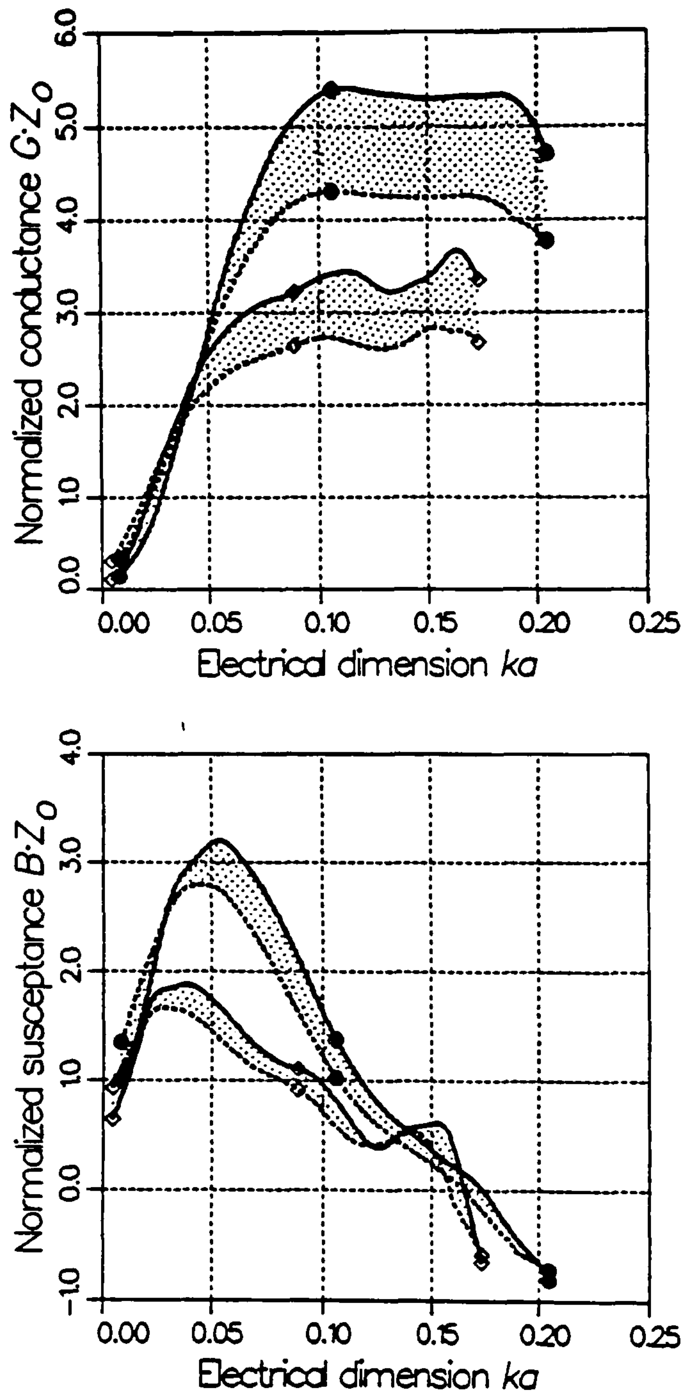

Fig. 5.5

Experimental and theoretical curves of normalized conductance and susceptance of open-ended coaxial lines: O.D. 6.35 mm • and O.D. 3.58 mm ◇ immersed in formamide at 25^oC. Solid lines experimental curves: dashed lines theoretical model. Shaded areas show the difference between theoretical and experimental data. Uncertainty of experimental data: $\pm 11.4\%$ in GZ_o and $\pm 0.6\%$ in BZ_o at 1 GHz.

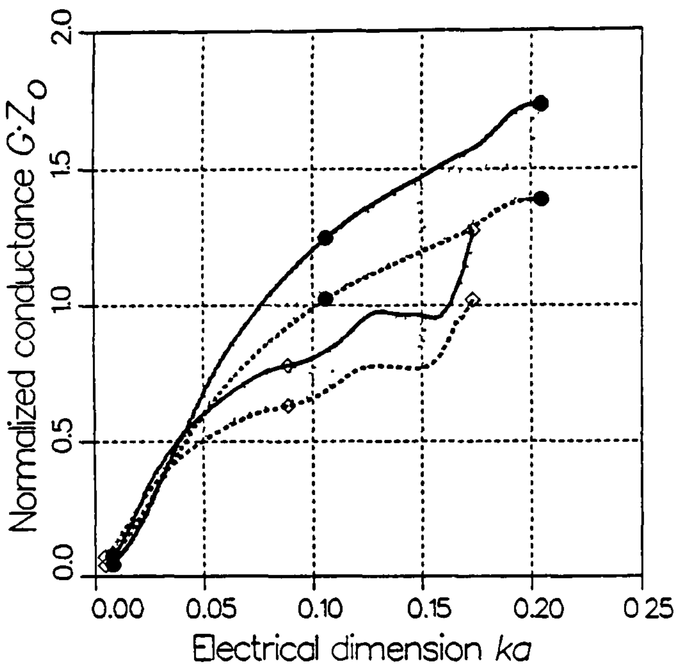

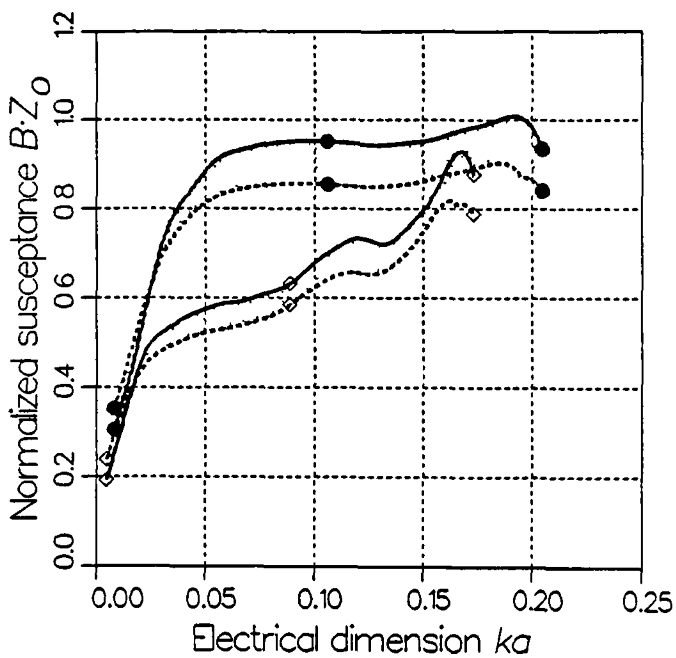

Fig. 5.6

Experimental and theoretical curves of normalized conductance and susceptance of open-ended coaxial lines: O.D. 6.35 mm • and O.D. 3.58 mm ◇ immersed in methanol at 25^oC Solid lines experimental curves· dashed lines theoretical model. Shaded areas show the difference between theoretical and experimental data. Uncertainty of experimental data. $\pm 11.4\%$ in GZ_o and $\pm 0.6\%$ in BZ_o at 1 GHz.

5.3 Analytical Determination of Lumped Elements of the Equivalent Circuit

5.3.1 The Terminal Region

The terminal region is understood as the volume of the coaxial line between the aperture plane S_a and the plane called the terminal plane S_t where all evanescent modes disappear. In the terminal region there are of evanescent modes which contribute to the value of the input admittance beyond the terminal plane. The length of the terminal region l is equal to the penetration depth of the lowest TM-mode as shown in Fig. 4.4 for two coaxial sensors. This region may be lumped provided that $l << 2\pi/(k_o\sqrt{\varepsilon_c})$. For -60 dB attenuation level of the first TM-mode, the penetration distance is given as

$$l = \frac{\ln 0.001}{\sqrt{\frac{\chi_1^2}{b^2} - k_o^2\varepsilon_c}} \; . \tag{5.3.1}$$

In order to establish the physical nature of the terminal function, consider the complex integral form [86] of (2.2.2) which is

$$\frac{1}{2}\oint_{S_v}(\vec{\mathbf{E}} \times \vec{\mathbf{H}}^*) \;\; d\vec{S} = 2j\omega\int_V\Big(\frac{\mu_0\vec{\mathbf{H}} \;\; \vec{\mathbf{H}}^*}{2} - \frac{\varepsilon_c\vec{\mathbf{E}} \;\; \vec{\mathbf{E}}^*}{2}\Big)dV + \frac{1}{2}\int_V \vec{\mathbf{E}} \;\; \vec{\mathbf{J}}^* dV \; , \tag{5.3.2}$$

where S_v denotes the surface surrounding volume V. The surface integral results from application of the divergence theorem to a volume integral of the complex Poynting vector divergence.

For the terminal region of the coaxial sensor, (5.3.2) reduces to

$$\frac{1}{2}\int_{S_t}(\vec{\mathbf{E}}_\rho \times \vec{\mathbf{H}}_\phi^*) \;\; \vec{\mathbf{e}}_z d\,S - \frac{1}{2}\int_{S_a}(\vec{\mathbf{E}}_\rho^- \times \vec{\mathbf{H}}_\phi^{*-}) \cdot \vec{\mathbf{e}}_z d\,S = 2j\omega(W_e - W_m) \; , \tag{5.3.3}$$

where W_e and W_m denote electric and magnetic energy stored in terminal area, respectively. The contribution from coaxial line walls vanishes because of the condition: $\vec{\mathbf{E}}_z \times \vec{\mathbf{H}}_\phi|_{\rho=a,\, \rho=b} = 0$.

Repeating the procedure leading to (4.5.17) with the use of the complex conjugate of $\vec{\mathbf{H}}_\phi$, it is found that

---

[86] R.E. Collin, "Field Theory of Guided Waves", *op. cit.*, p 181-182.

$$\frac{1}{2}\int_{S_a}(\vec{\mathbf{E}}\times\vec{\mathbf{H}}^*)\cdot\vec{\mathbf{e}}_z d\,S =$$

$$= \pi\frac{z_o}{\sqrt{\varepsilon_c}}\ln\frac{a}{b}\left[1+2j\Im\tilde{\Gamma}_o-(\Re\tilde{\Gamma}_o)^2-(\Im\tilde{\Gamma}_o)^2\right]$$

$$-j\pi\frac{z_o}{\sqrt{\varepsilon_c}}\sum_{n-1}^{\infty}\sqrt{\frac{\chi_n^2}{k_o^2b^2\varepsilon_c}-1}\left[(\Re\tilde{\Gamma}_n)^2+(\Im\tilde{\Gamma}_n)^2\right]\,. \tag{5.3.4}$$

Orthonormality of eigenfunctions for the coaxial region was used to derive the last term.

The sole contribution to the surface integral over the terminal plane S_t comes from the fundamental TEM mode. The result is:

$$\frac{1}{2}\int_{S_t}(\vec{\mathbf{E}}\times\vec{\mathbf{H}}^*)\cdot\vec{\mathbf{e}}_z d\,S =$$

$$= \pi\frac{z_o}{\sqrt{\varepsilon_c}}\ln\frac{a}{b}\left\{1-(\Re\tilde{\Gamma}_o)^2-(\Im\tilde{\Gamma}_o)^2-2j\left[\Im\tilde{\Gamma}_o\cos(2\gamma_c l)+\Re\tilde{\Gamma}_o\sin(2\gamma_c l)\right]\right\} \tag{5.3.5}$$

Substituting (5.3.4) and (5.3.5) into (5.3.3), it is found that

$$2j\omega(W_e-W_m)=$$

$$j\frac{2\pi z_o}{\sqrt{\varepsilon_c}}\left\{\ln\frac{b}{a}\Im\tilde{\Gamma}_o+\frac{1}{2}\sum_{n-1}^{\infty}\sqrt{\frac{\chi_n^2}{k_o^2b^2\varepsilon_c}-1}\left[(\Re\tilde{\Gamma}_n)^2+(\Im\tilde{\Gamma}_n)^2\right]-\ln\frac{b}{a}\left[\Im\tilde{\Gamma}_o\cos(2\gamma_c l)+\Re\tilde{\Gamma}_o\sin(2\gamma_c l)\right]\right\} \tag{5.3.6}$$

Noting that

$$W_e=\frac{1}{4}C_f VV^* \tag{5.3.7}$$

and

$$W_e=\frac{1}{4}L_f II^*\ , \tag{5.3.8}$$

we can evaluate VV^* and II^* at terminal plane S_t. Comparing with (5.3.3), it is found that

$$C_f = \frac{y_o\sqrt{\varepsilon_c}}{\omega}\frac{1}{\ln\frac{b}{a}} \times \\ \times \frac{\frac{1}{2}\sum_{n-1}^{\infty}\sqrt{\frac{\chi_n^2}{k_o^2 b^2 \varepsilon_c} - 1}\left\{(\Re\tilde{\Gamma}_n)^2 + (\Im\tilde{\Gamma}_n)^2\right\} + \Im\tilde{\Gamma}_o \ln\frac{b}{a}}{1 + 2\left(\Im\tilde{\Gamma}_o \sin(2\gamma_c l) - \Re\Gamma_o \cos(2\gamma_c l)\right) + (\Re\tilde{\Gamma}_o)^2 + (\Im\tilde{\Gamma}_o)^2} \tag{5.3.9}$$

and

$$L_f = \frac{z_o}{\omega\sqrt{\varepsilon_c}}\frac{1}{\ln\frac{b}{a}} \times \\ \times \frac{\Im\tilde{\Gamma}_o \cos(2\gamma_c l) + \Re\Gamma_o \cos(2\gamma_c l)}{1 + 2\left(\Re\tilde{\Gamma}_o \cos(2\gamma_c l) - \Im\Gamma_o \sin(2\gamma_c l)\right) + (\Re\tilde{\Gamma}_o)^2 + (\Im\tilde{\Gamma}_o)^2} . \tag{5.3.10}$$

The reference voltage and current are chosen at the terminal plane $z = -l$.

5.3.2 The Aperture Region

The aperture region consists of the interface between two media: the teflon of the coaxial sensor and the dielectric medium under investigation. Because of power loss across the aperture due to surface current, the complex Poynting theorem has the form

$$\frac{1}{2}\int_{S_a^-}(\vec{\mathbf{E}}_\rho^- \times \vec{\mathbf{H}}_\phi^{*-}) \ \vec{\mathbf{e}}_z d\,S - \frac{1}{2}\int_{S_a^+}(\vec{\mathbf{E}}_\rho^+ \times \vec{\mathbf{H}}_\phi^{*+}) \cdot \vec{\mathbf{e}}_z d\,S = P_l + 2j\omega(W_e - W_m) \tag{5.3.11}$$

Contributions due to infinitesimal surface corresponding to edges of the aperture vanish since $\vec{\mathbf{E}}_z \times \vec{\mathbf{H}}_\phi|_{\rho=a,\rho=b} = 0$.

Repeating the same procedure as that leading to (5.3.9) and (5.3.10) and noting that

$$C_a = \frac{4W_e}{VV^*} , \tag{5.3.12}$$

it is found that aperture capacitance C_a is given as

$$C_a = \frac{y_o \varepsilon_c}{\omega \pi \ln \frac{b}{a}} \times$$

$$\times \frac{\frac{2\pi}{\sqrt{\varepsilon_c}} \ln \frac{b}{a} \Re\tilde{\Gamma}_o + \frac{4}{\pi} \sum_{n=1}^{\infty} f_1\{\chi_n, \tilde{\epsilon}(\omega)\}\{(\Re\tilde{\Theta}_n)^2 + (\Im\tilde{\Theta}_n)^2\} \left(\frac{J_o^2(\chi_n \ell)}{J_o^2(\chi_n)} - 1\right)}{1 + 2\Big(\Im\tilde{\Gamma}_o \sin(2\gamma_c l) - \Re\Gamma_o \cos(2\gamma_c l)\Big) + (\Re\tilde{\Gamma}_o)^2 + (\Im\tilde{\Gamma}_o)^2} , \tag{5.3.13}$$

where

$$f_1(\chi_n, \tilde{\epsilon}(\omega)) = \Re\left(\frac{1}{\sqrt{\tilde{\epsilon}_m(\omega)}}\right) \Im\sqrt{1 - \frac{\chi_n}{k_o^2 b^2 \tilde{\epsilon}_m(\omega)}} + \Re\sqrt{1 - \frac{\chi_n}{k_o^2 b^2 \tilde{\epsilon}_m(\omega)}} \Im\left(\frac{1}{\sqrt{\tilde{\epsilon}_m(\omega)}}\right) \tag{5.3.14}$$

Reference voltage V^- is chosen at the same reference plane as for terminal region, i.e. at $z = -l$. By noting that the aperture conductance

$$G_a = \frac{2P_l}{VV^*} , \tag{5.3.15}$$

it is found that

$$G_a = \frac{y_o \varepsilon_c}{\pi \ln \frac{b}{a}} \times$$

$$\times \frac{\frac{\pi}{\sqrt{\varepsilon_c}} \ln \frac{b}{a} \left\{1 - \left[(\Re\tilde{\Gamma}_o)^2 + (\Im\tilde{\Gamma}_o)^2\right]\right\} - \frac{4}{\pi} \sum_{n=1}^{\infty} f_2\{\chi_n, \tilde{\epsilon}(\omega)\}\{(\Re\tilde{\Theta}_n)^2 + (\Im\tilde{\Theta}_n)^2\} \left(\frac{J_o^2(\chi_n \ell)}{J_o^2(\chi_n)} - 1\right)}{1 + 2\Big(\Im\tilde{\Gamma}_o \sin(2\gamma_c l) - \Re\Gamma_o \cos(2\gamma_c l)\Big) + (\Re\tilde{\Gamma}_o)^2 + (\Im\tilde{\Gamma}_o)^2} , \tag{5.3.16}$$

where

$$f_2\{\chi_n, \tilde{\epsilon}(\omega)) = \Im\left(\frac{1}{\sqrt{\tilde{\epsilon}_m(\omega)}}\right) \Im\sqrt{1 - \frac{\chi_n}{k_o^2 b^2 \tilde{\epsilon}_m(\omega)}} - \Re\sqrt{1 - \frac{\chi_n}{k_o^2 b^2 \tilde{\epsilon}_m(\omega)}} \Re\left(\frac{1}{\sqrt{\tilde{\epsilon}_m(\omega)}}\right) \tag{5.3.17}$$

The radiation conductance is found by using (5.3.15) with respect to power transferred into the medium.

The final result is given by

$$G_r = \frac{y_o \varepsilon_c}{\pi \ln \frac{b}{a}} \times \\ \times \frac{\frac{4}{\pi}\sum_{n=1}^{\infty} -f_2(\chi_n, \tilde{\epsilon}(\omega))\{(\Re\tilde{\Theta}_n)^2 + (\Im\tilde{\Theta}_n)^2\}\left(\frac{J_o^2(\chi_n \ell)}{J_o^2(\chi_n)} - 1\right)}{1 + 2\Big(\Im\tilde{\Gamma}_o \sin(2\gamma_c l) - \Re\Gamma_o \cos(2\gamma_c l)\Big) + (\Re\tilde{\Gamma}_o)^2 + (\Im\tilde{\Gamma}_o)^2}, \tag{5.3.18}$$

The net electric energy stored in the medium gives capacitance C_d from equation (5.3.7)

$$C_d = \frac{y_o \varepsilon_c}{\omega \pi \ln \frac{b}{a}} \times \\ \times \frac{\frac{4}{\pi}\sum_{n=1}^{\infty} f_1(\chi_n, \tilde{\epsilon}(\omega))\{(\Re\tilde{\Theta}_n)^2 + (\Im\tilde{\Theta}_n)^2\}\left(\frac{J_o^2(\chi_n \ell)}{J_o^2(\chi_n)} - 1\right)}{1 + 2\Big(\Im\tilde{\Gamma}_o \sin(2\gamma_c l) - \Re\Gamma_o \cos(2\gamma_c l)\Big) + (\Re\tilde{\Gamma}_o)^2 + (\Im\tilde{\Gamma}_o)^2}, \tag{5.3.19}$$

where $\tilde{\Gamma}_o$, $\tilde{\Gamma}_n$ and $\tilde{\Theta}_n$ are given by the solution of the diffraction problem at the aperture in section 4.4.1, i.e. equations (4.4.19), (4.4.20) and (4.4.21). Capacitance C_d corresponds to the radiation susceptance.

The terminal region has the characteristic impedance $Z_c = \sqrt{L_f/C_f}$. It represents the inhomogeneous section of the coaxial line. The parallel equivalent circuit of the coaxial sensor consists of the above components, namely C_f and L_f in the terminal region, C_a and G_a at the aperture and C_d and G_r at the dielectric medium. The modified circuit is depicted in Fig. 5.7-b.

This circuit lumps only several millimeters of the length of the line. The dielectric medium itself cannot, in general, be lumped since it occupies semi-infinite space and its dimensions do not satisfy condition $l << \lambda$. However, it may be represented as a distributed network.

The reference voltage is selected at the terminal plane. In this model, the ideal transformer may be used to separate the external and internal problems. However, if

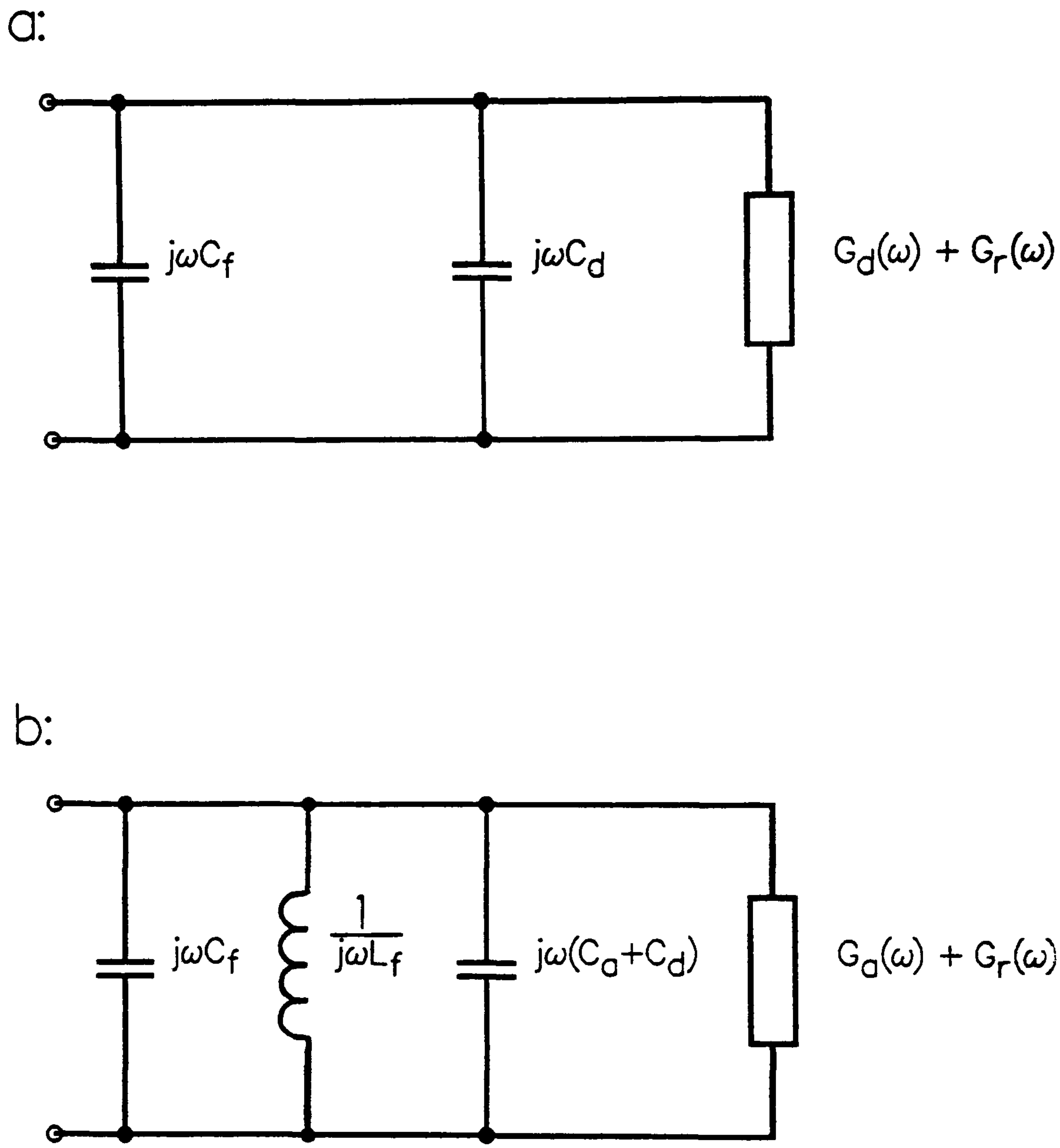

Fig. 5.7

Equivalent circuits for the open-ended coaxial line:
a: conventionally used,
b: modified in the course of this research.

the characteristic admittance were chosen n^2 times the characteristic admittance of the waveguide, then the transformer would not be needed. The susceptance $B_f = \omega C_f$ represents the fringing field within the teflon coaxial sensor, while B_d represents the fringing field of the external side of the aperture. At high frequencies, however, the "fringing field" is represented by a complete set of evanescent, higher order TM modes. The magnetic energy stored within the terminal area is represented by a negative susceptance $-jB_f$ or a positive reactance $jX_f(\omega)$. The presence of the dielectric outside the line is represented by a shunt admittance $Y_a = G_a + jB_a$. Finally, the radiated energy is depicted as the radiation conductance G_r and associated radiation susceptance ωC_d.

5.4 Determination of Lumped Elements of the Equivalent Circuit by the Identification Technique

This technique can be used to determine elements of the equivalent from experimental data.

The input admittance for the measurable fundamental TEM mode, given by (4.5.10), may be separated as

$$\begin{aligned}\tilde{Y}_{in} &= \Re\tilde{Y}_{in} + j\Im\tilde{Y}_{in} \\ &= G_d(\omega) + G_r(\omega) + j\left\{\omega C_f(\omega) + \omega C_d(\omega) - \frac{1}{\omega L(\omega)}\right\} .\end{aligned} \tag{5.4.1}$$

When $\Im\tilde{Y}_{in} = 0$, the following condition is implied

$$\omega_o^2 = \frac{1}{L\{C_f(\omega) + C_d(\omega)\}} . \tag{5.4.2}$$

When $\Im\tilde{Y}_{in} \neq 0$ one may write

$$\Im\tilde{Y}_{in} = \omega\{C_f(\omega) + C_d(\omega)\} - \frac{1}{\omega L} . \tag{5.4.3}$$

Using condition (5.4.2) it is found from (5.4.3) that

$$C_f(\omega) + C_d(\omega) = \Im\tilde{Y}_{in}\left(\frac{\omega}{\omega^2 - \omega_o^2}\right) \tag{5.4.4}$$

and

$$L = \frac{1}{\omega_o^2 \Im \tilde{Y}_{in}} \left(\frac{\omega^2 - \omega_o^2}{\omega} \right) \, . \tag{5.4.5}$$

At resonance frequency ω_o, values of the equivalent lumped elements are

$$C_f(\omega) + C_d(\omega) = \Im \tilde{Y}_{in} \frac{1}{2\omega_o} \tag{5.4.6}$$

and

$$L = \frac{2}{\omega_o \Im \tilde{Y}_{in}} \, . \tag{5.4.7}$$

This procedure represents rather a simple identification technique. Nevertheless, it may be very useful from a practical viewpoint. It allows to find the net equivalent circuit of the input admittance.

VI. Uncertainties in Dielectric Spectroscopy

6.1 State of Art in Uncertainty Analysis

Measurements of the dielectric properties of materials at radiowaves and microwaves usually consist of placing a test sample of a given material in a transmission line or a waveguide and measuring the reflection and/or transmission coefficient of the line [87]. For lossy materials such as biomaterials, the methods based on measurements of reflections are particularly suitable and various schemes have been investigated [88]. Because of the presence of losses, the measurement arrangement can be made very simple as shown in Fig.6.1. Even for test materials of moderate losses, the sample may be made sufficiently long to be considered as infinitely long. The dielectric properties of the test material are determined from the measured reflection coefficient at the test sample interface which is usually taken as a reference plane.

Many biological materials exhibit several dispersion regions at radio and microwaves and their properties at various frequencies may be presented in the form of the Cole-Cole diagram for a certain range of frequencies.

In practice, the reflection coefficient is measured with some known uncertainty in amplitude and phase determined by the instrument used, e.g., a network analyzer [89]. A question may then be posed: "What is the uncertainty in the complex permittivity resulting from the uncertainties in the measured values of reflection coefficient at various frequencies ?". This uncertainty can be relatively easily calculated for nondispersive materials using a direct analytical method, for example equations (6.4.1-2).

[87] L Altschuler, "Dielectric Constant", Chapter IX in "Handbook of Microwave Measurements", Vol 3, ed M Sucher and J Fox, Brooklyn Polytechnic Press, 1963, pp 495-518

[88] H E Bussey, "Measurement of RF Properties of Materials A survey", Proc IEEE, vol 55, 1967, pp 1046-1053

[89] "Automating the HP 8410B Microwave Network Analyzer", Hewlett Packard, Application Note 221A, June 1980, pp 5-10

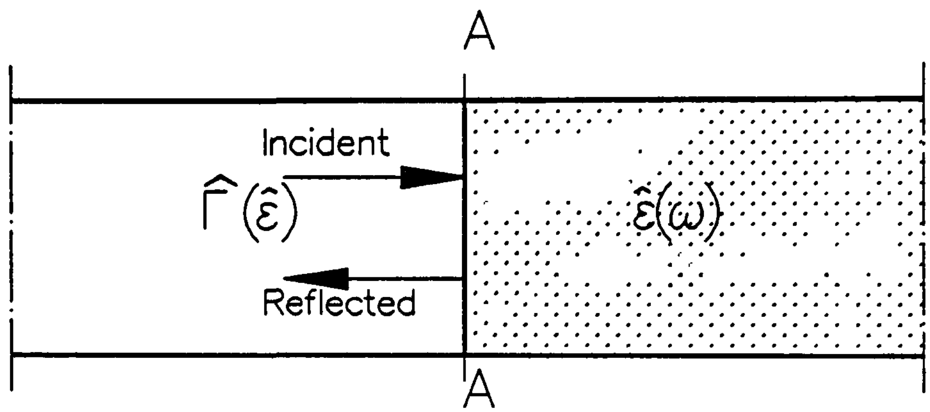

Fig. 6.1

Determination of dielectric properties using reflection method.

For dispersive dielectrics, numerical differentiation may be applied to calculate the uncertainties [90].

The usual procedure employed to determine the dielectric properties utilizes an appropriate mathematical model of the input admittance $\tilde{y}(\tilde{\epsilon})$ of the sample holder. Although the classical Debye model was originally used in the development of the Cole-Cole chart presentation [91], any permittivity model may be presented in this form. The main limitation of the Cole-Cole presentation is that the frequency appears as a parameter [92], [93].

In order to determine the uncertainties in the complex permittivity resulting from given uncertainties in the measured reflection coefficient, it is necessary to find a transformation from from the complex reflection coefficient plane $\tilde{\Gamma}$ to the complex permittivity plane $\tilde{\epsilon}$. In this chapter, a general form of such transformation has been derived and applied to a uniform transmission line filled with lossy dielectric as shown in Fig. 6.1. The formulas are relatively simple and are used to calculate the uncertainty in the complex permittivity as a function of frequency and may also be used to optimize the configuration to obtain minimum uncertainty in the complex permittivity.

6.2 Uncertainty Determination

6.2.1 Concept of Conformal Mapping in Dielectric Spectroscopy

Consider the normalized admittance $\tilde{y} = \tilde{Y}/\tilde{Y}_o$ at the reference plane A-A in Fig.6.1 which is related to the reflection coefficient $\tilde{\Gamma}$ by:

$$\tilde{y} = \frac{\tilde{Y}}{\tilde{Y}_o} = \frac{1-\tilde{\Gamma}}{1+\tilde{\Gamma}}, \tag{6.2.1}$$

[90] S S Stuchly, A Kraszewski, M A Stuchly, "Uncertainties in Radiofrequency Dielectric Measurements of Biological Substances", IEEE Trans on Instr and Measur , Vol IM-36, No 1, 1987, pp 67-70

[91] K Cole and R Cole, "Dispersion and Absorption in Dielectrics", J of Chem Physics, Vol 9, April 1941, pp 341-351

[92] V V Daniel, "Dielectric Relaxation", Academic Press, 1966

[93] A K Jonscher, "Dielectric Relaxations in Solids", Chelsea Dielectric Press, London, 1983, pp 36-61

for a given frequency ω, where $\tilde{Y}$ and $\tilde{Y}_o$ are the input admittance of the sample holder and the characteristic admittance of the transmission line, respectively.

Equation (6.2.1) represents an involutory bilinear conformal transformation which maps the unit circle $|\tilde{\Gamma}| \leq 1$ into the right half plane $\Re\, \tilde{Y}/\tilde{Y}_o \geq 0$.

Substituting $\tilde{\Gamma} = \rho e^{j\phi}$ we find that

$$\tilde{y}(\rho,\ \phi) = \frac{1-\rho^2}{1+2\rho\cos\phi+\rho^2} - j\frac{2\rho\sin\phi}{1+2\rho\cos\phi+\rho^2}\ . \tag{6.2.2}$$

The points $\tilde{\Gamma} = -1,\ 0\ ,\ 1,\ j,\ -j$ in the $\tilde{\Gamma}$-plane correspond to $\tilde{y} = \infty,\ 1,\ 0,\ -j,\ j$ in the $\tilde{y}$ plane, respectively. The two domains are shown in Fig. 6.2.

In general, the normalized admittance is an undetermined function of the sample complex permittivity, i.e.:

$$\tilde{y}(\tilde{\epsilon}) = \frac{\tilde{Y}(\tilde{\epsilon})}{\tilde{Y}_o} \tag{6.2.3}$$

where $\tilde{Y}(\tilde{\epsilon})$ is the input admittance of the dielectric sample holder.

The requirement that the normalized admittance be restricted to $\Re\tilde{y} > 0$ (the positive conductance) implies that the variation of the argument of $\tilde{y}$ is between 0 and $\pi/2$. Such a restriction is obtained by imposing a demarcation or cut line along the real axis from 0 to ∞ [94], as depicted in Fig. 6.3.

Let us consider the complex domain of the input admittance $\tilde{y}$ given by (6.2.2) and try to find the function (6.2.3) which maps the upper half of the plane $\Re\ \tilde{y} \geq 0$, depicted in Fig. 6.2., into the whole upper half plane $\Im\ \tilde{\epsilon} > 0$. The cut is here considered as a polygon having two vertices at $\tilde{y} = 0$ and $\tilde{y} = \infty$ whose angles are equal to $-\pi$ and 3π, respectively.

In effect, we obtain the following form of Schwarz-Christoffel transformation [95], [96]

[94] G Arfken, "Mathematical Methods for Physicists", Academic Press, Orlando, 1985, pp 388-390
[95] Z Nehari, "Conformal Mapping", McGraw-Hill, 1952, pp 148-198
[96] H Kober, "Dictionary of Conformal Representation", Dover Publications Inc , 1952, pp 3,35 and 141-169

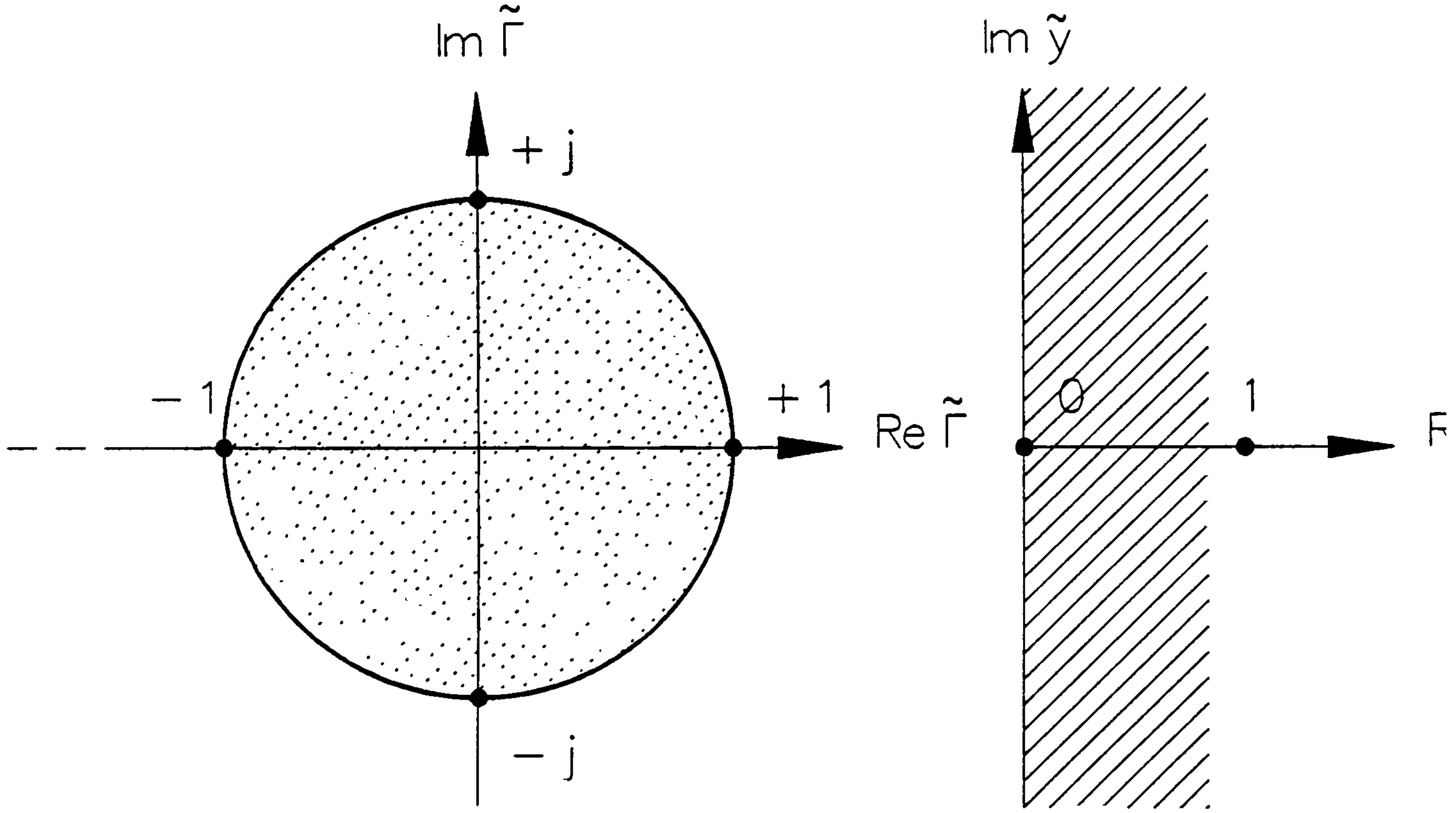

Fig. 6.2

Complex reflection coefficient and normalized admittance domains.

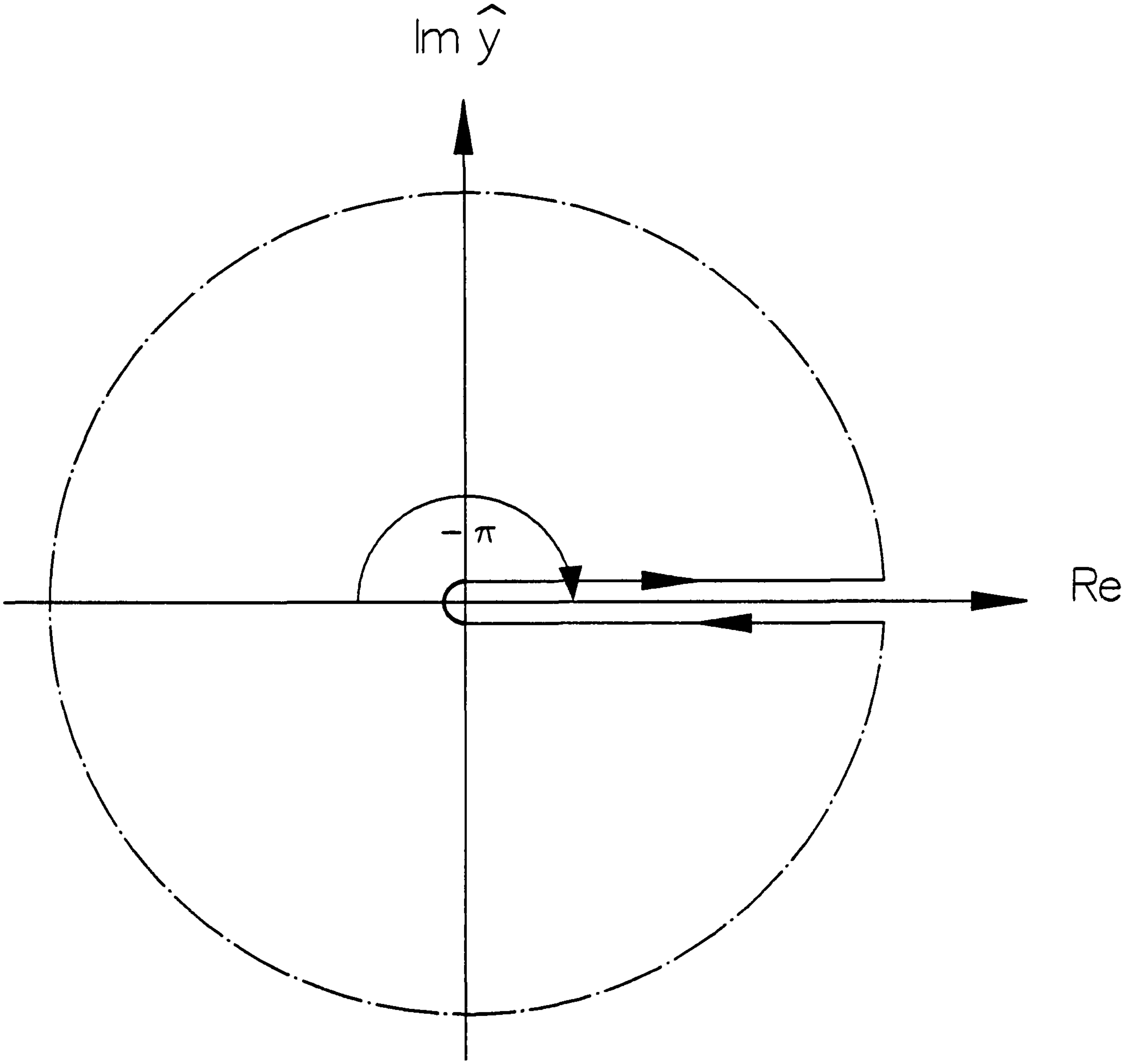

Fig. 6.3

Contour for parameter determination of Schwarz-Christoffel transformation.

$$\frac{d\tilde{\epsilon}}{d\tilde{y}} = C_1 \tilde{y} \;, \tag{6.2.4}$$

where C_1 is a real constant to be determined from physical considerations. Integration of the latter equation gives

$$\tilde{\epsilon} = \frac{C_1}{2}\tilde{y}^2 + C_2 \;. \tag{6.2.5}$$

Let us determine the unknown coefficients for the simplest, limiting case of a TEM wave normally incident at an unbounded semi-space filled with a homogeneous and isotropic dielectric medium.

The wave equation solution in the above defined space is given by [97]

$$\vec{E} = \vec{E}_1 e^{j\vec{k}\cdot\vec{x} - j\omega t}, \tag{6.2.6}$$

where

$$\vec{k} = \frac{2\pi}{\lambda}\, \vec{a}_x = \frac{\omega}{v}\, \vec{a}_x = \sqrt{\mu_0 \tilde{\epsilon}}\, \frac{\omega}{c}\, \vec{a}_x = \tilde{y}\; k_0\; \vec{a}_x \tag{6.2.7}$$

and $\tilde{y} = \tilde{\text{n}}$ is the complex index of refraction, and k_0 is the free space propagation constant.

The relation between electric and magnetic field components at a point is

$$\vec{H}_z = \tilde{Y}\; \vec{a}_x \times \vec{E}_y = \tilde{y} Y_0\; \vec{a}_x \times \vec{E}_y \tag{6.2.8}$$

for the case of TEM wave. When a homogeneous plane wave is normally incident upon a half space, defined by $\mu_0, \tilde{\epsilon}$, the normalized intrinsic admittance $\tilde{y}$ in (6.2.1) becomes the index of refraction $\tilde{\text{n}}$.

From (6.2.7), the relation between the complex permittivity and complex index of refraction is

$$\tilde{\epsilon} = \tilde{y}^2 = \tilde{\text{n}}^2 \;. \tag{6.2.9}$$

By comparing (6.2.5) and (6.2.9), we find that $C_1 = 2$ and $C_2 = 0$.

[97] J.D. Jackson, *op. cit.*, pp. 269-273.

Thus, the topological method lead to the result which is in complete agreement with well known physical behavior.

For the above example the considered transformation has the following properties:

- The half line $\Im\tilde{y} = 0$, $0 < \Re\tilde{y} < \infty$ is transformed into the line $\Im\tilde{\epsilon} = 0$, $0 < \Re\tilde{\epsilon} < \infty$
- The half lines $\Re\tilde{y} = 0$, $0 \leq \Im\,\tilde{y} \leq \infty$ and $\Re\,\tilde{y} = 0$, $-\infty < \Im\,\tilde{y} < 0$ into $\Im\tilde{\epsilon} = 0$, $-\infty \geq \Re\tilde{\epsilon} \geq 0$.
- The points 0, 1 and ∞ remain fixed.

By writing (6.2.9) as

$$\tilde{\epsilon} = \Re\,\tilde{y}^2 - j\Im\,\tilde{y}^2\ , \tag{6.2.10}$$

we find the real and imaginary components in terms of magnitude ρ and phase ϕ of the measured reflection coefficient as

$$\Re\,\tilde{y}^2(\rho,\ \phi) = \frac{1+\rho^4-2\rho^2(2-\cos 2\phi)}{(1+2\rho\cos\phi+\rho^2)^2} \tag{6.2.11}$$

and

$$\Im\,\tilde{y}^2(\rho,\ \phi) = \frac{4\rho\sin\phi(1-\rho^2)}{(1+2\rho\cos\phi+\rho^2)^2}. \tag{6.2.12}$$

Equations (6.2.11) and (6.2.12) are valid for the systems in which an electromagnetic wave enters the sample at normal incidence and therefore such systems may be described by a transmission line model, i.e. (6.2.1) is valid. However, this condition is satisfied for a coaxial transmission line only if the reflection coefficient at the interface is measured.

The internal consistency of (6.2.11) and (6.2.12) results from the fact that they satisfy Kramers-Krönig relations (2.3.6) and (2.3.7).

6.2.2 Uncertainty Analysis

In practical situations such as, e.g., infinite sample methods, one more element must be considered. This element is a window or a bead which is necessary to hold the sample in case of samples of materials other than solids to define the boundary between the sample and the transmission line. The presence of the window or the bead modifies the input admittance by changing the amplitude of the dominant wave. It is evident that the admittance then undergoes another transformation [98].

Most measurement techniques based on the substitution principle allow us, however, to eliminate this unwanted transformation by an appropriate calibration of the measuring system e.g., placement of short, open and matched load calibration procedures prior to measurement.

In order to find the complex uncertainty function of the permittivity, $\Delta\tilde{\varepsilon}$, it is required that the uncertainty function be independent of integration constants C_1 and C_2 of the model. When this is satisfied, this uncertainty function depends only on the uncertainties of the measurement system.

To eliminate constants C_1 and C_2, the Schwarz procedure can be employed [99] by taking the logarithm of (6.2.5) and differentiating it with respect to $\tilde{\Gamma}$. This transformation can be used for a wide class of permittivity models. Performing this procedure, one obtains

$$\frac{d}{d\tilde{\Gamma}} \ln \frac{d\tilde{\varepsilon}}{d\tilde{y}} = \frac{d \ln \tilde{y}}{d\tilde{\Gamma}} \; . \tag{6.2.13}$$

Substituting (6.2.1) into (6.2.13), evaluating right and left hand sides of the obtained expression and, subsequently, replacing differentials by finite differences, the following expression for the complex uncertainty is obtained:

$$\Delta\tilde{\varepsilon} = 2\,\frac{(\tilde{\Gamma}-1)}{(\tilde{\Gamma}+1)^3}\,\Delta\tilde{\Gamma}_{max} \; . \tag{6.2.14}$$

[98] R.E. Collin, Foundation for Microwave Engineering, *op. cit.*, pp. 93-95.

[99] H.A. Schwarz, "Über einige Abbildungausgaben", Journal für reine und angewandte Mathematik, V.70, 1869, pp. 105-120.

Let us introduce the notation

$$\Delta\tilde{\epsilon} = \pm\Delta\epsilon' \pm j\Delta\epsilon'' , \tag{6.2.15}$$

for the complex uncertainty in the Cole-Cole domain, and

$$\Delta\tilde{\Gamma} = \tilde{\Gamma}_m - \tilde{\Gamma} \tag{6.2.16}$$

for the complex uncertainty in the measurement domain, where

$$\tilde{\Gamma}_m = \rho_m e^{j\phi_m} \tag{6.2.17}$$

and

$$\tilde{\Gamma} = \rho e^{j\phi} . \tag{6.2.18}$$

$\tilde{\Gamma}_m$ and $\tilde{\Gamma}$ denote the measured and exact values of reflection coefficient, respectively. If we denote $\Delta\tilde{\Gamma} = \Delta\rho e^{j\theta}$ which represents an uncertainty vector randomly varying in time with respect to modulus and phase, then we can express the measured reflection coefficient by the following expressions

$$\rho_m = \rho\sqrt{1 + \left(\frac{\Delta\rho}{\rho}\right)^2 + 2\frac{\Delta\rho}{\rho}(\cos\phi\cos\theta + \sin\phi\sin\theta)} \tag{6.2.19}$$

and

$$\phi_m = \tan^{-1}\frac{\rho\sin\phi + \Delta\rho\sin\theta}{\rho\cos\phi + \Delta\rho\cos\theta} \tag{6.2.20}$$

where $\phi_{min} \leq \phi \leq \phi_{max}$, $0 \leq \theta \leq 2\pi$, $\rho \leq 1$ and $\Delta\rho \leq \rho$.

A graphical representation of the complex uncertainty on the Smith chart is shown in Fig. 6.4. If $\theta = \phi$, then the error with respect to the amplitude of reflection coefficient is significant and $\phi_{max} = \phi$. For the critical value of angle $\theta = \theta_{cr}$, the dominant error is due to ϕ_m. Therefore, the total maximum vector of measured reflection coefficient, $\tilde{\Gamma}_{max}$, is defined on the Smith chart as the complex maximum norm of the measured vector of reflection coefficient, $\tilde{\Gamma}_m$ (6.2.16), of the form

$$\tilde{\Gamma}_{max} = \| \tilde{\Gamma}_m \|_\infty = \max|\Delta\tilde{\Gamma}_j| \sum \tilde{\Gamma}_i + \Delta\tilde{\Gamma}, \tag{6.2.21}$$

where index i refers to coordinates ρ and ϕ, while j refers to the value of the residual uncertainty vector. This procedure is equivalent to writing (6.2.21) as

$$\tilde{\Gamma}_{max} = (\rho \pm \Delta\rho_{max}) e^{j\phi \pm \Delta\phi_{max}} \; , \tag{6.2.22}$$

where $\Delta\rho_{max}$ and $\Delta\phi_{max}$ are upper bounds for an uncertainty in the modulus and in the phase, respectively.

Defining the characteristic uncertainty $\psi = \Delta\phi_{max}$ as the maximum uncertainty of measurement, it is found that $\Delta\rho = \psi$ at $\rho = 1$. When an uncertainty in phase is different from that in amplitude, we always select $\Delta\rho = max(\psi,\ \Delta\rho_m)$ at $\rho = 1$, otherwise we have to consider elliptic circulation of the uncertainty vector around the exact value of the reflection coefficient. The first variant represents the worst situation.

Substituting (6.2.22) in (6.2.14) and using (6.2.17), the complex uncertainty transformed from the Smith chart into complex dielectric constant domain is expressed as

$$\Delta\tilde{\epsilon} = \pm\, 2\, \tilde{\Gamma}\, \frac{(\tilde{\Gamma} - 1)}{(\tilde{\Gamma} + 1)^3} \left[e^{-j\Delta\phi_{max}} \left(1 + \frac{\Delta\rho_{max}}{\rho} \right) - 1 \right] \tag{6.2.23}$$

where, for the chosen case, the maximal deviation of the phase angle, $\Delta\phi_{max}$, is related to $\Delta\rho_{max}$ by

$$\Delta\phi_{max} = 2 \sin^{-1} \frac{\Delta\rho_{max}}{\rho} \; . \tag{6.2.24}$$

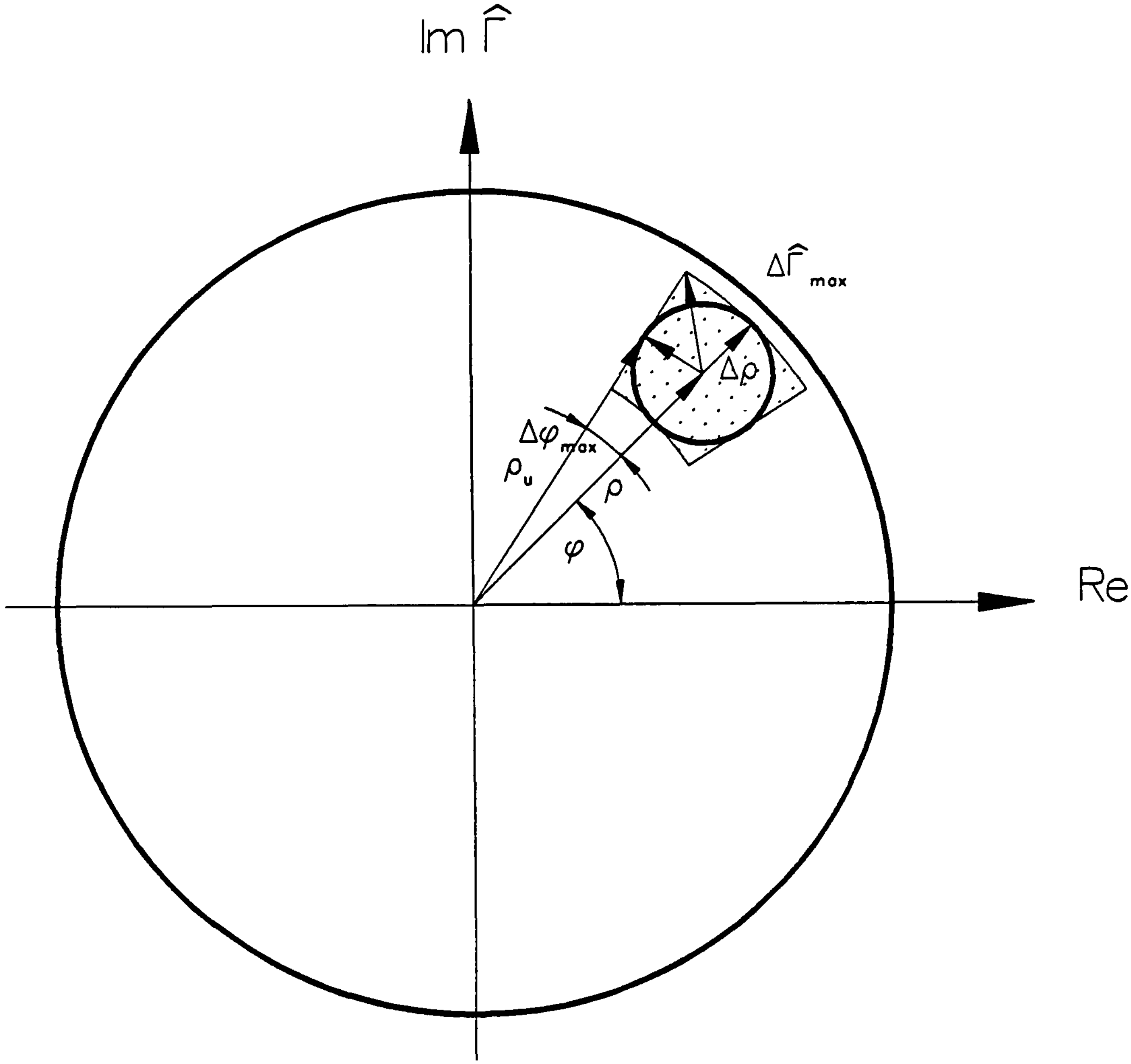

Fig. 6.4

Definition of complex uncertainty in reflection coefficient on a Smith chart.

For a dielectric whose electrical properties can be represented by the Debye's model, the Cole-Cole equation has the following form

$$\left[\epsilon^{'}(\omega) - \frac{\epsilon_L + \epsilon_\infty}{2}\right]^2 + \left[\epsilon^{''}(\omega)\right]^2 = \left(\frac{\epsilon_L - \epsilon_\infty}{2} \pm \Delta R\right)^2 , \qquad (6.2.25)$$

(see also (3.3.6)) where

$$\Delta R = \pm\frac{\epsilon_L - \epsilon_\infty}{2} \pm 2\sqrt{\left(\frac{\epsilon_L - \epsilon_\infty}{2}\right)^2 \pm 2\left(\epsilon_L + \epsilon_\infty + \epsilon^{'}\frac{\Delta\epsilon^{'}}{2}\right)\Delta\epsilon^{'} \pm 2\left(\epsilon^{''} + \frac{\Delta\epsilon^{''}}{2}\right)\Delta\epsilon^{''}} \, . \qquad (6.2.26)$$

Equation (6.2.25) represents an uncertainty ring in the complex permittivity domain.

6.3 Discussion

The proposed approach to determination of the uncertainty in the permittivity is simple. The uncertainty is regarded as a complex quantity. Distilled water at 20^o C, a well known dielectric material, is chosen to demonstrate the method of uncertainty analysis. In Fig.6.5, the locus of reflection coefficient is shown on the Smith chart for the frequency range up to 1000 GHz. The agreement with analysis based on different approach in [100] is evident.

The corresponding uncertainties (6.2.23) for distilled water are superimposed on the Cole-Cole diagram according to (6.2.25) and are depicted in Figs. 6.6 , 6.7 and 6.8 for three different characteristic uncertainties: $\psi = 0.6^o$, $\psi = 0.2^o$, $\psi = 0.1^o$, respectively. The measured uncertainty is a function of the resolution angle $\psi = \Delta\phi_{max}$ at $\rho = 1$. One may observe that the accuracy of measurements deteriorates as $\omega \rightarrow 0$.

[100] M A Rzepecka, S S Stuchly and M A K Hamid, "Modified Infinite Sample Method for Routine Permittivity Measurements at Microwave Frequencies", IEEE Trans on Instr and Measur , Vol IM-22, 1973, pp 41-46

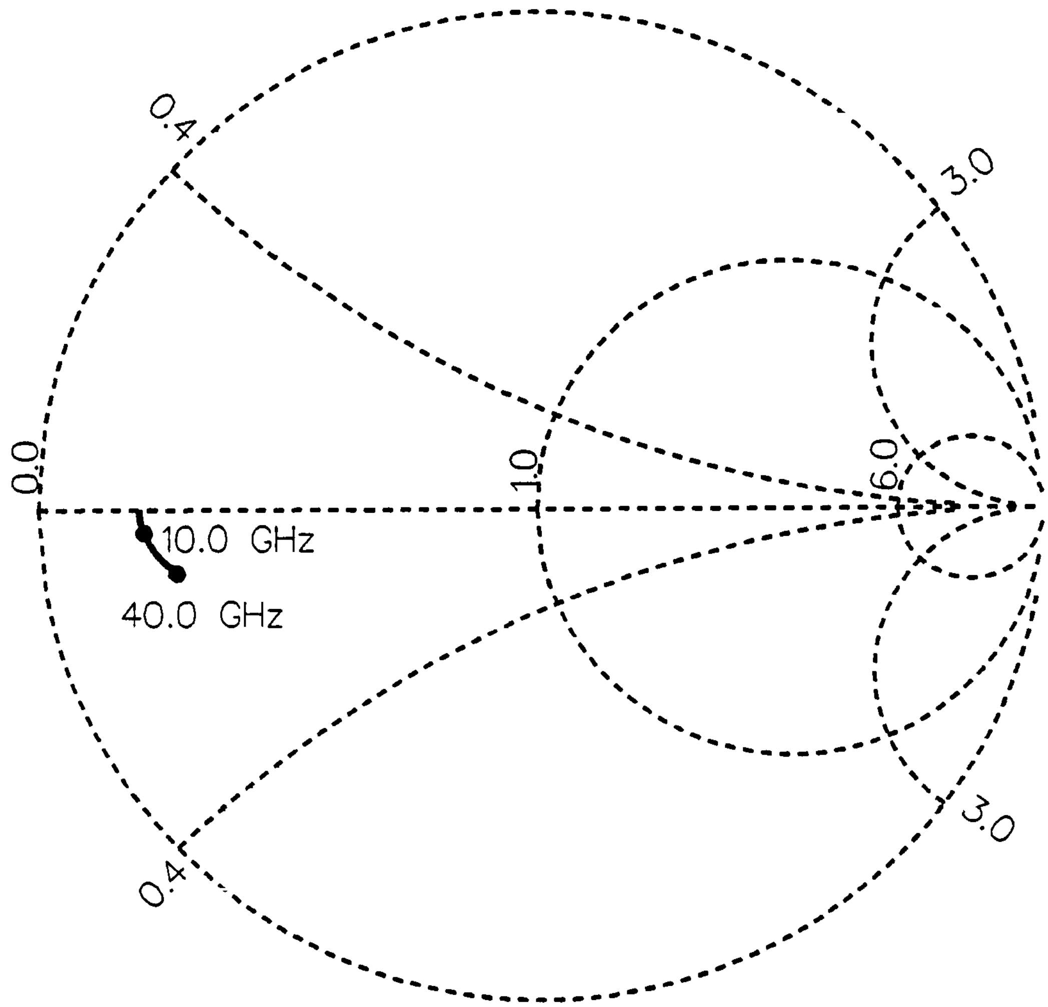

Fig. 6.5

Smith chart diagram showing reflection coefficient of distilled water at normal incidence.

For resolution angle $\psi = 0.6^o$ shown in Fig. 6.6, the uncertainty increases up to an unacceptable level of more than 20.0 % at the range of interest. From Figs. 6.7 and 6.8 it is evident that the configuration of the sample (Fig.6.1) may provide accurate results only at frequencies above 11 GHz for $\psi = 0.2^o$ and above 8 GHz for $\psi = 0.1^o$. From Fig. 6.8 it is evident that, for a resolution angle $\psi = 0.1^o$, the resulting uncertainty varies from a minimum of less than 0.1 % to a maximum of greater than 1.0 % at radio- and microwave frequencies.

In order to achieve good accuracy in dielectric measurements of materials containing water, e.g., biomaterials, it is necessary to use equipment of high accuracy. Although this has been known for long time, it has not been quantified. The derived formulas for uncertainties may explain a large discrepancy in published data for permittivity of water at lower frequencies, particularly regarding the loss factor.

Every measurement system introduces errors into the measured results. Hence calibration of the Computerized Network Analyzer is the most important part of the measuring procedure. The measurement errors can be separated into two categories: random and systematic errors. Random errors are non-repeatable measurement variations due to noise, temperature drift, and other physical changes in the test setup between calibration and measurement. These errors can only be reduced through careful system design and by time-averaging the measurements. Systematic errors are the repeatable errors which the system can measure. They include mismatch and leakage terms in the test setup, isolation characteristics between the reference and the test signal paths, and system frequency response. Since each of these errors produces a predictable effect upon the measured data, their effects can be removed to obtain a corrected value for the test device response. These uncertainties are quantified as directivity, source match, load match, isolation, and tracking (frequency response). The values of the effective source match and reflection tracking are computed and stored in the computerized network analyzer and are next used for elimination of these errors during the measurement

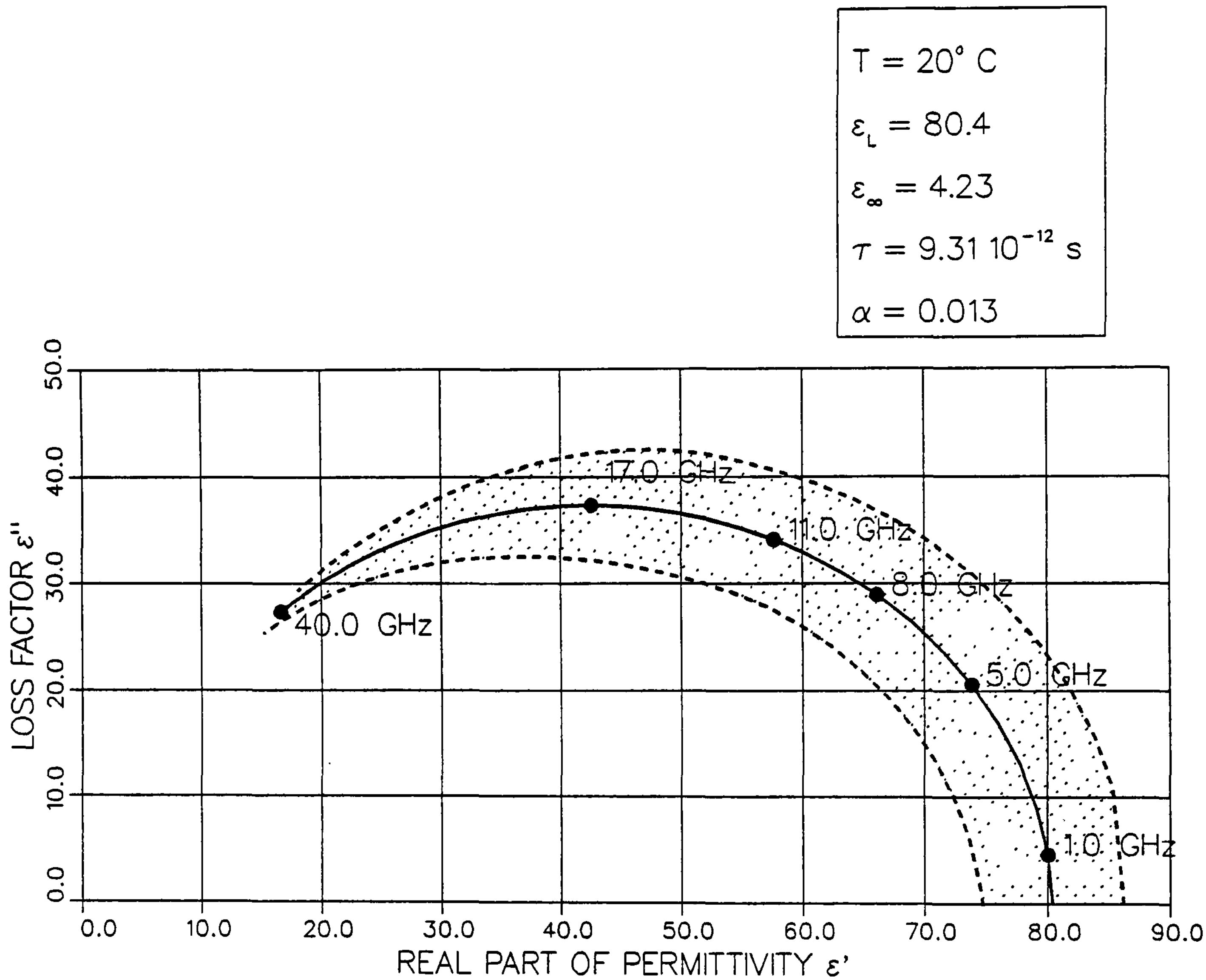

Fig. 6.6

Cole-Cole presentation of permittivity of distilled water and related uncertainty bounds for characteristic uncertainty $\psi = 0.6^o$ in the Smith chart domain.

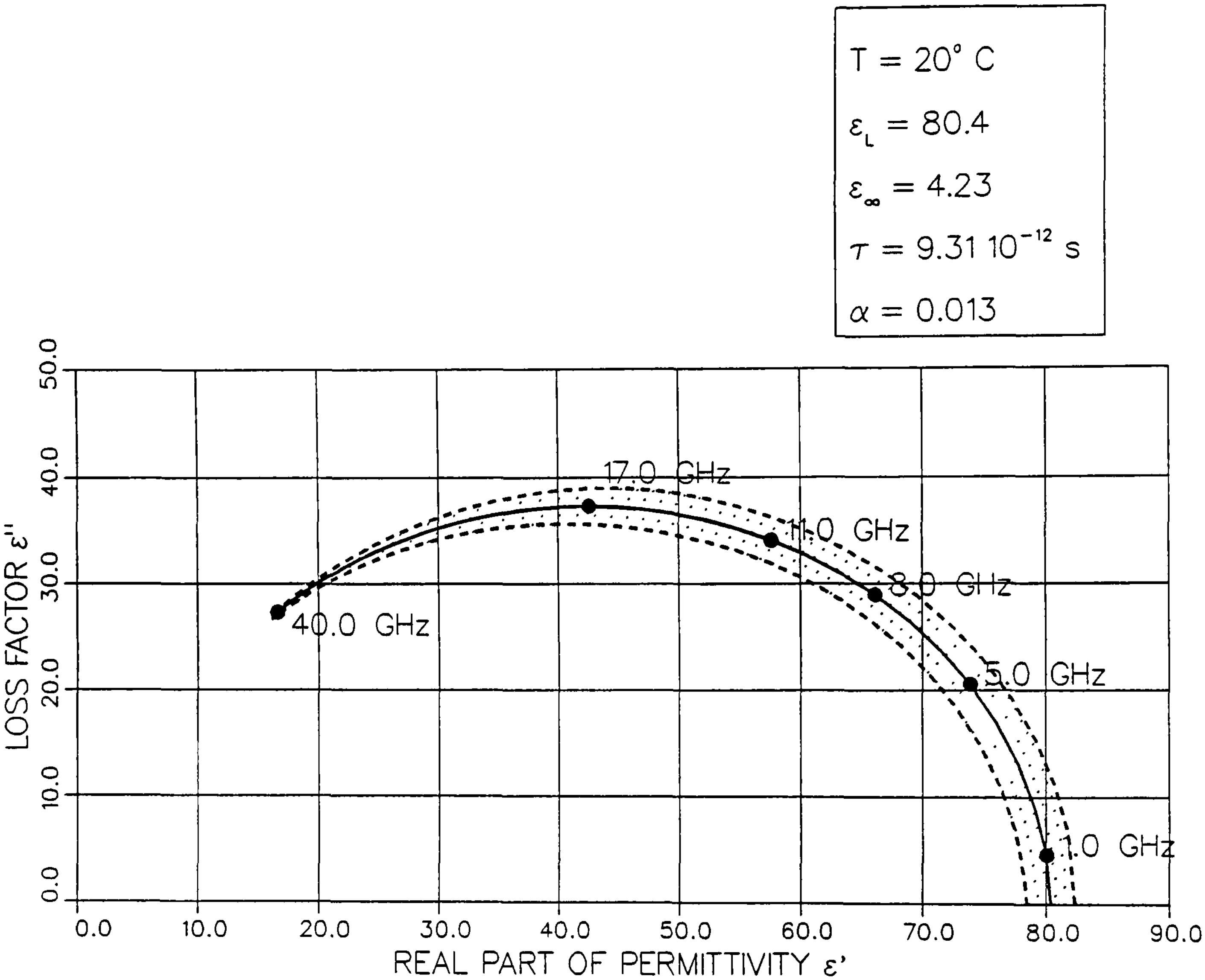

Fig. 6.7

Cole-Cole presentation of permittivity of distilled water and related uncertainty bounds for characteristic uncertainty $\psi = 0.2^o$ in the Smith chart domain.

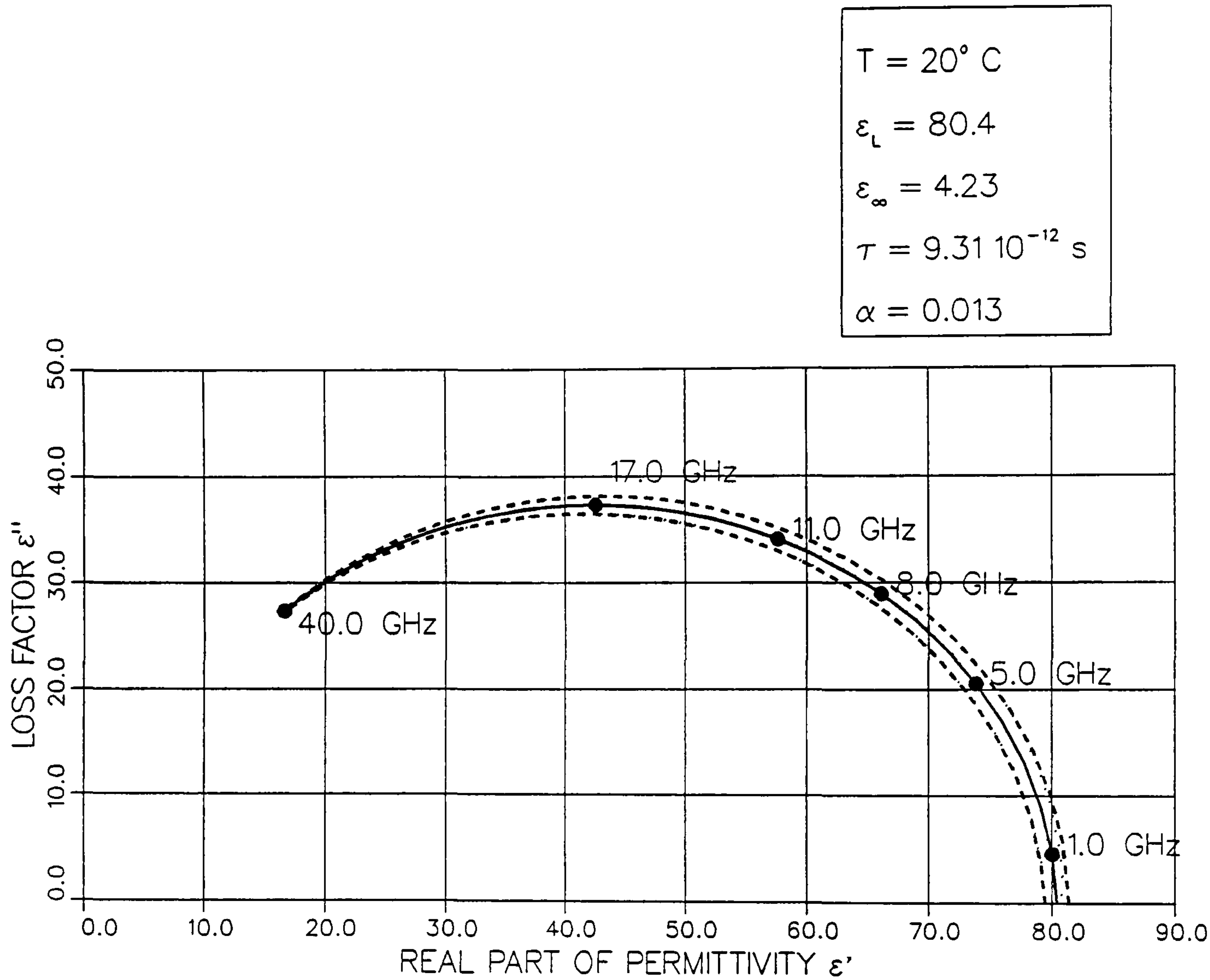

Fig. 6.8

Cole-Cole presentation of permittivity of distilled water and related uncertainty bounds for characteristic uncertainty $\psi = 0.1^o$ in the Smith chart domain.

procedure. For the purpose of accuracy enhancement, eight term or twelve term error models may be utilized. For reflection measurements of one port devices, the eight term error model provides sufficient measurement accuracy. This model provides directivity, source match and frequency response vector error correction for reflection measurements. The error correcting coefficients may be determined by calibration of the measuring system with three independent standard terminations whose actual reflection coefficient is known at all frequencies.

The first standard applied is a "matched load" at the reference plane which imposes the condition $|\tilde{\Gamma}| = 0$ and essentially measures the effective directivity. The perfect matched load cannot be practically achieved and any reflection measurement contain uncertainties. Hence the system effective directivity becomes the actual reflection coefficient of the perfect load. In general, any termination having a return loss value greater than the uncorrected system directivity reduces reflection measurement uncertainty.

The short circuit termination is used to establish the second standard. This standard corresponds to the condition that $\tilde{\Gamma} = -1$. These two techniques are fundamental for the reduction of resolution angle ψ in the presented method of the uncertainty analysis.

Sometimes the third condition for calibration procedure is used, namely the open circuit. This is used for calibration of open-ended coaxial lines, but its application is limited to the range of frequencies below the radiation range. There is no complete theoretical substantiation of the third calibration condition. This procedure may be performed on the Computerized Network Analyzer. The typical system is comprised of a 8410 Network Analyzer, a HP 8745A or HP 8743A Test Set, a HP 8620C RF Signal Source, the source phase-lock subsystem consisting of a HP 8656 Synthesized Signal Generator, a HP 8709A Synchronizer, a HP 59306A Relay Actuator and a HP 59313A A/D converter controlled by a computer using an IEEE 488 interface bus. Such a system operates in the frequency range 100 MHz to 18 GHz. The source phase-lock subsystem used in the measurement set-up virtually provides the synchronizer class frequency, accuracy and repeatability. In each measurement, the control computer sets the sweep oscillator and the network analyzer to the required frequency range and then routes the RF signal through the multiplexer to the test unit. The IF attenuation is automatically ranged to position the trace on the polar display. Once the S-parameter to be measured is selected, the measurement is performed and the resulting amplitude and phase information are digitized and transferred to the computer.

In summary, the developed Schwartz-Christoffel transformation is only the first step of a general formulation of the inverse problem utilizing conformal transform techniques. This analysis indicates that the solution may be complicated even for the very simple problem treated here. The engineering implication of this chapter is that a method of uncertainty evaluation is developed. However, this method has also one important limitation, namely its validity is restricted to travelling wave transmission lines and waveguides where only the forward wave exists in the dielectric medium. The treatment of the open-ended coaxial line by this method couldn't be obtained due to complexity of the analysis. The main advantage of this approach is that the uncertainties are treated as complex quantities what causes the ease to compute uncertainties in the permittivity when the transformation between the measurement domain and Cole-Cole domain is known.

VII. Discussion and Conclusions

A summary of the results and contributions contained within this dissertation follows. A significant step has been taken towards the determination of the complete performance of open-ended coaxial sensors. The background for future research has been established. The classical diffraction and reflection theories are merged to introduce a general theory for modelling phenomena associated with field singularities at the interface of a dielectric sample. A method for evaluation of field quantities is developed in circular regions, where the mixed boundary conditions exist. The theory of the methods is developed in the second part of the theses.

A new formulation of the admittance or impedance boundary conditions introduced here is based on physical considerations. It contains an important generalization and extension of the previously published results. The calculations of the surface admittance is based on the knowledge of fields inside the dielectric satisfying appropriate boundary conditions. The main feature of this formulation is that it allows us to transform a general diffraction problem into a reflection one which is fundamental for dielectric reflection spectroscopy. The surface admittance for TM-polarized waves is presented. The solution of a coaxial line open into a dispersive dielectric was the main application described in this dissertation.

The analysis of the open-ended coaxial line is particularly important since it also includes higher order modes and the nature of the electromagnetic field in the dielectric region. Thus, extension of the range of application of the open-ended coaxial line up to upper range of operation of the Computerized Network Analyzer is obvious. An oversized line (with respect to cutoff wavelength for the TM_{o1} mode) and a finite flange are essential realistic elements included in the analysis. The method of analysis developed in

Chapter IV is also suitable for other problems with circular symmetry involving dielectric media. The problem of diffraction of the electromagnetic wave at the open end of the coaxial line is solved rigorously by the use of properties of the Fourier-Bessel expansion. This solution was obtained for the first time to the best of the author's knowledge. It was found that the diffraction process at the aperture of the coaxial sensor predominates reflection process for the fundamental mode wave at high frequencies.

In the first part of chapter V, the numerical results for the open-ended coaxial line were compared with the available experimental data. A general equivalent circuit was derived for the open ended coaxial line from the field theory standpoint, although explicit equations for its elements were not simplified for the practical use because the complexity of equations.

The uncertainty analysis consists of a formulation of the infinite sample problem. It is a natural extension of the inverse problem of the reflection spectroscopy. A simple equation is derived for the complex uncertainty calculation. The system with the finite sample length is the modification of this type of analysis.

The results presented in the theory section of the dissertation may be used to analysis the following problems:

- Short monopole antenna sensor;
- Grounded high-permittivity dielectric antenna;
- Excitation of antennas by coaxial cables;
- Modes in fiber-optic multilayer cables;
- Open ended shielded coaxial lines.

Possibilities for further studies are:

- Experimental investigation of oversized coaxial lines with various flange sizes;
- Comparison between theory and experiment.

The FHT method applied to a complex problem leads to a complicated solution. The solution is rigorous, but not easily applicable to solutions of engineering problems. A simplified approach based on utilization of the surface impedance concept and the limiting form of the solution by FHT method is developed and it leads to the acceptable solution for practical problems. Solutions require the knowledge of eigenvalues of transcendental equations to the full extent.

APPENDIX A

Finite Hankel Transform

Any twice differentiable function $f(x)$ that satisfies the boundary condition of a boundary value problem, say over (a, b), may be expanded into a uniformly convergent series of the normal orthogonal set of eigenfunctions pertaining to that boundary-value problem [101]

$$f(x) = \sum_{n=1}^{\infty} c_n \psi_n \ . \tag{A.1}$$

Multiplying(A.1) by ψ_m and integrating over (a,b) we obtain

$$c_n = \int_a^b f(x)\psi_n(x)dx \ , \tag{A.2}$$

where orthogonality of the set of eigenfunctions is used. The normalization usually is achieved by the following euclidean norm condition

$$\|\psi_n\|_2^2 = \int_a^b \psi_n^2(x)dx = 1 \ . \tag{A.3}$$

Turning this general formulation into one for the circular symmetry problems, one may define the expansion eliminating radial dependence from the partial differential equation. Following [102], we define the finite Hankel transform by

$$\mathcal{F}(\kappa) = \int_0^a f(\rho)\rho\mathcal{K}_m(\kappa\rho)d\rho \ , \tag{A.4}$$

where $\mathcal{K}_m(\kappa\rho)$ is an appropriately chosen kernel pertaining to the properties of the domain under consideration. If a cylinder of radius a is the object of interest, κ_k is the $k-th$ positive root of the equation

$$J_m(\kappa_k a) = 0 \ . \tag{A.5}$$

[101] S.G. Mikhlin, "Linear Equations of Mathematical Physics", Holt, Rinehart and Winston, Inc , New York, 1967, pp 96-99
[102] I.N. Sneddon, *op. cit.* pp. 17-25

By the well-known theory of Fourier-Bessel series [103], the function $f(\rho)$ may be represented in the range $0 \leq \rho < a$ by

$$f(\rho) = \sum_{k=1}^{\mathrm{K}} a_k J_m(\kappa_k \rho) \ , \tag{A.6}$$

where K denotes the summation limit. Upon finding the coefficient a_k, the inverse finite Hankel transform is

$$f(\rho) = \frac{2}{a^2} \sum_{k=1}^{K} \mathcal{F}(\kappa_k \rho) \frac{J_m(\kappa_k \rho)}{J_{m+1}^2(\kappa_k a)} \ . \tag{A.7}$$

This transform may also be applied to an infinite domain which is internally bounded with the integration range in ρ given by (5.3.16). For the finite circular domain bounded both from below and above the kernel of the transformation becomes:

$$\mathcal{K}_m(\kappa\rho) = J_m(\kappa\rho) Y_m(\kappa a) - Y_m(\kappa\rho) J_m(\kappa a) \ . \tag{A.8}$$

For this case the inverse formula becomes

$$f(\rho) = \frac{\pi^2}{2} \sum_{k=1}^{K} \frac{\kappa_k^2 J_m^2(\kappa_k b)}{J_m^2(\kappa_k a) - J_m^2(\kappa_k b)} \mathcal{F}(\kappa_k) \mathcal{K}_m(\kappa_k \rho) \ , \tag{A.9}$$

where κ_k is a positive root of the equation:

$$J_m(\kappa_k b) Y_m(\kappa_k a) - Y_m(\kappa_k b) J_m(\kappa_k a) = 0 \ . \tag{A.10}$$

A special treatment is required when the impedance boundary condition at $z = 0$ is applied. Consider a circular annulus in the interval $\rho \in (a,\ b)$. The solution of the vector Helmholtz equation for magnetic field density $\vec{\mathbf{H}}$ expressed in terms of the scalar wave function Ψ^+ gives the following components of the TM-wave at the discontinuity

$$E_\rho^+ = \frac{1}{j\omega\epsilon_o\tilde{\varepsilon}(\omega)} \frac{\partial^2 \Psi^+}{\partial\rho\partial z} \tag{A.11}$$

$$\begin{aligned} E_z^+ &= -\frac{1}{j\omega\epsilon_o\tilde{\varepsilon}(\omega)} \frac{\partial}{\partial\rho} \left(\rho \frac{\partial \Psi^+}{\partial\rho}\right) \\ &= \frac{z_o(\omega)}{jk_o} \left(\frac{\partial^2 \Psi^+}{\partial z^2} + k_o^2 \tilde{\epsilon}(\omega) \Psi^+\right) \end{aligned} \tag{A.12}$$

$$H_\phi^+ = -\frac{\partial \Psi^+}{\partial\rho} \ . \tag{A.13}$$

[103] G.N. Watson, *op. cit.* pp. 576-582

The surface impedance for a TM-wave is defined as*

$$Z_S = \frac{E_\rho^+}{H_\phi^+} \, . \tag{A.14}$$

Substituting (A.11) and (A.12) into (A.13) we obtain the following boundary condition

$$\frac{\partial^2 \Psi^+(\rho, z)}{\partial \rho \partial z} - \tilde{h} \frac{\partial \Psi^+(\rho, z)}{\partial \rho} = 0 \tag{A.15}$$

which is equivalent to writing

$$\frac{\partial f_1(\rho)}{\partial \rho} = 0 \tag{A.16}$$

where

$$\frac{\partial \Psi^+(\rho, z)}{\partial z} - \tilde{h}\Psi^+ = 0 \tag{A.17}$$

and

$$\begin{aligned} \tilde{h} =& \frac{\sqrt{\tilde{\varepsilon}(\omega)}}{z_o} Z_{TM}, \\ =& \frac{\tilde{\vartheta} - 1}{\tilde{\vartheta}^2 + 1} \, . \end{aligned} \tag{A.18}$$

Applying the FHT** with the kernel given by (A.8) to (A.16), we obtain

$$\begin{aligned} \mathcal{H}^{(3)}\{f_1(\rho)\} =& \int_a^b \frac{\partial f_1(\rho)}{\partial \rho} \mathcal{K}_m(\kappa\rho) \rho d\rho \\ =& \mathcal{K}_m(\kappa\rho) f_1(\rho) \Big|_a^b - \kappa \int_a^b \frac{\partial \mathcal{K}_m(\kappa\rho)}{\partial \rho} f_1(\rho) \rho d\rho \\ =& -\kappa \int_a^b \frac{\partial \mathcal{K}_m(\kappa\rho)}{\partial \rho} f_1(\rho) \rho d\rho \\ =& 0 \, . \end{aligned} \tag{A.19}$$

The last identity holds for $a \le \rho \le b$ and $z = 0$.

Since $k \neq 0$ and $\frac{\partial \mathcal{K}_m(\kappa\rho)}{\partial \rho} \neq 0 \quad \forall \quad \rho \in (a,\, b)$, the conclusion is that

$$\begin{aligned} f_1(\rho) =& 0 \\ \frac{\partial \Psi^+(\rho, z)}{\partial z} - \tilde{h}\Psi^+(\rho, z) =& 0 \, . \end{aligned} \tag{A.20}$$

* As it is shown in chapter III, section 3 4

** This transform is called the FHT of third kind (Sneddon, [76], *op cit*)

This is an important finding for the application of boundary conditions at transverse to z surfaces. The Hankel transform of the third kind for this surface is correctly given by (4.3.17) in chapter IV.

Consider restrictions implied upon Helmholtz equation (4.3.1) in the composite domain, when the Finite Hankel Transform is applied with kernel of transformation given by (A.10). This implies that the value of function $\Psi^{+}(a, z)$, $\Psi^{+}(b, z)$, and $\Psi^{+}(d, z)$ are independent of ρ. These values enter into the transformed boundary as parameteric functions and can be found using the electromagnetic continuity conditions. These conditions are introduced during the construction of the global solution in Chapter IV.

APPENDIX B

Hankel-Weber Transform

Consider (4.2.1) in region IV, namely

$$\frac{1}{\rho}\frac{\partial}{\partial\rho}\left(\rho\frac{\partial\Psi^{+}(\rho,z)}{\partial\rho}\right)-\frac{m^2}{\rho^2}\Psi^{+}(\rho,z)+\frac{\partial^2\Psi^{+}(\rho,z)}{\partial z^2}+k_o^2\tilde{\epsilon}(\omega)\Psi^{+}(\rho,z)=0 \qquad (B.1)$$

with the following boundary condition

$$\frac{\partial^2\Psi^{+}(\rho,z)}{\partial\rho\partial z}+\frac{1}{\alpha}\frac{\partial\Psi^{+}(\rho,z)}{\partial\rho}=0 \qquad (B.1.1)$$

for $z=0$, $d\leq\rho<\infty$ and a general Cauchy's boundary condition

$$\left.\frac{\partial\Psi^{+}(\rho\ ,z)}{\partial\rho}\right|_{\rho=d}+\beta_d\Psi^{+}(d,z)=0 \qquad (B.1.2)$$

for $0<z<+\infty$.

In order to derive a transform with respect to ρ-variable in the region $d<\rho<\infty$ and $z>0$, the auxillary singular Sturm-Liouville equation for the rotational problem is of interest, i.e.,

$$\frac{1}{\rho,z}\frac{\partial}{\partial\rho}\left(\rho\frac{\partial\Psi^{+}(\rho)}{\partial\rho}\right)+\frac{\partial^2\Psi^{+}(\rho,z)}{\partial z^2}+\left(\iota^2+k_o^2\tilde{\epsilon}(\omega)-\frac{m^2}{\rho^2}\right)\Psi^{+}(\rho,z)=0 \qquad (B.2)$$

with the boundary condition at $\rho=d$, $0\leq z<+\infty$ given by (B.1.2).

Introducing the substitutions

$$\Psi^{+}=\rho^{-\frac{1}{2}}\Psi_1^{+} \qquad (B.3)$$

and

$$\nu^2=\iota^2+k^2\tilde{\epsilon}(\omega)\ , \qquad (B.3.1)$$

we obtain

$$\frac{\partial^2\Psi_1^{+}(\rho,z)}{\partial\rho^2}+\frac{\partial^2\Psi_1^{+}(\rho,z)}{\partial z^2}+\left(\nu^2-\frac{m^2-\frac{1}{4}}{\rho^2}\right)\Psi_1^{+}(\rho,z)=0\ . \qquad (B.4)$$

The general solution of this equation is given by

$$\Psi_1^+(\rho,\ \nu) = A\sqrt{\rho}H_m^{(1)}(\nu\rho) + B\sqrt{\rho}H_m^{(2)}(\nu\rho)\ . \tag{B.4.1}$$

If $\Im\nu > 0$, then the first of the Hankel functions is square-integrable, thus it represents the only linearly independent solution. The solution $\Psi^+(\rho)$ must satisfy the following condition

$$\int_d^\infty |\Psi_1^+(\rho)|^2 d\rho < \infty\ . \tag{B.4.2}$$

On the other hand, from the general theory of singular Sturm-Liouville systems results that [104]

$$\Psi_1^+(\rho,\nu) = \Theta(\rho,\ \nu) + \mu(\nu)\Lambda(\rho,\ \nu)\ . \tag{B.4.3}$$

Functions $\Lambda(\rho,\ \nu)$ and $\Theta(\rho,\ \nu)$ are solutions of (B.4) such that they satisfy the following condition at $\rho = d$

$$\begin{bmatrix} \Lambda_m(d,\ \nu) & \Theta(d,\ \nu) \\ \Lambda_m'(d,\ \nu) & \Theta'(d,\ \nu) \end{bmatrix} = \begin{bmatrix} 0 & -1 \\ 1 & 0 \end{bmatrix}, \tag{B.4.4}$$

whose Wronskian is equal to 1. When the complex operator in (B.1.2) $\beta_d \to \infty$, the Dirichlet boundary condition is implied.

For this case

$$\Theta(\rho,\ \nu) = \frac{\pi}{2}\sqrt{d\rho}\nu\left\{J_m(\nu\rho)Y_m'(\nu d) - Y_m(\nu\rho)J_m'(\nu d)\right\} \tag{B.4.5}$$

and

$$\Lambda(\rho,\ \nu) = \frac{\pi}{2}\sqrt{d\rho}\left\{J_m(\nu\rho)Y_m(\nu d) - Y_m(\nu\rho)J_m(\nu d)\right\} \tag{B.4.6}$$

are also solutions of (B.4), so the first solution must be multiple $\mu(\nu)$ of this (or alternatively both solutions are linearly dependent).

Substituting (B.4.5) and (B.4.6) into (B.4.3), equating to (B.4.1) and subsequently comparing coefficients associated with $J_m(\nu\rho)$ and $Y_m(\nu\rho)$ we obtain

$$\nu Y_m'(\nu d) + \mu(\nu)Y_m(\nu d) = A$$

$$-\nu J_m'(\nu d) - \mu(\nu)J_m(\nu d) = iA\ , \tag{B.4.7}$$

[104] E C Titchmarsh, "Eigenfunction Expansions Associated with Second-Order Differential Equations" Part I, Oxford at the Clarendon Press, 1958, p 25

from which

$$\mu(\nu) = \nu \left\{ \frac{J'_m(\nu d) + jY'_m(\nu d)}{J_m(\nu d) + jY_m(\nu d)} \right\}$$
$$= -\nu \frac{H_m^{(1)'}(\nu d)}{H_m^{(1)}(\nu d)} \ . \qquad (B.4.8)$$

Imposing ν real and thus requiring $\nu^2 > 0$,

$$-\Im\mu(\nu) = \nu \frac{J_m(\nu d)Y'_m(\nu d) - Y_m(\nu d)J'_m(\nu d)}{J_m^2(\nu d) + Y_m^2(\nu d)}$$
$$= \frac{2}{\pi d} \frac{1}{J_m^2(\nu d) + Y_m^2(\nu d)} \qquad (B.4.9)$$

is obtained.

Taking into account that

$$\frac{2}{j\pi} e^{-j\frac{\nu\pi}{2}} K_m(\hat{z}) = H_m^{(1)}(j\hat{z}) \qquad (B.4.10)$$

where the Kelvin function $K_m(\hat{z})$ is real for real $\hat{z}$, it may be concluded that right hand side of (B.4.8) is real for purely imaginary ν (hence for $\nu^2 < 0$). It also implies that $-\Im\mu(\nu) = 0$ in (B.4.8) for $\nu^2 < 0$.

Using (B.4.9), the solution of the form (B.4.3) has the form as originally proven in [114]

$$\Psi_1^+(\rho) = \int_0^\infty \sqrt{\rho} \frac{J_m(\nu\rho)Y_m(\nu d) - Y_m(\nu\rho)J_m(\nu d)}{J_m^2(\nu d) + Y_m^2(\nu d)} \nu d\nu$$
$$\times \int_d^\infty \sqrt{\nu}\{J_m(\nu\rho)Y_m(\nu d) - Y_m(\nu\rho)J_m(\nu d)\}\Psi_1^+(\rho)d\rho \ . \qquad (B.4.11)$$

This is Weber's integral equation which also defines the Hankel-Weber transform (in contrast to the Hankel transform for which $0 < \rho < \infty$) for a semi-infinite region $d < \rho < \infty$. By using the substitution (B.3) and multiplying by $\Psi_2(z)$, thus obtaining the original problem (B.1), an appropriate transform is

$$\mathcal{P}^+(\nu) = \int_d^\infty \mathcal{K}_m(\rho\ ,\nu)\rho\Psi^+(\rho)d\rho \qquad (B.5)$$

[114] E C Titchmarsh, "Weber's Integral Theorem", Proceedings of the London Mathematical Society, V 22, 1923, pp 15-28

and its inverse is

$$\Psi^{+}(\rho) = \int_0^\infty \mathcal{P}^{+}(\nu)\mathcal{K}_m(\rho\ ,\nu)\nu d\nu\ , \tag{B.6}$$

where $\mathcal{K}_m(\rho\ ,\nu)$ is the kernel of transformation whose form depends on the boundary condition at $\rho = d$.

When a more general Cauchy's boundary condition (B.2.1) is applied at $\rho = d$, the procedure leads to the following kernel of transformation

$$\mathcal{K}_m(\rho\ ,\nu) =$$

$$\frac{J_m(\nu\rho)\left\{Y_m'(\nu d)\sin\left(\nu\sin^{-1}\frac{1}{\sqrt{1+\beta_d^2+\beta_d d^{-1}(2d)^{-2}}}\right) - \frac{\beta_d}{\sqrt{1+\beta_d^2+\beta_d d^{-1}+(2d)^{-2}}}Y_m(\nu d)\right\}}{\left[\left\{J_m'(\nu d)\sin\left(\nu\sin^{-1}\frac{1}{\sqrt{1+\beta_d^2+\beta_d d^{-1}+(2d)^{-2}}}\right) - \frac{\beta_d}{\sqrt{1+\beta_d^2+\beta_d d^{-1}+(2d)^{-2}}}J_m(\nu d)\right\}^2\right.}\cdots$$

$$\cdots\frac{-Y_m(\nu\rho)\left\{J_m'(\nu d)\sin\left(\nu\sin^{-1}\frac{1}{\sqrt{1+\beta_d^2+\beta_d d^{-1}+(2d)^{-2}}}\right) - \frac{\beta_d}{\sqrt{1+\beta_d^2+\beta_d d^{-1}+(2d)^{-2}}}J_m(\nu d)\right\}}{\left.+\left\{Y_m'(\nu d)\sin\left(\nu\sin^{-1}\frac{1}{\sqrt{1+\beta_d^2+\beta_d d^{-1}+(2d)^{-2}}}\right) - \frac{\beta_d}{\sqrt{1+\beta_d^2+\beta_d d^{-1}+(2d)^{-2}}}Y_m(\nu d)\right\}^2\right]^{-\frac{1}{2}}}\ . \tag{B.7}$$

When $\beta_d \to 0$, this reduces to Neumann's problem kernel

$$\mathcal{K}_m(\rho\ ,\nu) = \frac{J_m(\nu\rho)Y_m'(\nu d) - Y_m(\nu\rho)J_m'(\nu d)}{\sqrt{J_m'^2(\nu d) + Y_m'^2(\nu d)}} \tag{B.8}$$

and when $\beta_d \to \infty$, the kernel of (B.4.11) is obtained for Dirichlet's problem

$$\mathcal{K}_m(\rho\ ,\nu) = \frac{J_m(\nu\rho)Y_m(\nu d) - Y_m(\nu\rho)J_m(\nu d)}{\sqrt{J_m^2(\nu d) + Y_m^2(\nu d)}}\ . \tag{B.9}$$

Applying the Hankel-Weber transform to (B.1) and integrating twice by parts,

$$\frac{\partial^2\mathcal{P}^{+}}{\partial z^2} + \{k_o^2\tilde{\epsilon}(\omega) - \nu^2\}\mathcal{P}^{+} = \left[\rho\Big(\mathcal{K}_m(\nu,\rho)\frac{d\Psi^{+}(\rho)}{d\rho} - \Psi^{+}(\rho)\frac{d\mathcal{K}_m(\nu,\rho)}{d\rho}\Big)\right]_{\rho=d}^{\rho=\infty}\ . \tag{B.10}$$

is obtained.

APPENDIX C

Selection of Vector Potential in the Dielectric Medium Region

The boundary conditions satisfied by the magnetic vector potential $\vec{\mathbf{A}}$ on the surface of a perfect electric conductor are, e.g. [106],

$$\vec{\mathbf{n}} \times \vec{\mathbf{A}} = 0 \, , \tag{C.1}$$

$$\nabla_n \cdot \vec{\mathbf{A}} = 0 \, . \tag{C.2}$$

These boundary conditions may have to be simultaneously satisfied for the vector potential. If condition (2.1.28) is satisfied then a medium is a dielectric. It implies that the magnetic flux and magnetic density vectors are linearly dependent, namely $\vec{\mathbf{B}} = \mu_o \vec{\mathbf{H}}$. Since the magnetic flux density $\vec{\mathbf{B}}$ possessess vanishing source density, both $\vec{\mathbf{B}}$ and $\vec{\mathbf{H}}$ are solenoidal fields by virtue of their linear dependence. For the class of solenoidal fields, the representation theorem for the vector Helmholtz equation [107] allows a solution of a vector Helmholtz equation, say for $\vec{\mathbf{H}}$, to be represented by a solution of the corresponding scalar Helmholtz equation, say for Ψ_{tot}, such that $\vec{\mathbf{H}} = \nabla \times \hat{\mathbf{e}}_i \, \Psi_{tot}$, where $\hat{\mathbf{e}}_i$ denotes a properly chosen unit vector. This choice of the vector $\hat{\mathbf{e}}_i \Psi_{tot}$ requires great ingenuity in selection of the direction vector. When the choice is inadequate, it may lead to an ill-posed problem. Nevertheless, as far as the dielectric medium is considered, it is advantageous to work with vector potential $\vec{\mathbf{A}}$, since the solution is achieved by solving a scalar partial differential equation and no gauge transformation is required.

At first, choose the longitudinal vector $\vec{\mathbf{A}} = \hat{\mathbf{e}}_z \Psi_{tot}$. Then, the conditions (C.1-2)

---

[106] W F. Richards, K. Mcinturff and P D. Simon, "An Efficient Technique for Computing the Potential Green's Functions for a Thin, Periodically Prallel-Plate Waveguide Bounded by Electric and Magnetic Walls", IEEE Trans. M T T , V 35, No 3, 1987, pp. 276-281

[107] P.M. Morse and H. Feshbach, *op. cit.* pp. 1764-1765

give on the center conductor and flange surfaces (denoted here $S_\imath$):

$$\hat{\mathbf{e}}_z \times \hat{\mathbf{e}}_z \Psi_{tot}|_{S_\imath} = 0 \cdot \Psi_{tot}|_{S_\imath} = 0 \tag{C.3}$$

and

$$\frac{\partial}{\partial z}\hat{\mathbf{e}}_z \cdot \hat{\mathbf{e}}_z \Psi_{tot}|_{S_\imath} = \frac{\partial \Psi_{tot}}{\partial z}\Big|_{S_\imath} = 0 \ , \tag{C.4}$$

respectively. Conditions (C.1-2) are satisfied for an arbitrary Ψ_{tot} and the Neumann boundary condition is implied.

Consider (5.2.1) in region I or II with the following transformed Neumann boundary condition at $z = 0$

$$\frac{d\mathcal{P}^+}{dz}\Big|_{S_\imath} = 0 \ . \tag{C.5}$$

Then the solutions of (5.2.1) are in region I

$$\mathcal{P}_I^+(\kappa, z) = \frac{\kappa}{k_o^2\tilde{\epsilon}(\omega) - \kappa^2} a\Psi^+(a)J_m'(\kappa a) + C\cos\left(\sqrt{k_o^2\tilde{\epsilon}(\omega) - \kappa^2}\ z\right) \tag{C.6}$$

and in region II

$$\mathcal{P}_{III}^+(\kappa, z) = \frac{\left\{\frac{2}{\pi}\Psi^+(b) - \frac{2}{\pi}\frac{J_m(\chi b)}{J_m(\chi d)}\Psi^+(d)\right\}}{[k_o^2\tilde{\epsilon}(\omega) - \chi^2]} + C\cos\left(\sqrt{k_o^2\tilde{\epsilon}(\omega) - \chi^2}\ z\right) \ . \tag{C.7}$$

The boundary condition (C.5) on the perfectly conducting surfaces at $z = 0$ lead to nonunique solutions in regions I and III, respectively. Therefore, this choice of vector potential leads to an ill-posed problem, namely relations (C.6-7) are solutions for an arbitrary value of C. The above consideration also invalidates results in [108] and [109]

Consider the second choice for the vector potential*:

$$\vec{\mathbf{A}} = (\hat{\mathbf{e}}_z + \hat{\mathbf{e}}_\rho)\Psi_{tot} \ . \tag{C.8}$$

Conditions (C.1-2) give on perfect electric conductor surfaces:

$$\hat{\mathbf{e}}_z \times (\hat{\mathbf{e}}_z + \hat{\mathbf{e}}_\rho)\Psi_{tot} = \hat{\mathbf{e}}_\phi \Psi_{tot}|_{S_\imath} = 0 \tag{C.9}$$

[108] J R Mosig, J E. Besson, M Gex-Fabry and F Gardiol, *op. cit.*, pp 46-51

[109] C Fray, N Khayata and A Papiernik, *op cit*, pp 107-110

* This choice is allowed on the basis of the extended representation theorem for the vector Helmholtz equation

and

$$\frac{\partial}{\partial z}\hat{\mathbf{e}}_z \cdot (\hat{\mathbf{e}}_z + \hat{\mathbf{e}}_\rho)\Psi_{tot} = \frac{\partial \Psi_{tot}}{\partial z}\Big|_{S_i} = 0 \ . \tag{C.10}$$

From the first equation, we infer that $\Psi_{tot}|_{S_i} = 0$ while from the second, $\partial\Psi_{tot}/\partial z|_{S_i} = 0$. The Neumann boundary condition is an additional constraint imposed upon wave function. These two conditions cannot be satisfied on the same surface of a perfect electric conductor. However, this choice may be appropriate for region II which is associated with the annular aperture at $z = 0$.

The third choice is

$$\vec{\mathbf{A}} = (\hat{\mathbf{e}}_\rho + \hat{\mathbf{e}}_\phi)\Psi_{tot} \ . \tag{C.11}$$

For this choice, conditions (C.1-2) give:

$$\hat{\mathbf{e}}_z \times (\hat{\mathbf{e}}_\rho + \hat{\mathbf{e}}_\phi)\Psi_{tot} = (\hat{\mathbf{e}}_\phi - \hat{\mathbf{e}}_\rho)\Psi_{tot}|_{S_i} = 0 \tag{C.12}$$

and

$$\frac{\partial}{\partial z}\hat{\mathbf{e}}_z \cdot (\hat{\mathbf{e}}_\rho + \hat{\mathbf{e}}_\phi)\Psi_{tot}|_{S_i} = 0 \cdot \frac{\partial \Psi_{tot}}{\partial z}\Big|_{S_i} = 0 \ . \tag{C.13}$$

From the two last equations, the Dirichlet boundary condition $\Psi_{tot}|_S = 0$ is satisfied and $\partial\Psi_{tot}/\partial z|_{S_i}$ is equal to an arbitrary function.

Transforming this boundary condition into FHT domain, we obtain

$$\mathcal{P}^+|_{S_i} = 0 \ . \tag{C.14}$$

The solutions of (5.2.1) in regions I and III are thus given by

$$\mathcal{P}_I^+(\kappa, z) = \frac{\kappa a}{k_o^2\tilde{\epsilon}(\omega) - \kappa^2}\Psi^+(a)J_m'(\kappa a)\Big\{1 - e^{-j\sqrt{k_o^2\tilde{\epsilon}(\omega)-\kappa^2}z}\Big\} \tag{C.15}$$

and

$$\mathcal{P}_{III}^+(\kappa, z) = \frac{\left\{\frac{2}{\pi}\Psi^+(b) - \frac{2}{\pi}\frac{J_m(\chi b)}{J_m(\chi d)}\Psi^+(d)\right\}}{[k_o^2\tilde{\epsilon}(\omega) - \chi^2]}\Big\{1 - e^{-j\sqrt{k_o^2\tilde{\epsilon}(\omega)-\chi^2}z}\Big\} \ , \tag{C.16}$$

respectively.

These solutions are unique. The choice of the vector potential, the subsequent boundary condition and the solution of the ordinary differential equation for wave function represent a consistent system. Thus, the natural conclusion is that, in the near field, this configuration of the sensor-medium structure supports at $z > 0$ the hybrid waves HE_{mn} consisting of TM_{mn} to z and TE_{mn} to z modes.

For this choice of the vector potential, i.e. (C.11), components of the TE_{mn} to z field are given:

$$E_\rho = \frac{1}{j\omega\tilde{\epsilon}(\omega)}\left\{\frac{1}{\rho^2}\frac{\partial}{\partial\rho}\left(\rho\frac{\partial\Psi_{tot}}{\partial\phi}\right) - \frac{1}{\rho^2}\frac{\partial^2\Psi_{tot}}{\partial\phi^2} - \frac{\partial^2\Psi_{tot}}{\partial z^2}\right\} \tag{C.17}$$

$$H_\phi = \frac{\partial\Psi_{tot}}{\partial z} \tag{C.18}$$

$$H_z = \frac{1}{\rho}\frac{\partial}{\partial\rho}(\rho\Psi_{tot}) - \frac{1}{\rho}\frac{\partial\Psi_{tot}}{\partial\phi}\ , \tag{C.19}$$

while those of TM_{mn} to z are:

$$E_\phi = -\frac{1}{j\omega\tilde{\epsilon}(\omega)}\left\{\frac{\partial}{\partial\rho}\left(\frac{\Psi_{tot}}{\rho} + \frac{\partial\Psi_{tot}}{\partial\rho}\right) - \frac{1}{\rho}\frac{\partial^2\Psi_{tot}}{\partial\rho\partial\phi} + \frac{\partial^2\Psi_{tot}}{\partial z^2}\right\} \tag{C.20}$$

$$E_z = \frac{1}{j\omega\tilde{\epsilon}(\omega)}\left(\frac{1}{\rho}\frac{\partial\Psi_{tot}}{\partial z} + \frac{\partial^2\Psi_{tot}}{\partial\rho\partial z} + \frac{1}{\rho}\frac{\partial^2\Psi_{tot}}{\partial z\partial\phi}\right) \tag{C.21}$$

$$H_\rho = -\frac{\partial\Psi_{tot}}{\partial z} \tag{C.22}$$

These fields are located in regions I and III.

When region II is considerd, the proper choice of the magnetic vector potential is (C.8). In this case the fields are:

for the TE_{mn} to z field

$$E_\rho = -\frac{1}{j\omega\tilde{\epsilon}(\omega)}\left(\frac{\partial^2\Psi_{tot}}{\partial z^2} + \frac{1}{\rho^2}\frac{\partial^2\Psi_{tot}}{\partial\phi^2} - \frac{\partial^2\Psi_{tot}}{\partial\rho\partial z}\right) \tag{C.23}$$

$$H_\phi = \frac{\partial\Psi_{tot}}{\partial z} - \frac{\partial\Psi_{tot}}{\partial\rho} \tag{C.24}$$

$$H_z = -\frac{1}{\rho}\frac{\partial\Psi_{tot}}{\partial\phi}\ , \tag{C.25}$$

and for the TM_{mn} to z field

$$E_\phi = \frac{1}{j\omega\tilde{\epsilon}(\omega)}\left\{\frac{1}{\rho}\frac{\partial^2\Psi_{tot}}{\partial\phi\partial z} + \frac{1}{\rho}\frac{\partial}{\partial\rho}\left(\frac{1}{\rho}\frac{\partial\Psi_{tot}}{\partial\phi}\right)\right\} \tag{C.26}$$

$$E_z = \frac{1}{j\omega\tilde{\epsilon}(\omega)} \left\{ \frac{1}{\rho} \left(\frac{\partial \Psi_{tot}}{\partial z} - \frac{\partial \Psi_{tot}}{\partial \rho} \right) + \frac{\partial^2 \Psi_{tot}}{\partial z \partial \rho} - \frac{\partial^2 \Psi_{tot}}{\partial \rho^2} - \frac{1}{\rho^2} \frac{\partial^2 \Psi_{tot}}{\partial \phi^2} \right\} \qquad (C.27)$$

$$H_\rho = \frac{1}{\rho} \frac{\partial \Psi_{tot}}{\partial \phi} \ . \qquad (C.28)$$

If we restrict consideration to TM_{on} and TE_{on} modes, the ϕ-dependence vanishes, i.e., $\Phi^+ \equiv 1$ in (5.2.3). In effect, a simplified form of modal equations in the region I and III follows:

for the TE_{on} to z

$$E_\rho = -\frac{1}{j\omega\tilde{\epsilon}(\omega)} \frac{\partial^2 \Psi^+}{\partial z^2} \qquad (C.29)$$

$$H_\phi = \frac{\partial \Psi^+}{\partial z} \qquad (C.30)$$

$$H_z = \frac{\partial \Psi^+}{\partial \rho} + \frac{\Psi^+}{\rho} \ , \qquad (C.31)$$

while those of the TM_{on} to z are

$$E_\phi = -\frac{1}{j\omega\tilde{\epsilon}(\omega)} \left\{ \frac{\partial}{\partial \rho} \left(\frac{\Psi^+}{\rho} + \frac{\partial \Psi^+}{\partial \rho} \right) + \frac{\partial^2 \Psi^+}{\partial z^2} \right\} \qquad (C.32)$$

$$E_z = \frac{1}{j\omega\tilde{\epsilon}(\omega)} \left(\frac{1}{\rho} \frac{\partial \Psi_{tot}}{\partial z} + \frac{\partial^2 \Psi_{tot}}{\partial \rho \partial z} \right) \qquad (C.33)$$

$$H_\rho = -\frac{\partial \Psi^+}{\partial z} \ , \qquad (C.34)$$

and for the TM_{on} to z field in the region II

$$E_\rho = -\frac{1}{j\omega\tilde{\epsilon}(\omega)} \left(\frac{\partial^2 \Psi^+}{\partial z^2} - \frac{\partial^2 \Psi^+}{\partial \rho \partial z} \right) \qquad (C.35)$$

$$H_\phi = \frac{\partial \Psi^+}{\partial z} - \frac{\partial \Psi^+}{\partial \rho} \qquad (C.36)$$

$$E_z = \frac{1}{j\omega\tilde{\epsilon}(\omega)} \left\{ \frac{\partial^2 \Psi^+}{\partial z \partial \rho} - \frac{\partial^2 \Psi^+}{\partial \rho^2} + \frac{1}{\rho} \left(\frac{\partial \Psi^+}{\partial z} - \frac{\partial \Psi^+}{\partial \rho} \right) \right\} \ . \qquad (C.37)$$

APPENDIX D

Computation of Roots of Transcendental Equations for Application of Finite Hankel Transform

The theory introduced in chapter IV has meaning only in terms of the existence and ordering of the solution for transcendental equation (4.3.19).

The solution of the boundary value problem in multiply connected regions requires the specification of boundary conditions on every surface. The simplest structures belonging to this class are the coaxial waveguide or cavity. The use of finite integral transforms with respect to space variables considerably simplifies the solution of the boundary value problems. For problems described in cylindrical coordinate systems, the Finite Hankel Transform offers a comparatively simple tool for solving mixed boundary value problem of Helmholtz equation. Despite this, it has not obtained wide usage because the existing largest tables of Bessel functions [110] are not sufficient to provide all needed values for computation of transcendental equations of appropriate problem. They do not contain Neumann functions; hence its use would be extremely laborious. The important problem to overcome, is to compute Bessel and Neumann functions with the desired accuracy for the required order and argument.

Modern engineering applications require numerical results. Therefore, it is required that for any value of the characteristic dimension ℓ of the coaxial region the eigenvalues be available, thus the points of characteristic equation lying in $\chi - \ell$ plane be linked such that to create $\ell(\chi)$ curves of zero contours. A condition for this is to provide the tables of roots χ_{mn} for the desired value of parameter $\ell = a/b$. There are 18 possible kernels of the transformation resulting in nine transcendental equations in the circular annulus region of

[110] The Staff of the Comput. Lab. of Harvard University, "The Annals of the Computation Laboratory of Harvard University", Cambridge, Massachusetts, Harvard University, 1949

interest. Two symmetric cases: Dirchlet-Dirichlet (D-D) and Neumann-Neumann (N-N) are fundamental both from practical and theoretical point of view. The first gives rise TM_{mn} modes while the second TE_{mn}. There are also other areas of research where these equations are of interest. The advent of optical fibre transmission technology, the higher order modes are again focused interest of researchers [111].

For annular domain with symmetric Dirichlet boundary conditions (D-D) , i.e., the first boundary value problem, give the following transcendental equation

$$J_m(\chi_{mn})Y_m(\chi_{mn}\ell) - Y_m(\chi_{mn})J_m(\chi_{mn}\ell) = 0 \ . \qquad (D-1)$$

When symmetric Neumann boundary conditions (N-N), i.e., the second boundary value problem, are applied the transcendental equation is

$$J_m'(\chi_{m\,n})Y_m'(\chi_{m\,n}\ell) - J_m'(\chi_{m\,n}\ell)Y_m'(\chi_{m\,n}) = 0 \ . \qquad (D-2)$$

In both equations, χ_{mn} is the eigenvalue and $\ell = a/b$ is the characteristic dimension of the coaxial structure. Indexes m and n denote order of Bessel and Neumann functions and number of root (or alternatively zero), respectively. These equations have the following properties [112] as $\ell \to 0$:

- the eigenvalues of (D-1) approach the corresponding root of

$$J_m(\chi) = 0 \ ; \qquad (D-3)$$

- and the eigenvalues of (D-2) approach the corresponding root of

$$J_m'(\chi) = 0 \ . \qquad (D-4)$$

The most extensive table of roots of (D-1) and (D-2) are published in [113]. In fact, (D-1) is tabulated up to the order $m = 3$ of Bessel function involved and up to 5-th root

[111] H M Barlow, "Optical Fibre Transmission in the TE_{mn} Mode", Journal of Physics, D Applied Physics, V 13, 1980, pp 369-75

[112] M Kline, "Some Bessel Equations and Their Application to Guide and Cavity Theory", Journal of Mathematical Physics V 28, 1950, pp 37-48

[113] H B Dwight, "Table of Roots for Natural Frequencies in Coaxial Type Cavities", Journal of Mathematical and Applied Physics, v 27, 1948, pp 90-97

for limited number of parameter ℓ. This is not sufficient for rigorous application of the FHT. When $\ell \rightarrow 0$, the roots of (D-1) approach the corresponding roots of (D-2) for the same order m.

The nonlinear equation defined by (D-1) and (D-2) are subset of a general function which is written in simplified form as

$$\mathcal{K}_m = f_m(\chi\,,\ell) \qquad (D-5)$$

of which arguments are constrained $0 < \chi \leq \chi_{max} < \infty$ and $0 \geq \ell < 1$.

Two mutually-related codes were developed to accomplish the solution of (D-5):

- First the zero-contour determination, $\ell(\chi)$;
- Second high accuracy eigenvalue χ_{mn} evaluation for the given parameter ℓ.

The first one deals with 3-dimensional problem and allows us to determine properties of the characteristic dimension-eigenvalue domain $\ell - \chi$ and provide information about behavior of the function and approximate (and values) location of all eigenvalues. This code uses initialization of searching procedure of which concept is described in [114], however, the details of the solution are different. Once values of both variables are imposed on boundaries of the region in the parameter statement at the beginning of the program, the search procedure begins by examining values of function on the perimeter of the $\chi - \ell$ plane. Each point on the perimeter is controlled by a member of a logical vector of which values are set to "true" at the beginning of the search process. For the search process along the boundary $\ell = 0$, the equations (3) and (4) are used. When brackets of the first eigenvalue are detected, the automatic search process is carried out. For this purpose, the values of the function are examined at four vertices of the adjacent to the bracket grid. A logical function of two variables describes each grid. This function describes the search strategy in a systematic way. The first variable may assume sixteen distinct values, each of them associated with a combination of values of function at vertices of a grid. The second

[114] M. Mrozowski, "An Efficient Algorithm for Finding Zeros of a Real Function of Two Variables", IEEE Trans. on Microwave Theory and Tech., V 36, No. 3, March 1988, pp. 601-604.

variable may take four values and is associated with a side of a current grid. The present and the past states of the grid function determine the next grid to be examined. This method causes that no rotation of a grid is required in contrast to the code described in [142]. The value of the "output" point of the zero contour is determined by interpolation procedure using values of the function $\mathcal{K}_m$ at the associated grid points. Therefore, the accuracy of the method is affected by the grid size. When the zero-contour is determined and its end point lies on the perimeter, a member of the logical vector controlling each perimeter point is set to false. The search procedure is then resumed on the perimeter from the next point to that at which last eigenvalue was found.

The second code utilizes similar to the first technique of search, however, the search strategy is carried out on members of a vector

$$\mathcal{K}_m = f_m(\chi) \qquad \text{for} \qquad \ell = \text{const} \;, \tag{D-6}$$

where $\chi_{min} < \chi < \chi_{max}$. The numerical procedure of finding nodal points between which the eigenvalue lies, is called the root bracketing. When the eigenvalue is bracketed, the iterative process starts. This is carried out by a subroutine based on modified Van Wijingaarden-Dekker-Brent Method [115]. This method combines root bracketing, bisection, and inverse quadratic interpolation. The program is capable of finding eigenvalues with the uncertainty 10^{-8} at the expense of increase of computation time. The convergence of the code has been proven, although, for large eigenvalues presented in Tab. 1.1 and Tab. 1.2, the number of iterations exceeds 200.

[115] W H Press, B P Flannery, S A Teukolsky, W T Vettering, "Numerical Recipes", Cambridge University Press, Cambridge, 1986, p 269

Roots χ_{on} of the transcendental equation $J_o(\chi_{on})Y_o(\chi_{on}\ell) - J_o(\chi_{on}\ell)Y_o(\chi_{on}) = 0$						
n	$\ell = 0.100$	$\ell = 0.250$	$\ell = 0.333$	$\ell = 0.500$	$\ell = 0.667$	$\ell = 0.833$
1	3.3252	4.1002	4.6502	6.2503	9.4255	18.8259
2	6.8503	8.3004	9.3755	12.5256	18.8509	37.6019
3	10.4005	12.5506	14.1257	18.8509	28.3014	56.4528
4	13.8757	16.7258	18.8009	25.1012	37.7269	75.2287
5	17.4009	20.9260	23.5512	31.4266	47.1773	94.0797
6	20.8760	25.1012	28.2264	37.6769	56.5778	112.8556
7	24.4012	29.3265	32.9766	43.9772	66.0533	131.7066
8	27.8764	33.4767	37.6519	50.2525	75.4538	150.4825
9	31.4016	37.7019	42.4021	56.5528	84.9292	169.3084
10	34.8517	41.8521	47.0773	62.8031	94.3297	188.1094
11	38.3769	46.0773	51.8276	69.1284	103.7802	206.9353
12	41.8521	50.2525	56.5028	75.3788	113.2056	225.7363
13	45.3522	54.4527	61.2280	81.6791	122.6561	244.5622
14	48.8274	58.6279	65.9283	87.9544	132.0566	263.3630
15	52.3526	62.8281	70.6535	94.2547	141.5320	282.1887
16	55.8278	67.0033	75.3537	100.5050	150.9325	300.9900
17	59.3280	71.2035	80.0790	106.8303	160.3830	319.8157
18	62.8031	75.3788	84.7542	113.0806	169.8085	338.5918
19	66.3283	79.6040	89.5045	119.3810	179.2589	357.4424
20	69.7785	83.7542	94.1797	125.6562	188.6594	376.2187
21	73.3036	87.9794	98.9299	131.9566	198.1349	395.0696
22	76.7538	92.1296	103.6052	138.2069	207.5353	413.8455
23	80.2790	96.3548	108.3304	144.5322	217.0108	432.6965
24	83.7542	100.5050	113.0306	150.7825	226.4113	451.4724
25	87.2543	104.7302	117.7559	157.0828	235.8618	470.2983
26	90.7295	108.8804	122.4561	163.3581	245.2872	489.0994
27	94.2547	113.1056	127.1813	169.6584	254.7377	
28	97.7049	117.2808	131.8566	175.9088	264.1379	
29	101.2300	121.4810	136.6068	182.2341	273.6133	
30	104.7052	125.6562	141.2820	188.4844	283.0139	
31	108.2054	129.8565	146.0323	194.7847	292.4641	
32	111.6806	134.0317	150.7075	201.0600	301.8899	
33	115.2057	138.2319	155.4327	207.3603	311.3401	
34	118.6559	142.4071	160.1330	213.6106	320.7410	
35	122.1811	146.6073	164.8582	219.9109	330.2161	
36	125.6313	150.7825	169.5584	226.1863	339.6167	
37	129.1564	154.9827	174.2837	232.4866	349.0671	
38	132.6316	159.1579	178.9589	238.7369	358.4927	
39	136.1318	163.3831	183.7092	245.0622	367.9431	
40	139.6069	167.5333	188.3844	251.3125	377.3437	
41	143.1321	171.7586	193.1096	257.6125	386.8191	
42	146.5823	175.9088	197.8099	263.8879	396.2197	
43	150.1075	180.1340	202.5351	270.1880	405.6951	
44	153.5576	184.2842	207.2353	276.4387	415.0955	
45	157.0828	188.5094	211.9606	282.7637	424.5461	
46	160.5580	192.6596	216.6358	289.0144	433.9714	
47	164.0582	196.8848	221.3860	295.3145	443.4219	
48	167.5333	201.0350	226.0613	301.5898	452.8225	
49	171.0585	205.2602	230.8115	307.8899	462.2979	
50	174.5087	209.4354	235.4867	314.1406	471.6985	

Table D.1.1

Roots of the transcendental equation $\mathcal{K}_o(\chi, \ell) = 0$ with the uncertainty ± 0.0001.

Roots χ_{on} of the transcendental equation $J_o(\chi_{on})Y_o(\chi_{on}\ell) - J_o(\chi_{on}\ell)Y_o(\chi_{on}) = 0$						
n	$\ell = 0.100$	$\ell = 0.250$	$\ell = 0.333$	$\ell = 0.500$	$\ell = 0.667$	$\ell = 0.833$
51	178.0339	213.6357	240.2120	320.4656	481.1489	
52	181.4840	217.8109	244.9122	326.7161	490.5742	
53	185.0092	222.0111	249.6374	333.0164		
54	188.4844	226.1863	254.3377	339.2668		
55	191.9846	230.3865	259.0625	345.5918		
56	195.4597	234.5617	263.7380	351.8425		
57	198.9849	238.7619	268.4880	358.1426		
58	202.4351	242.9371	273.1636	364.4180		
59	205.9603	247.1373	277.9136	370.7183		
60	209.4104	251.3125	282.5889	376.9687		
61	212.9356	255.5377	287.3140	383.2939		
62	216.4108	259.6877	292.0144	389.5442		
63	219.9109	263.9128	296.7395	395.8447		
64	223.3861	268.0632	301.4399	402.1199		
65	226.9113	272.2883	306.1648	408.4202		
66	230.3615	276.4387	310.8403	414.6707		
67	233.8867	280.6636	315.5903	420.9958		
68	237.3368	284.8140	320.2659	427.2461		
69	240.8620	289.0391	324.9907	433.5464		
70	244.3372	293.1895	329.6914	439.8218		
71	247.8373	297.4146	334.4163	446.1221		
72	251.3125	301.5898	339.1167	452.3723		
73	254.8377	305.7898	343.8418	458.6729		
74	258.2878	309.9653	348.5173	464.9480		
75	261.8127	314.1653	353.2673	471.2483		
76	265.2632	318.3408	357.9426	477.4988		
77	268.7881	322.5408	362.6926	483.8240		
78	272.2634	326.7161	367.3682	490.0742		
79	275.7634	330.9160	372.0935	496.3745		
80	279.2388	335.0916	376.7937			
81	282.7388	339.2915	381.5188			
82	286.2141	343.4670	386.2192			
83	289.7390	347.6919	390.9443			
84	293.1895	351.8425	395.6196			
85	296.7144	356.0674	400.3699			
86	300.1899	360.2178	405.0452			
87	303.6897	364.4429	409.7954			
88	307.1653	368.5933	414.4705			
89	310.6650	372.8184	419.1958			
90	314.1406	376.9687	423.8960			
91	317.6655	381.1938	428.6213			
92	321.1160	385.3440	433.3215			
93	324.6409	389.5693	438.0466			
94	328.1162	393.7446	442.7219			
95	331.6162	397.9448	447.4722			
96	335.0916	402.1199	452.1475			
97	338.5916	406.3201	456.8726			
98	342.0669	410.4954	461.5730			
99	345.5918	414.6956	466.2981			
100	349.0422	418.8708	470.9983			

Table D.1.2

Roots of the transcendental equation $\mathcal{K}_o(\chi\,,\ell) = 0$ with the uncertainty ± 0.0001.

Roots χ_{1n} of the transcendental equation $J_1(\chi_{1n})Y_1(\chi_{1n}\ell) - J_1(\chi_{1n}\ell)Y_1(\chi_{1n}) = 0$						
n	$\ell = 0.100$	$\ell = 0.250$	$\ell = 0.333$	$\ell = 0.500$	$\ell = 0.667$	$\ell = 0.833$
1	3.9502	4.4502	4.9252	6.4003	9.5005	18.8509
2	7.3254	8.5254	9.5255	12.6006	18.8759	37.6269
3	10.7505	12.7006	14.2257	18.9009	28.3264	56.4528
4	14.1757	16.8258	18.8759	25.1512	37.7269	75.2287
5	17.6509	21.0260	23.6012	31.4516	47.2023	94.0797
6	21.1010	25.1763	28.2764	37.7019	56.6028	112.8556
7	24.6012	29.3764	33.0266	44.0022	66.0533	131.7066
8	28.0514	33.5517	37.7019	50.2775	75.4788	150.4825
9	31.5516	37.7519	42.4271	56.5778	84.9292	169.3334
10	35.0017	41.9021	47.1023	62.8281	94.3297	188.1094
11	38.5019	46.1273	51.8526	69.1284	103.8052	206.9353
12	41.9521	50.2775	56.5278	75.4037	113.2056	225.7363
13	45.4773	54.5027	61.2531	81.7041	122.6561	244.5622
14	48.9274	58.6529	65.9533	87.9544	132.0816	263.3630
15	52.4526	62.8781	70.6785	94.2797	141.5320	282.1887
16	55.9028	67.0283	75.3537	100.5300	150.9325	300.9900
17	59.4279	71.2535	80.1040	106.8303	160.4080	319.8157
18	62.8781	75.4037	84.7792	113.0806	169.8085	338.5918
19	66.4033	79.6290	89.5045	119.4059	179.2589	357.4424
20	69.8535	83.7792	94.2047	125.6562	188.6844	376.2187
21	73.3786	88.0044	98.9299	131.9566	198.1349	395.0696
22	76.8288	92.1546	103.6302	138.2319	207.5353	413.8455
23	80.3540	96.3798	108.3554	144.5322	217.0108	432.6965
24	83.8042	100.5300	113.0306	150.7825	226.4113	451.4724
25	87.3293	104.7552	117.7809	157.1078	235.8618	470.3232
26	90.7795	108.9054	122.4561	163.3581	245.2872	489.0994
27	94.3047	113.1306	127.1813	169.6584	254.7377	
28	97.7549	117.2808	131.8816	175.9088	264.1379	
29	101.2800	121.5061	136.6068	182.2341	273.6133	
30	104.7552	125.6562	141.3070	188.4844	283.0139	
31	108.2554	129.8815	146.0323	194.7847	292.4641	
32	111.7306	134.0317	150.7075	201.0600	301.8899	
33	115.2307	138.2569	155.4577	207.3603	311.3401	
34	118.7059	142.4071	160.1330	213.6106	320.7410	
35	122.2061	146.6323	164.8582	219.9360	330.2161	
36	125.6813	150.7825	169.5584	226.1863	339.6167	
37	129.2064	155.0077	174.2837	232.4866	349.0920	
38	132.6566	159.1829	178.9839	238.7619	358.4927	
39	136.1818	163.3831	183.7092	245.0622	367.9431	
40	139.6320	167.5583	188.3844	251.3125	377.3687	
41	143.1571	171.7586	193.1346	257.6375	386.8191	
42	146.6323	175.9338	197.8099	263.8879	396.2197	
43	150.1325	180.1340	202.5601	270.1880	405.6951	
44	153.6077	184.3092	207.2353	276.4387	415.0955	
45	157.1078	188.5094	211.9606	282.7637	424.5461	
46	160.5830	192.6846	216.6608	289.0144	433.9714	
47	164.1082	196.8848	221.3860	295.3145	443.4219	
48	167.5583	201.0600	226.0863	301.5898	452.8225	
49	171.0835	205.2602	230.8115	307.8899	462.2979	
50	174.5337	209.4354	235.4867	314.1406	471.6985	

Table D.2.1

Roots of the transcendental equation $\mathcal{K}_1(\chi, \ell) = 0$ with the uncertainty ± 0.0001.

Roots χ_{1n} of the transcendental equation

$$J_1(\chi_{1n})Y_1(\chi_{1n}\ell) - J_1(\chi_{1n}\ell)Y_1(\chi_{1n}) = 0$$

n	$\ell = 0.100$	$\ell = 0.250$	$\ell = 0.333$	$\ell = 0.500$	$\ell = 0.667$	$\ell = 0.833$
51	178.0589	213.6357	240.2370	320.4656	481.1489	
52	181.5340	217.8109	244.9122	326.7161	490.5742	
53	185.0342	222.0361	249.6374	333.0164		
54	188.5094	226.1863	254.3377	339.2917		
55	192.0096	230.4115	259.0625	345.5918		
56	195.4847	234.5617	263.7629	351.8425		
57	199.0099	238.7869	268.4880	358.1675		
58	202.4601	242.9371	273.1636	364.4180		
59	205.9853	247.1623	277.9136	370.7183		
60	209.4354	251.3125	282.5889	376.9687		
61	212.9606	255.5377	287.3389	383.2939		
62	216.4358	259.6877	292.0144	389.5442		
63	219.9360	263.9128	296.7395	395.8447		
64	223.4111	268.0632	301.4399	402.1199		
65	226.9113	272.2883	306.1648	408.4202		
66	230.3865	276.4636	310.8655	414.6707		
67	233.9117	280.6636	315.5903	420.9958		
68	237.3618	284.8391	320.2659	427.2461		
69	240.8870	289.0391	325.0159	433.5464		
70	244.3372	293.2146	329.6914	439.8218		
71	247.8624	297.4146	334.4163	446.1221		
72	251.3375	301.5898	339.1167	452.3723		
73	254.8377	305.7898	343.8418	458.6978		
74	258.3127	309.9653	348.5422	464.9480		
75	261.8376	314.1653	353.2673	471.2483		
76	265.2881	318.3408	357.9426	477.4988		
77	268.8130	322.5657	362.6926	483.8240		
78	272.2634	326.7161	367.3682	490.0742		
79	275.7883	330.9412	372.1184	496.3745		
80	279.2639	335.0916	376.7937			
81	282.7637	339.3167	381.5188			
82	286.2393	343.4670	386.2192			
83	289.7390	347.6919	390.9443			
84	293.2146	351.8425	395.6445			
85	296.7395	356.0674	400.3699			
86	300.1899	360.2178	405.0452			
87	303.7148	364.4429	409.7954			
88	307.1653	368.5933	414.4705			
89	310.6902	372.8184	419.1958			
90	314.1655	376.9937	423.8960			
91	317.6655	381.1938	428.6213			
92	321.1409	385.3691	433.3215			
93	324.6658	389.5693	438.0466			
94	328.1162	393.7446	442.7219			
95	331.6411	397.9448	447.4722			
96	335.0916	402.1199	452.1475			
97	338.6165	406.3201	456.8977			
98	342.0920	410.4954	461.5730			
99	345.5918	414.6956	466.2981			
100	349.0674	418.8708	470.9983			

Table D.2.2

Roots of the transcendental equation $\mathcal{K}_1(\chi, \ell) = 0$ with the uncertainty ± 0.0001.

Computations ascertained by these two codes were performed on the Amdahl 5860 main frame University of Ottawa computer running the VM/CMS 4.2 operating system. Subroutines were written in VS/FORTRAN-77 in double precision. The plotting software is in single precision so that the DISSPLA graphics library can be used. The evaluation of Bessel and Neumann functions was performed using the IMSL double precision library adapted from the NATS FUNPACK library [116]. The basic limitation is based on the machine precision which for double precision approximately is 15 hexadecimal digits within the range $(10^{-78}, 10^{75})$.

The process of determination of a bracket of an eigenvalue for a transcendental equation is sometimes very difficult due to lack of an algorithm which includes the sign change caused by a pole of the equation. However, this problem was not found to be very severe for equations (1) and (2). The accuracy of the first code suffers from the choice of the mesh size. Nevertheless, it provides quite good engineering insight into eigenvalues For the illustration of the first code, equation (D-1) was chosen with index $m = 1$, i.e. the first non-rotationally symmetric TM_{mn} mode.

Deficiency of the first code is compensated by the second one which provides high accuracy eigenvalues. Tables 1.1 and 1.2 show numerical values of eigenvalues of equation (D-1) for index $m = 1$ while Tables 2.1 and 2.2 for $m = 1$. The uncertainty of each eigenvalue is ± 0.0001. When only $m = 0$ is considered, these tables improve accuracy of the known eigenvalues up to $n = 5$ and extend them up to $n = 100$ for $\ell = 0.100, 0.250, 0.333$, $n = 79$ for $\ell = 0.500$, $n = 51$ for $\ell = 0.667$ and $n = 26$ for $\ell = 0.833$. The presented code has been tested up to order $m = 54$ of transcendental functions and number of eigenvalue $n = 100$. These data pave the way for application of the Finite Hankel Transform to the solution of boundary value problems in various circular symmetry electromagnetic objects.

In summary, the evaluation of eigenvalues for transcendental equations in the circular

[116] National Activity to Test Software (NATS) FUNPACK, Argonne National Laboratory, Argonne Code Center, Argonne, Illinois 60439, 1976.

coordinate system is considered. A new code has been developed for computation of eigenvalues. This is a fast algorithm for finding zero-contour of a real function of two variables. This algorithm searches for the interval in which function passes through the required value of transcendental equation and subsequently automatically starts to trace the zero-contour within a circular annulus region of interest. When the accurate values of proper number are required, another code provides them with the desired uncertainty. Numerical results are presented and compared with available data.

APPENDIX E

Field Matching at the Aperture of the Coaxial Sensor

Consider (4.3.5.1) for the simplest case: $m = 0$. Then (4.3.11) reduces to:

$$\mathcal{F}_1(\xi,0^+) = \Theta_o \int_a^b \ln\rho \mathcal{K}_o(\xi\rho)\rho d\rho + \sum_n^\infty \Theta_n \int_a^b \Psi_{Eon}(\kappa_n\rho)\mathcal{K}_o(\xi\rho)\rho d\rho \qquad \text{for} \quad a < \rho < b \;, \tag{E.1}$$

where the order of summation and integration is interchanged, and

$$\mathcal{K}_o(\xi\rho) = J_o(\xi\rho)Y_o(\xi a) - Y_o(\xi\rho)J_o(\xi a) \;. \tag{E.2}$$

The first integral is found by evaluation of (4.4.9). Evaluation of the second integral is easy, by noting that functions $\mathcal{K}_o(\xi\rho)$ and $\Psi^-_{on}(\kappa_n\rho)$ are orthogonal. Therefore, the integral is nonzero only if $\xi = \kappa_n$. This holds because variables of both integrand functions are evaluated over $a \le \rho \le b$, and the boundary conditions at a and b are the same. In effect, the following integral is evaluated

$$\int_a^b [J_o(\xi_n\rho)Y_o(\xi_n a) - J_o(\xi_n a)Y_o(\xi_n\rho)]^2 \rho d\rho = \frac{2}{\pi^2\xi_n^2}\left(\frac{J_o^2(\xi_n a)}{J_o^2(\xi_n b)} - 1\right) \;. \tag{E.3}$$

After substituting integrals into (E.1) one obtains

$$\mathcal{F}_1(\xi,0^+) = \Theta_o \frac{2}{\pi\xi^2}\left\{\ln b \frac{J_o(\xi a)}{J_o(\xi b)} - \ln a\right\} + \sum_n^\infty \Theta_n \frac{2}{\pi^2\xi_n^2}\left(\frac{J_o^2(\xi_n a)}{J_o^2(\xi_n b)} - 1\right) \;. \tag{E.4}$$

In order to construct electromagnetic fields at the aperture limiting forms of the solution for region I and II are required. For the external region, the limiting form of solution (4.3.25) for region II is of interest. Differentiating (4.3.25) with respect to ρ and evaluating the left hand limit at $z = 0^+$, it is found that

$$\lim_{z\to 0^+} \frac{\partial\Psi^+}{\partial\rho} = \sum_{k=1}^{K}\left\{\sum_{n=k}^{\infty}\Theta_n \frac{1}{\xi_n^2}\left(\frac{J_o^2(\xi_n a)}{J_o^2(\xi_n b)} - 1\right)\right\} \frac{\xi_k^2 J_o^2(\xi_k b)}{J_o^2(\xi_k a) - J_o^2(\xi_k b)} \frac{\partial B_o(\xi_k, a, \rho)}{\partial\rho} \;. \tag{E.5}$$

The second term in (E.5) may be simplified by using condition that $n = k$ to the following form

$$S_2 = \sum_{n=k}^{\infty} \Theta_n \frac{\partial B_o(\xi_k, a, \rho)}{\partial \rho} . \tag{E.6}$$

Thus, the Fourier-Bessel expansion of the Fourier-Bessel series is the series itself. By similar differentiation of (4.3.25) with respect to ρ, and subsequently with respect to z, and evaluating the left hand limit at $z = 0^+$, it is found that

$$\lim_{z\to 0^+} \frac{\partial^2 \Psi^+}{\partial\rho\partial z} = j\Theta_o\pi \sum_{k=1}^{K} \sqrt{k_o^2\tilde{\epsilon}(\omega) - \xi_k^2} \left\{ \ln b \frac{J_o(\xi a)}{J_o(\xi b)} - \ln a \right\} \frac{J_o^2(\xi_k b)}{J_o^2(\xi_k a) - J_o^2(\xi_k b)} \frac{\partial B_o(\xi_k, a, \rho)}{\partial \rho}$$
$$- j \sum_{k=1}^{K} \sqrt{k_o^2\tilde{\epsilon}(\omega) - \xi_k^2}\, \Theta_n \frac{\partial B_o(\xi_k, a, \rho)}{\partial \rho} , \tag{E.7}$$

where (E.5) was used. It is clear from (E.7) that the tangential component of the electric field density at the aperture depends on local properties of the semi-space $z > 0^+$.

By noting that

$$\lim_{z\to 0^-} \frac{\partial \Psi^-}{\partial \rho} = \frac{1}{\rho}(1 + \tilde{\Gamma}_o) + \sum_{n=1}^{\infty} \tilde{\Gamma}_n \Psi'_{E_n}(\rho) \tag{E.8}$$

and

$$\lim_{z\to 0^-} \frac{\partial^2 \Psi^-}{\partial\rho\partial z} = \frac{j\beta_o}{\rho}(1 - \tilde{\Gamma}_o) - \sum_{n=1}^{\infty} j\beta_n \tilde{\Gamma}_n \Psi'_{E_n}(\rho) , \tag{E.9}$$

one obtains four field matching conditions according to (3.4.7):

$$\tilde{Z}_s = \frac{E_\rho^-}{H_\phi^-} = -\frac{1}{j\omega\epsilon_o\epsilon_c} \frac{\lim_{z\to 0^-} \frac{\partial^2\Psi^-}{\partial\rho\partial z}}{\lim_{z\to 0^-} \frac{\partial\Psi^-}{\partial\rho}} \tag{E.10}$$

$$\tilde{Z}_s = \frac{E_\rho^-}{H_\phi^+} = -\frac{1}{j\omega\epsilon_o\epsilon_c} \frac{\lim_{z\to 0^-} \frac{\partial^2\Psi^-}{\partial\rho\partial z}}{\lim_{z\to 0^+} \frac{\partial\Psi^+}{\partial\rho}} \tag{E.11}$$

$$\tilde{Z}_s = \frac{E_\rho^+}{H_\phi^-} = -\frac{1}{j\omega\epsilon_o\tilde{\epsilon}_m(\omega)} \frac{\lim_{z\to 0^+} \frac{\partial^2\Psi^+}{\partial\rho\partial z}}{\lim_{z\to 0^-} \frac{\partial\Psi^-}{\partial\rho}} \tag{E.12}$$

$$\tilde{Z}_s = \frac{E_\rho^+}{H_\phi^+} = -\frac{1}{j\omega\epsilon_o\tilde{\varepsilon}_m(\omega)} \frac{\lim_{z\to 0^+} \frac{\partial^2\Psi^+}{\partial\rho\partial z}}{\lim_{z\to 0^+} \frac{\partial\Psi^+}{\partial\rho}} \tag{E.13}$$

However, when equation (3.4.8) is used, two equations are implied

$$\tilde{Y}_s = \frac{H_\phi^+ - H_\phi^-}{E_\phi^-} = j\omega\epsilon_o\epsilon_c \frac{\lim_{z\to 0^-} \frac{\partial\Psi^-}{\partial\rho} - \lim_{z\to 0^+} \frac{\partial\Psi^+}{\partial\rho}}{\lim_{z\to 0^-} \frac{\partial^2\Psi^-}{\partial\rho\partial z}} \tag{E.14}$$

$$\tilde{Y}_s = \frac{H_\phi^+ - H_\phi^-}{E_\phi^+} = j\omega\epsilon_o\tilde{\varepsilon}_m(\omega) \frac{\lim_{z\to 0^-} \frac{\partial\Psi^-}{\partial\rho} - \lim_{z\to 0^+} \frac{\partial\Psi^+}{\partial\rho}}{\lim_{z\to 0^+} \frac{\partial^2\Psi^+}{\partial\rho\partial z}} \tag{E.15}$$

The remaining condition is:

$$\begin{aligned} &\lim_{z\to 0^-}\left(\frac{\partial^2\Psi^-}{\partial z^2} + k_o^2\epsilon_o\varepsilon_c\Psi^-\right) - \lim_{z\to 0^+}\left(\frac{\partial^2\Psi^+}{\partial z^2} + k_o^2\tilde{\varepsilon}(\omega)\Psi^+\right) \\ &= \lim_{z\to 0^-} \frac{\tilde{Y}_s}{j\omega\epsilon_o\varepsilon_c}\frac{\partial}{\partial z}\left(\frac{\partial^2\Psi^-}{\partial z^2} + k_o^2\epsilon_o\varepsilon_c\Psi^-\right) . \end{aligned} \tag{E.16}$$

Three conditions are needed in order to determine three constants $\tilde{\Gamma}_o$, $\tilde{\Gamma}_n$ and $\tilde{\Theta}_n$ corresponding to TEM and TM_{on} forward and backward scattered fields. Condition (E.16) results from the discontinuity of the normal component of electric flux density across the dielectric surface.

APPENDIX F

Experimental Results for Reflection Coefficient

The objective of this Appendix is to present the verifying experiment of the results in Chapter III. The infinite sample method allows us to compare measured values of the reflection coefficient with values of the reflection coefficient computed by equations (3.4.12) and (3.4.13).

Experimental arrangement is shown in Fig. F.1. Standard calibration procedure was performed as described in Section 6.3. Distilled water filled long coaxial line when the experiment was carried out.

The comparison between measured and computed results is shown in Fig. F.2. Systematic error occur because of non-ideal components, for instance, leakage of microwave signals in system components. The error bounds of the automated network analyzer HP8410B were estimated in [117]. These error bounds correspond to the measured standard deviations and are estimated as 0.20 dB in magnitude (return loss) and 0.1^o in phase for the range of the measured magnitudes.

Experimental results agree with (3.4.13) derived in Chapter III.

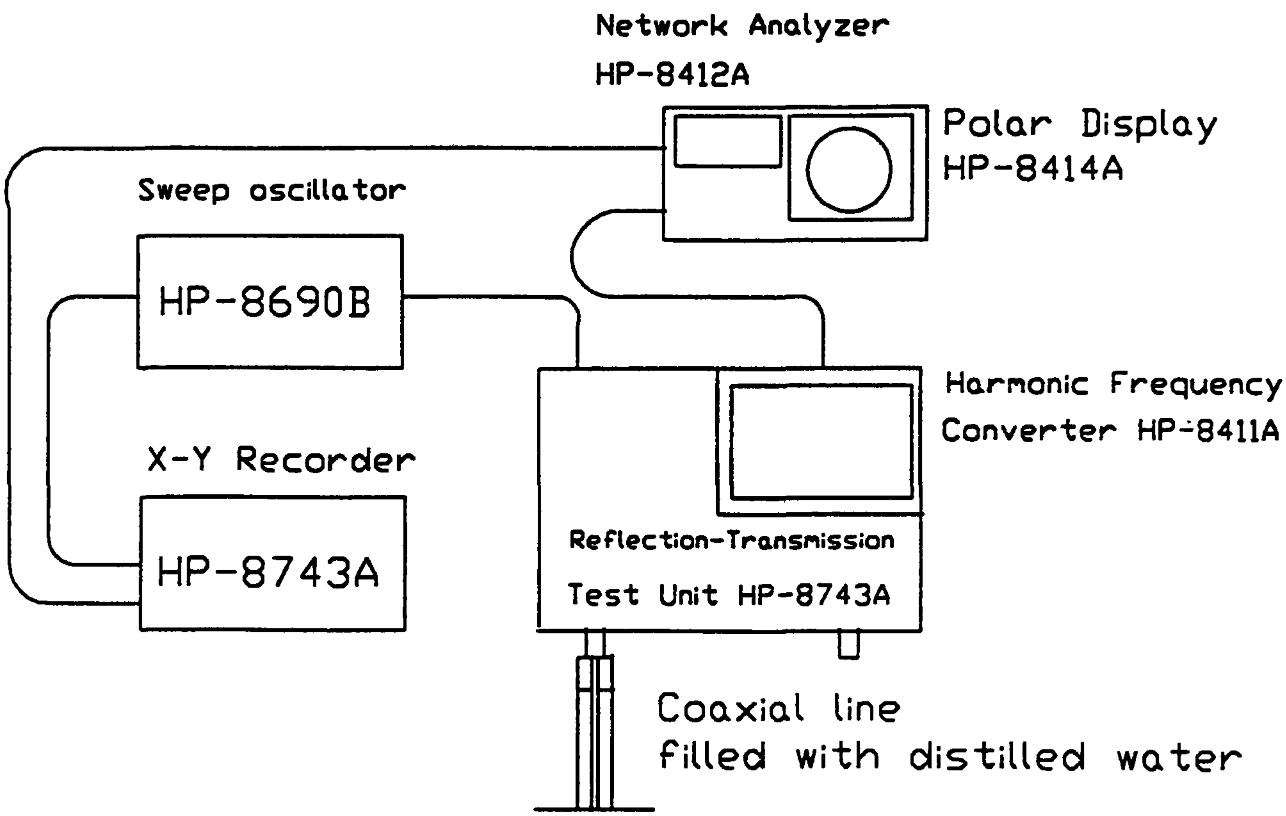

Fig. F.1

Experimental setup for determination reflection coefficient by the infinite sample method utilizing the HP8410B network analyzer.

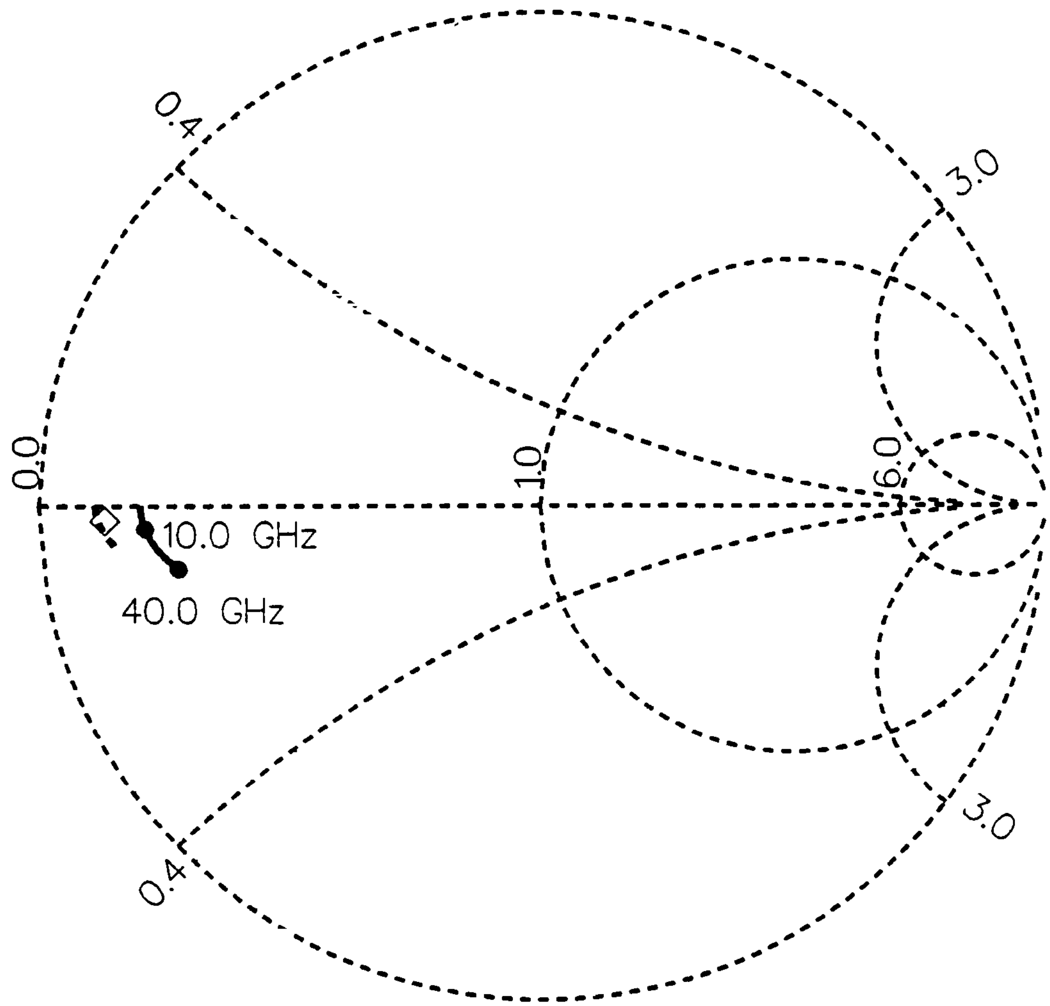

Fig. F.2

The input impedance of distilled water in the infinite sample method. Solid line corresponds to (3.4.12) while dashed line to (3.4.13). ◇ shows the measured result at f=2.7 GHz and T= 25° C.

VIII. References

[1] J.A. Stratton, "Electromagnetic Theory", McGraw-Hill, New York, 1941, p. 466.

[2] G.J. Burke and A.J. Poggio, "Numerical Electromagnetic Code (NEC) Method of Moments", Technical Document 116, Naval Ocean Systems Center, San Diego, USA, 1980, pp.1-179.

[3] C.T. Tai, "Dyadic Green's Functions in Electromagnetic Theory", Intext Educational Publishers, San Francisco-Toronto-London, 1971, pp. 17-27.

[4] A.P. Wills, "Vector Analysis with an Introduction to Tensor Analysis", Prentice-Hall, Inc., 1950, pp. 121-122.

[5] W.F. Brown, "Dielectrics", Encyclopedia of Physics, ed. by S. Flügge, V. XVII, Springer-Verlag, Berlin, 1956, pp. 1-153.

[6] J. Meixner, "Einige Folgerungen aus einer Identität für Electromagnetische Felder", Acta Physica Polonica, V. XXVII, 1965, pp. 113-121.

[7] G. Russakoff, "A Derivation of the Macroscopic Maxwell Equations", American Journal of Physics, V.38, No. 10, 1970, pp. 1188-1195.

[8] R.W.P. King, "Quasi-Stationary and Nonstationary Currents in Electric Circuits", Encyclopedia of Physics, ed. by S. Flügge, V.XVI, Springer-Verlag, Berlin, 1958, pp. 165-172.

[9] J.D. Jackson, "Classical Electrodynamics", John Wiley & Sons, New York, 1975, pp. 226-235.

[10] A.C. Eringen, "On the Foundations of Electroelastostatics", International Journal of Engineering Science, V. 1, pp. 127-153, 1963.

[11] J. Van Bladel, "Relativity and Engineering", Springer Verlag, Berlin, 1984, pp. 106-109.

[12] R.M. Fano, L.J. Chu and R.B. Adler, "Electromagnetic Fields, Energy and Forces", John Wiley & Sons, 1960, pp. 269-316.

[13] J.A. Stratton, *op. cit.*, pp. 464-470.

[14] N. Marcuvitz and J. Schwinger, "On the Representation of the Electric and Magnetic Fields Produced by Currents and Discontinuities in Waveguides", Journal of Applied Physics, V. 22., No. 6, June 1951, pp. 806-819.

[15] H. Levine and J. Schwinger, "On the Theory of Electromagnetic Wave Diffraction by an Aperture in an Infinite Plane Conducting Screen", Communications on Pure and Applied Mathematics, No. 3, 1950, pp. 355-391.

[16] R.W.P. King, G. Smith, M.Owens and T.T. Wu, "Antennas in Matter", The MIT Press, Massachusetts, 1981, pp. 316-361.

[17] N.P. Zhuk and O.A. Tret'yakov, "Green's Functions for Maxwell's Equations for a Plane-Layered Medium", Raditekhnika i Elektronika, No. 5, 1985, pp. 76-81 (*English trans.*)

[18] B.W. Braude, "Ob Odnoj Oszibke pri Ispolzowanii Metoda Integralnych Urawneniy Teorii Antenn", Jurnal Technitcheskoy Fiziki *(in Russian)*, V. XXV, No. 10, 1955, pp. 1819-1824.

[19] A.Z Fradin, "Microwave Antennas", Pergamon Press, Oxford, 1961, pp. 48-58.

[20] A.Sommerfeld, "Über die Fortpflanzug des Lichtes in dispergierenden Medien", Annalen der Physik, B. 44, 1914, pp. 177-203.

[21] L.Brillouin, "Über die Fortpflanzüg des Lichtes in dispergierenden Medien", Annalen der Physik, B. 44, 1914, pp. 204-240.

[22] R.W. Ditchburn, "Light", Interscience Publishers, New York, 1963, pp. 772-776.

[23] M. Born and E. Wolf, "Principles of Optics", Pergamon Press, Oxford, 1980, pp. 494-499.

[24] H.A. Kramers, "Estratto dagli Atti del Congresso Internationale de Fisici Como", Nicolo Zanichelli, Bologna, V.2, 1928, p. 545.

[25] R. Krönig, Ned. Tijdschr. Natuurk, No. 9, 1942, p. 402.

[26] J. Meixner, "Impedanz and Lagrange Funktion linearen dissipativen Systeme", Zeitschrift der Physik, 156, 1959, pp. 200-210.

[27] E.C. Titchmarsh, "Introduction to the Theory of Fourier Integrals", Oxford at the Clarendon Press, 1948, pp. 119-151.

[28] J.D. Jackson,*op. cit.*, pp. 307-309.

[29] J.D. Jackson,*op. cit.*, pp. 17-25.

[30] C.T. Tai, *op. cit.*, pp. 20-23.

[31] S.A. Schelkunoff, "On Teaching the Undergraduate Electromagnetic Theory", IEEE Transactions on Education, V. 15, 1972, pp. 15-25.

[32] F.N.H. Robinson, "Macroscopic Electromagnetism", Pergamon Press, 1973, pp.71-72.

[33] Ch. Hafner, "Numerische Berechnung electromagnetischer Felder", Springer Verlag, New York, 1987, pp. 63-66.

[34] Ch.H. Papas, "Theory of Electromagnetic Wave Propagation", McGraw-Hill, 1965, pp. 8-9.

[35] T.B.A. Senior, "Impedance Boundary Conditions for Imperfectly Conducting Surfaces", Appl. Sci. Research, Sec. B, V. 8, 1960, pp. 418-436.

[36] G. Boudouris, "Une Nouvelle Solution du Problème de Propagation au-dessus d'une Terre Plane", Supplemento Del Nuovo Cimento, V. X, No. 1, 1957, pp. 71-91.

[37] E.L. Feinberg, "Propagation of Radio Waves along an Inhomogeneous Surface", Supplemento Del Nuovo Cimento, V. XI, No. 1, 1959, pp. 147-170.

[38] I.J. Ciric and L. Shafai, "Comparison of Surface Impedance Models for Quasistationary Electromagnetic Field Scatterers", IEEE Symposium on Antenna Technology and Applied Electromagnetics, Winnipeg, Canada, 1986.

[39] A.J. Poggio and E.K. Miller, "Integral Equation Solutions of Three-Dimensional Scattering Problems", Chapter 4 in "Computer Techniques for Electromagnetics", ed. by R. Mittra, Pergamon Press, Oxford, 1973, pp.159-261.

[40] S.O. Rice, "Reflection of Electromagnetic Wave From Slightly Rough Surfaces", Commun. on Pure and Applied Math., No. 40, 1951, pp. 351-378.

[41] T.B.A. Senior, "Impedance Boundary Conditions for Statistically Rough Surfaces", Appl. Sci. Research, Sec. B, V. 8, 1960, pp. 437-462.

[42] R. Del Sole, "Response Functions at Surfaces", in "Electromagnetic Surface Excitations", Proceedings of an International Summer School at the Ettore Majorana Centre, Erice, Italy, edited by R.F. Wallis and G.I. Stegman, Springer-Verlag, 1985, pp. 162-179.

[43] D. Winebrenner and A. Ishimaru, "Investigation of a Surface Field Phase Perturbation Technique for Scattering from Rough Surfaces", Radio Science, V. 20, No. 2, 1985, pp. 161-170.

[44] N.G. Alexopoulos, "Accuracy of the Leontovich boundary condition for continuous and discontinuous surface impedances", Journal of Applied Physics, V. 46, No. 8, 1975, pp. 3326-3332.

[45] R.E. Collin, "Foundations for Microwave Engineering", McGraw-Hill, 1966 pp. 43-47.

[46] J. Fritz, "Plane Waves and Spherical Means", Interscience Publishers, New York, 1955, pp. 7-13.

[47] N. Marcuvitz and J. Schwinger, *op. cit.*, p. 810.

[48] K.S.H. Lee and C.E. Baum, "Application of Modal Analysis Braided-Shield Cables", IEEE Trans. on Electromagnetic Compatibility, V. 17, No. 3, 1975, pp. 159-169.

[49] S.A Schelkunoff, "Electromagnetic Waves", Van Nostrand Company, New York, 1956, Sec. 4.5, pp. 74-75.

[50] V. Fock, "Generalization of the Reflection Formulae to the Case of Reflection of an

Arbitrary Wave from a Surface of Arbitrary Form", Chapter 8 in "Electromagnetic Diffraction and Propagation Problems", Pergamon Press, Oxford, 1965, pp. 147-170.

[51] J. N. Feld, "Difraktiya Skalarnoy Vny na Nyezamknutoy Poverkhnosti s Krayevym Uslovyem Dirichle" *(in Russian)*, Doklady Akademii Nauk USSR, 1972, No.6 ,pp. 1321-1324.

[52] M. Nakayama, "Theory of Electromagnetic Response of Solid Surface", Journal of the Physical Society of Japan, V. 39, No. 2, August, 1975, pp. 265-274.

[53] R.E. Collin, "Field Theory of Guided Waves", McGraw-Hill Book Company, New York, 1960, pp. 76-77.

[54] M.A. Stuchly and S.S. Stuchly, "Coaxial Line Reflection Methods for Measuring Dielectric Properties of Biological Substances at Radio and Microwave Frequencies A Review", IEEE Trans. on Instr. and Measur.,V.IM-29, No 3, 1980, pp. 176-183.

[55] T.W. Athey, M.A. Stuchly, and S.S. Stuchly, "Measurement of Radiofrequency Permittivity of Biological Tissues With an Open-Ended Coaxial Line: Part I", IEEE Trans. M.T.T. V 30, 1982, pp. 82-86.

[56] T.W. Athey, M.A. Stuchly, and S.S. Stuchly, "Measurement of Radiofrequency Permittivity of Biological Tissue with an Open Ended Coaxial Line. Part II Experimental Results", IEEE Trans M.T.T., V. 30, pp 87-92, 1982.

[57] H. Levine and C.H. Papas, "Theory of Circular Diffraction Antenna", Journal of Applied Physics, V. 22, No. 1, 1951, pp. 29-43.

[58] J. Galejs, "Antennas in Inhomogeneous Media", Pergamon Press, Oxford, 1969, pp. 39-44.

[59] J.R. Mosig, J.E. Besson, M. Gex-Fabry and F Gardiol, "Reflection of an Open-Ended Coaxial Line and Application to Nondestructive Measurement of Materials", IEEE Trans. M.T.T., V. IM-30, 1981, pp. 46-51.

[60] G. Gajda and S.S. Stuchly, "Numerical Analysis of Open-ended Coaxial Lines", IEEE Trans. M.T.T., V. IM-32, 1983, pp. 380-384.

[61] D.K. Misra, "A Quasi-static Analysis of Open-Ended Coaxial Lines", IEEE Trans. M.T.T., V. IM-35, No. 10, 1987, pp. 925-928.

[62] E.W. Risley, "Discontinuity Capacitance of a Coaxial Line a Circular Waveguide", IEEE Trans. M.T.T., V. IM-17, 1969, pp. 86-92.

[63] J.P. Grant, R.N. Clarke, G.T. Symm and N.M. Spyrou, "A Critical Study of the Open-Ended Coaxial Line Sensor Technique for RF and Microwave Complex Permittvity Determination", unpublished, Department of Physics, University of Surrey, Guildford, England, GU2 5XH.

[64] P.M. Morse and H. Feshbach, "Methods of Theoretical Physics", McGraw-Hill, New York, Part II, 1953, pp. 1764-1767.

[65] N. Marcuvitz, "Waveguide Handbook", Boston Technical Publishers, Lexington, 1964, pp.72-80.

[66] M. Abramovitz and I. Stegun, "Handbook of Mathematical Functions", Dover Publications, 1972, pp. 371-373.

[67] Chen-To Tai, "Dyadic Green's Function for a Coaxial Line", IEEE Trans. on Antennas & Propag., V. AP-31, No.2, 1983, pp.355-358.

[68] I. N. Vekua, "New Methods for Solving Elliptic Equations", John Wiley & Sons, New York, 1968, pp. 315-339.

[69] L.B. Felsen and N. Marcuvitz, "Radiation and Scattering of Waves", Prentice-Hall, New Jersey, 1973, pp. 278-361.

[70] A. Leitner and R.D. Spence, "Effect of a Circular Groundplane on Antenna Radiation", Journal of Applied Physics, V. 21, No. 10, 1950, pp. 1001-1006.

[71] J.E. Storer, "The Impedance of an Antenna over a Large Circular Screen", Journal of Applied Physics, V. 22, No. 8, 1951, pp. 1058-1066.

[72] E.C. Titchmarsh, "Eigenfunction Expansions Associated with Second-Order Differential Equations", Part II, Oxford at the Clarendon Press, 1958, pp. 123-126.

[73] G.N. Watson, "A Treatise on the Theory of Bessel Functions", Cambridge University Press, 1966, pp. 576-582.

[74] I.N. Sneddon, "Finite Hankel Transforms", Philosophical Magazine, V 37, No.264, 1946, pp. 17-25.

[75] G. Cinelli, "An Extension of the Finite Hankel Transform and Applications", International Journal of Engineering Science, V. 3, No.5, 1965, pp. 539-559.

[76] I. N. Sneddon, "The Use of Integral Transforms", McGraw-Hill, New York, 1972, pp. 446-454.

[77] Z.A. Delecki and S.S. Stuchly, "Electromagnetic Power Propagation in Dielectric Lossy Media", accepted by J. of Microwave Power, 1989.

[78] H.S. Carslaw and J.C. Jaeger, "Conduction of Heat in Solids", Oxford at Clarendon Press, 1959, pp. 188-229.

[79] H.B. Dwight, "Table of Roots for Natural Frequencies in Coaxial Type Cavities", Journal of Mathematical and Applied Physics, V. 27, No. 1, 1949, pp. 84-89.

[80] R.F Harrington, "Time-harmonic Electromagnetic Fields", Mc-Graw-Hill, 1961, p. 202.

[81] F.E. Borgnis and C.H. Papas, "Randwertprobleme der Mikrowellenphysik", Springer-Verlag, Berlin, 1955, pp. 88-101.

[82] G.N. Watson, *op. cit.*, pp. 605-606

[83] S.A Schelkunoff, "Electromagnetic Waves", *op. cit.*, pp. 74-75..

[84] C. Fray, N. Khayata and A. Papiernik, "TM_{01} Admittance and Radiation from Open-ended Waveguide into Layered Absorbing Media", Archiv für Elektronik und Übertragungtechnik, B.36, No.3, 1982, pp. 107-110.

[85] R.F. Harrington, *op. cit.*, pp. 420-422.

[86] R.E. Collin, "Field Theory of Guided Waves", *op. cit.*, pp. 181-182.

[87] L. Altschuler, "Dielectric Constant", Chapter IX in "Handbook of Microwave Measurements", V. 3, ed. M. Sucher and J. Fox, Brooklyn Polytechnic Press, 1963, pp. 495-518.

[88] H.E. Bussey, "Measurement of RF Properties of Materials. A survey.", Proc. IEEE, V.55, 1967, pp. 1046-1053.

[89] "Automating the HP 8410B Microwave Network Analyzer", Hewlett Packard, Application Note 221A, June 1980, pp. 5-10.

[90] S.S. Stuchly, A. Kraszewski, M.A. Stuchly, "Uncertainties in Radiofrequency Dielectric Measurements of Biological Substances", IEEE Trans. on Instr. and Measur., V.IM-36, No.1, 1987, pp. 67-70.

[91] K. Cole and R. Cole, "Dispersion and Absorption in Dielectrics", J. of Chem. Physics, V. 9, April 1941, pp.341-351.

[92] V. V. Daniel, "Dielectric Relaxation", Academic Press, 1967.

[93] A.K. Jonscher, "Dielectric Relaxations in Solids", Chelsea Dielectric Press, London, 1983, pp.36-61.

[94] G. Arfken, "Mathematical Methods for Physicists", Academic Press, Orlando, 1985, pp. 388-390.

[95] Z. Nehari, "Conformal Mapping", McGraw-Hill, 1952, pp. 148-198.

[96] H. Kober, "Dictionary of Conformal Representation", Dover Publications Inc., 1952, pp. 3-35 and 141-169.

[97] J.D. Jackson,*op. cit.*, pp. 269-273.

[98] R.E. Collin, *op. cit.*, pp. 93-95.

[99] H.A. Schwarz, "Über einige Abbildungausgaben", Journal für reine und angewandte Mathematik, V.70, 1869, pp. 105-120.

[100] M.A. Rzepecka, S.S. Stuchly and M.A.K. Hamid, "Modified Infinite Sample Method for Routine Permittivity Measurements at Microwave Frequencies", IEEE Trans. Instrum. and Meas., V.IM-22, 1973, pp. 41-46.

[101] S.G. Mikhlin, "Linear Equations of Mathematical Physics", Holt, Rinehart and Winston, Inc., New York, 1967, pp. 96-99.

[102] I.N. Sneddon, *op. cit.*, pp. 17-25.

[103] G.N. Watson, *op. cit.*, pp. 576-582.

[104] E.C. Titchmarsh, "Eigenfunction Expansions Associated with Second-Order Differential Equations", Part I, Oxford at the Clarendon Press, 1958, p. 25.

[105] E.C. Titchmarsh, "Weber's Integral Theorem", Proceedings of the London Mathematical Society, V.22, 1923, pp. 15-28.

[106] W.F. Richards, K. Mcinturff and P.D. Simon, "An Efficient Technique for Computing the Potential Green's Functins for a Thin, Periodically Prallel-Plate Waveguide Bounded by Electric and Magnetic Walls", IEEE Trans. M.T.T., V. 35, No. 3, 1987, pp. 276-281.,

[107] P.M. Morse and H. Feshbach *op. cit.*, pp. 1764-1765.

[108] J.R. Mosig, J.E. Besson, M. Gex-Fabry and F. Gardiol, *op. cit.*, pp. 46-51.

[109] C. Fray, N. Kayata and A. Papiernik, *op. cit.*, pp. 107-110.

[110] The Staff of the Comput. Lab. of Harvard University, "The Annals of the Computation Laboratory of Harvard University", Cambridge, Massachusetts, Harvard University, 1949.

[111] H.M. Barlow, "Optical Fibre Transmission in the TE_{mn} Mode", Journal of Physics, D: Applied Physics, V. 13, 1980, pp. 369-75.

[112] M. Kline, "Some Bessel Equations and Their Application to Guide and Cavity Theory", Journal of Mathematical Physics, V 28, 1950, pp. 37-48.

[113] H.B. Dwight, "Table of Roots for Natural Frequencies in Coaxial Type Cavities", Journal of Mathematical and Applied Physics, v. 27, 1948, pp.90-97.

[114] M. Mrozowski, "An Efficient Algorithm for Finding Zeros of a Real Function of Two Variables", IEEE Trans. M.T.T., V. 36, No. 3, March 1988, pp. 601-604.

[115] W.H. Press, B.P. Flannery, S.A. Teukolsky, W.T. Vettering, "Numerical Recipes", Cambridge University Press, Cambridge, 1986, p. 269

[116] National Activity to Test Software (NATS) FUNPACK, Argonne National Laboratory, Argonne Code Center, Argonne, Illinois 60439. 1976.

[117] J.A. Kozlowski, "Computing Numerical Solutions to the Electromagnetic Two-

Dimensional Scalar Inverse Scattering Problem", Ph.D. thesis, University of Ottawa, 1988, pp. 98-103.